Foam formation in a PMMA-methanol system

A dissertation submitted for the degree of

Doctor of Philosophy

submitted by

Angelika Marianne Beinert

Lucy Cavendish College

DEPARTMENT OF MATERIALS SCIENCE AND METALLURGY

UNIVERSITY OF CAMBRIDGE

MAY 2021

Supervisor:
Prof James Elliott

Advisor:
Prof Alan Windle

To my grandmothers Stefanie and Veronika, who didn’t have access to higher education in their days, but have encouraged and supported the following generations to pursue their goals.

I. Declaration

This dissertation is the result of my own work and does not include the outcome of work done in collaboration, except where specifically indicated in the text in chapter 3.3.1.2..

It does not exceed the word limit of 65,000 words including appendices, bibliography, footnotes, tables and equations and has fewer than 150 figures. No part of this dissertation has been or will be submitted for any other degree or qualification except for small pieces of work that led to the Certificate of Post-Graduate Studies (CPGS) and on which further research was built on.

The final stages of this work were affected by the lab closure due to the spread of SARS-CoV-19. No experimental work could be done between 20.03.20 - 31.07.20. Therefore, some experiments couldn’t be completed and in particular the foam characterising data sets in chapters 7 and 8 lack completion. However, the available data still revealed interesting aspects about foam development. So, it was decided to present them despite incompletion.

May 2021

Angelika Beinert

II. Acknowledgements

First and foremost, I want to thank my supervisor Prof James Elliott for his great support and our fruitful discussions through all the stages of this work. Thanks for the space, freedom and patience to grow personally and scientifically and for great advice and care, in particular during the more difficult times that are experienced throughout a PhD.

I also want to thank my advisor Prof Alan Windle, for his trust, kindness and enthusiastic interest in my topic and for encouraging discussions on foam formation that in particularly helped my approach towards the first experimental steps that were probably the hardest. He also taught me how important detailed observation is.

I am very appreciative of Dr Sergio Estravis who initially supported this project in its first stages for his advice, patience and openness towards discussing all of questions, no matter how big or small. For moral support and guidance during this initial period I also want to thank Dr Patrick Kiley and Dr Thurid Gspann.

I also want to thank Martin van Es from Sabic who is the primary industrial collaborator for the project. The discussions with him have been very helpful and important.

For technical support I want to thank Jenifer Mizen, Andrew Raymond, Mary Vickers, Andrew Moss and Wayne Skeleton-Slough. A special thank you for support with coding go to Dr Jerónimo Terrones Portas and Andrew Fowler.

Especially I also want to thank Dr Fiona Smail, Dr Andrew Fowler and Philipp Kloza for carefully revising this thesis.

A big thanks goes to all the MML group members and friends. The group was a really great space to learn and work, not just from a scientific perspective. Thanks for all the inspiring lunch time discussions and coffees from Brexit to Pooh, it was always a pleasure.

In particularly, I want to thank Dr Andrew Fowler for being a great co-PhD candidate for sharing all the ups and downs, giving great advise, helping with coding and learning how British humour can help to work out surprisingly easy scenarios to save the world. Thanks also for introducing me to the fajita crew and elephant polo.

Special thanks also go to Dr Adarsh Kaniyoor and Dr Jerónimo Terrones Portas for great desk neighborship, moral support and after work movies and music.

Thanks as well to Dr Cesar Miranda Reyes and Dr Georg Schusterisch. for good chats in German and great advice on many things when needed most.

Thanks to Dr Chunlei Pei and Dr Xizhong Zheng for some discussions on FE modelling and their great kindness. Thanks to Dr Peter Vanya for being Peter and for keeping the department save from our noise, thanks to the cool kids (Philipp Kloza, Ben Shires, Yoshitake Yamamoto, Philip McKweon for being cool and awesome new group members who keep proper, world saving lunch time conversations alive. Thanks as well to Elaine Kelly for always being up for plans, sharing gym and outdoor passion with signature calmness and great humour.

I also want to thank the people in the Cambridge University German society committee. Thanks for all the great events and trips that we did and for the experience of being part of the team that we became.

Furthermore, I want to thank Dr Lakshana Mohee, Wilhelm Hüttenes, Florian Fuchs and Dr Julia Woitischek for being amazing friends when needed most.

Massive thanks go as well to Dr Fiona Smail for being an amazing flatmate and giving great advice and massive moral support during the final stages of this work. Big thanks go as well to Andreas and Leonie Beinert for massive support and a roof over the head during the chaotic times after the outbreak of CoViD-19.

Furthermore, I want to thank Anne Hummel, Franzi Marbe, Konny Kiefer, Toni Strübig and “die Mädels”, who accompanied me through great parts of my life. Thanks as well to Georg Mülhöfer for being a great friend and awesome mountain partner.

Last, but not least, the biggest thank goes towards my parents for their love, support, trust and advice only parents can give.

III. Abstract

The overall objective of this PhD thesis is to contribute to a greater understanding of the mechanisms involved in the generation of low density and low cell size polymeric foams. Specifically, this means to understand what parameters contribute to an increase in nucleation density and a decrease in cell size.

Polymeric foams with low cell size and density serve a lot of different applications such as lightweight insulation, filtration, catalysis as well as tissue engineering. A decrease in density and cell size below 70 nm leads to an increase in mechanical properties and a decrease in thermal conductivity compared to conventional foams with cell sizes in the micrometer range. Below a cell size of 40 nm, optical transparency can be achieved.

Such nanocellular foams are produced using high-pressure infiltration of CO_2 in an autoclave followed by rapid depressurisation. This makes it difficult to observe the process experimentally and determine mechanisms and parameters influencing nucleation and growth.

In order to obtain an insight into nucleation and growth mechanisms that are potentially relevant for nanofoam formation, a novel solid-state foaming process employing PMMA and methanol was developed. The process is partly analogous to the CO_2-based nanofoam development process, but experimentally more accessible. This foam and its development were characterized and important mechanisms in the process for nucleation and void development were identified.

The most important finding was that methanol-desorption-induced stresses develop and gradually expand post-critical nuclei into a foamable state. This desorption-induced stress-development and consequent nuclei expansion was identified as a necessary parameter to achieve foam formation within the PMMA and methanol system. It was shown that externally applied stresses also contribute to nuclei expansion towards a foamable state. Furthermore, the expansional effect of externally applied stresses superimposes with the expansional effect on nuclei development of desorption-induced stresses. Altogether, desorption-induced stress development could be identified as a so far unrecognized mechanism that influences foam development.

Furthermore, it was observed that an increase in sample (methanol-charged PMMA in unfoamed state) temperature following a freeze is also a source of stress resulting from density differences.

Since the nano-foam production process comprises desorption as well as a temperature increase following a freeze, the hereby resulting stresses are potentially relevant in the nano-foam production process as well. The implications of this work for the production of nanofoams is therefore the identification of production-accompanied stress development as a foam properties influencing magnitude.

IV. Table of Contents

1. Introduction

Polymer foams serve many different applications such as lightweight insulation, filtration, catalysis as well as tissue engineering. (Vonka et al. 2016) The global polymer foam market size was valued at 90.7 billion USD in 2020 and is projected to expand to 114,8 billion in 2025 USD at a growth rate of 4.8%.("Polymer Foam Market Size | Global Industry Forecast Report, 2027")

The porous architecture can be influenced by manufacturing conditions and is key to tailor made mechanical, thermal, acoustic and optical properties.

As can be seen from Figure 1, a decrease in density leads to a decrease in thermal conductivity, which makes rigid low density polymer foams perfect insulation materials.

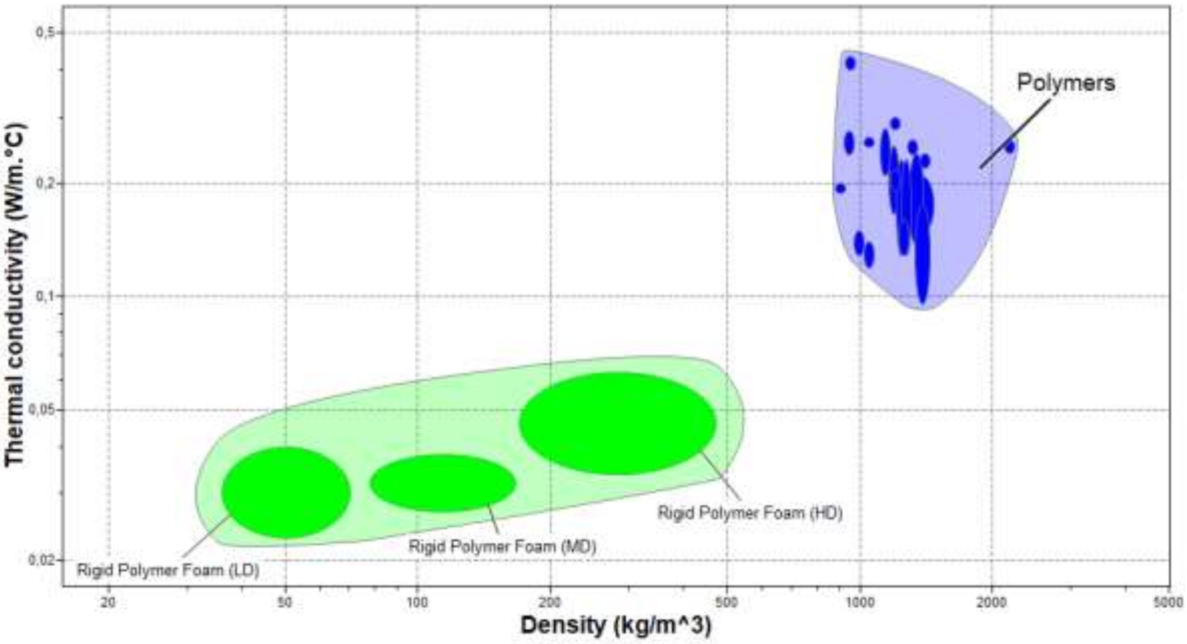

Figure 1: A thermal conductivity-density Ashby plot for different foam classes. Rigid polymer foams posess the lowest thermal conductivity.

The thermal conductivity is even lowered by a factor around 2.5 for cell sizes lower than the mean free path of gas molecules (~ 70 nm). (Notario et al. 2015) This is described by the so called Knudsen effect. (Notario et al. 2015) On the mechanical side, for nanocellular foams potential beneficial property changes arising from the confinement of the polymer on the nanoscale close to their molecular size are expected. (Stéphane Costeux 2014), (Pinto et al. 2017). Furthermore, it has been shown that semi-transparency can be achieved in foams with cell size around 40 nm. (Martín-de León, Bernardo, and Rodríguez-Pérez 2017)

Therefore, there is a high interest to find methods to further decrease density and cell size.

The process nowadays employed to reach cell sizes on the nanoscale is based on the so called solid state foaming process developed by Martini in 1981.(Martini 1981) This is a batch foaming process in which CO_2 is employed as a foaming agent. The CO_2 is mixed with the polymer in a pressure vessel under high pressure and at low temperatures as this increases the solubility of CO_2 in the most commonly employed rigid polymers (PMMA, PC). After the mixing step the vessel is depressurized, which leads to phase separation resulting in nuclei formation and subsequent void growth by the expanding CO_2. The first foams produced by solid state foaming were microcellular foams. However, nowadays cell size below 50 nm can be reached.(Martín-de León, Bernardo, and Rodríguez-Pérez 2017)

In order to create highly porous nanofoams, the decrease in the cell size has to go along with an increase in the number of cells (see Figure 9). As of today, the goal is to reach pore sizes below 70 nm with a porosity above 80 % to achieve a material with low thermal conductivity. This requires the generation of ca. 10^{17} voids/cm^3.(Notario, Pinto, and Rodriguez-Perez 2016a) The challenge is to generate a high initial density of postcritical nuclei, then expand and stabilize them as foam cells.

To achieve smaller cell sizes and higher porosities with the solid state nanofoam fabrication process, it is necessary to acquire a better understanding of the mechanisms involved. Besides changing pressure and temperature that change phase separation conditions the question is whether there might be other mechanisms that influence polymer foam development.

The problem about gaining a deeper understanding about the foam formation mechanisms within the CO_2 - assisted solid state foaming process is that foam development occurs in a fast and experimentally difficult to access process. The reason is that in the standard solid state foaming process, CO_2 is pushed in the polymer under high pressure and phase separation initiated by fast depressurisation, which prevents detailed observation of any accompanying mechanisms. Therefore, in order to understand the foam generation process better, an almost analogue polymer foaming process was developed based on methanol in a liquid state. Solvent desorption, accompanied phase separation and nucleation therefore is not sped up by depressurisation and nucleation and growth occurs on a relatively long time scale compared to the standard process. This developed process leads to a microcellular foam. However, because of the partial analogy between the processes, the mechanisms found to influence foam cell development are potentially also playing a role for the CO_2-assisted foaming process.

The development of this process, as well as the characterization of resulting foam, is described in chapter 4.

In chapter 5, it is shown that a stress state develops in the polymer from solvent desorption and is most likely a necessary condition for foamable nuclei development. The stress state development is qualitatively and quantitatively described and characterized with the help of birefringence and geometry measurements.

Based on the observation in chapter 5 that stress development seems to influence foam formation, the influence of additionally applied tensile stress on foam formation is examined in chapter 6.

In chapter 7, the stress induced by a liquid nitrogen quench as an analogue to the depressurisation associated cooling in the standard nanofoam process and its impact on nuclei development is experimentally evaluated.

In chapter 8, the influence of different solvent concentrations and desorption conditions on stress state and nuclei development is evaluated.
In chapter 9 the magnitude of the hydrostatic component of desorption-induced stress is evaluated with the help of FE modelling

2. Theoretical Background

2.1 Phase separation as origin of nucleation

Foaming usually refers to a porous structure that is generated with the help of a foaming agent. A foaming agent either leads to a physical process e.g. a gas that is expanded by changing physical process conditions (like increasing the temperature) or a chemical blowing agent can be employed that usually generates a chemical reaction, which product is e.g. a gas which expands the structure. A typical example for foams generated with chemical blowing agents are polyurethane-foams.

Other ways of inserting in small structures into a polymer matrix include templating or electro spinning, but these are often material and cost intensive. (Notario, Pinto, and Rodriguez-Perez 2016a).

The most widely adopted and successful way to generate nanofoams is based on employing CO_2 as a physical blowing agent.(Di Maio and Kiran 2017) The details are discussed in section 2.2.3. Nucleation is hereby essentially based on polymer-solvent phase separation dynamics.

A foaming process based on phase separation can be split in the following steps, which will be discussed in more detail in the assigned sections.

- a diffusion process of a solvent into the polymer (details in section 2.1.1.1)
- a phase separation process (details in section 2.1.2)
- a nucleation step (details in section 2.1.4)
- a nuclei expansion step (details in section 2.1.5)
- a stabilization step

In the diffusion step a solvent is diffused into the polymer. The conditions at which the diffusion takes place determines the available conditions (pressure, temperature, concentration) for phase separation.

A change of equilibrium conditions, e.g. a temperature or pressure, initiates the phase separation. Depending on the conditions it will lead to either spinodal decomposition or nucleation.(Stephane Costeux et al. 2012) With a gas as a solvent, a pressure change is the employed to trigger phase separation in most cases. This is referred to as pressure-induced phase separation. However, temperature also plays a role for mixing and demixing. There are cases in which phase separation in CO_2 assisted foaming is also triggered by a change in temperature. (Stéphane Costeux 2014) This is then referred to as temperature-(or sometimes thermally) induced phase separation.

The expansion of the nuclei is normally reached by heating the polymer above its glass transition temperature T_g and the blowing agent above its boiling point so that expansion is driven by the vapourizing blowing agent.

The expanded nuclei become stable as soon as the polymer is below its T_g. Bringing the polymer below its T_g, is sometimes realized by quenching the foam structure in a cooling ice bath. It has also been observed that if a stable foam is brought above T_g, it will shrink back into a transparent polymer.(Forest et al. 2015)

2.1.1 Solvent sorption in glassy polymers

The for nano-foam generation more promising CO_2-assisted batch foaming process as well as the in this thesis developed methanol-assisted batch foaming process starts with solvent sorption in glassy polymers. In the CO_2-assisted process absorption usually occurs at low temperatures and high pressures and therefore CO_2 is usually also in a liquid state.

Below T_g, the diffusion of solvents into glassy polymers is described by Case II diffusion. Its theoretical derivation is described in the next section. Case II behaviour was first described by Alfrey (Alfrey 1947) and has been well studied for the case of PMMA in methanol by Thomas and Windle (N. Thomas and Windle 1981). The case II diffusion process is characterized by a sharp front between a glassy core and swollen polymer, which is propagating at constant velocity. Therefore, the diffusion rate-controlling process is assumed to happen at the front. It is assumed that the diffusion rate controlling mechanism is the movement of the polymer segments in response to the osmotic swelling stress (see section A.3) of the solvent.(N. L. Thomas and Windle 1980)

Due to the sharp transition between methanol swollen material and glassy core, the sample dimensions swell anisotropically, with the exception of cubic samples. After the core has also swollen ("fronts met"), the sample shape readjusts partly. It was found by Thomas et al. that at higher absorption temperatures than 25 °C, the remaining shape anisotropy increases. This phenomena could be due to the fact that a lower viscosity during absorption doesn't allow for high enough restoring forces to develop from Case ll swelling accompanied stress development.(N. Thomas 1978)

2.1.1.1 Case II diffusion

Diffusion of freely moving particles under thermal agitations can be described by a random walk.(Comyn 1985) p. 342) Based on this assumption, the displacement of a particle can described by a Gaussian distribution. From these considerations it can be derived that the mean square displacement in one dimension $\langle \Delta x^2 \rangle$ of a particle increases linearly with time t and is given by:

$$\langle \Delta x^2 \rangle = 2Dt \tag{1}$$

Einstein and Smoluchowski showed that the particle's diffusivity D at a temperature T can be expressed as: (Parthasarathy 2008), (Einstein 1905), (von Smoluchowski 1906)

$$D = k_B T \mu \tag{2}$$

where μ is a friction coefficient depending on the size and shape of the particle as well as the friction coefficient of the solute. For a polymer, the equivalent is the polymer mobility $\mu = v/F$, which is determined by the stationary speed v of the polymer chain acted on by a force F (Gennes 1979)

If the relationship between t and $\langle \Delta x^2 \rangle$ is not linear (if the particle motion cannot be described by a Gaussian distribution), the diffusion behaviour is classified as anomalous. This is the case in a polymer network if the chain mobility is low and restricts the motion of solvent molecules.

This leads to a different type of diffusion in a polymer network that can be classified by the time-dependence of their sorption behaviour:(Comyn 1985)

$$\frac{M_t}{M_\infty} = kt^n \tag{3}$$

where M_t and M_∞ describe the solvent weight gain at time t and in equilibrium, respectively, k is a constant We can categorise the type of behaviour inherit to each diffusion process by the value of n.

- For $n = 0.5$ the solvent mass uptake corresponds to Fickian diffusion (see A.1). In this case the rate of diffusion is lower than the chain segment relaxation. This means the polymer chains adjust quickly enough to the solvent presence and do not affect Fickian diffusion.(Crank 1975)
- For $n = 1$ we have Case II diffusion. It applies in particular to glassy polymers in which the rate of diffusion is higher that the segmental relaxation. (Crank 1975)
- For $0.5<n<1$ non-Fickian or anomalous diffusion applies. In this case the segmental motion and the solvent mobility are comparable.(Comyn 1985)

Above T_g, the methanol uptake increases with temperature since the chain mobility is increasing the methanol absorption capacity. In contrast, below T_g, the temperature does not influence the polymer mobility as it is solely caused by methanol. Therefore, the total methanol uptake is independent below the PMMA-methanol equilibrium T_g. This has been demonstrated experimentally. (N. Thomas 1978)

2.1.2 Solubility of polymers

The thermodynamic condition for the homogenous mixture of two substances is the minimization of the Gibb's free energy of the mixed state G_{mix} compared to the sum of the free energies of the separated states G_1 and G_2. This means the difference ΔG_m in free energy between the mixed and the separated state has to be negative.

$$\Delta G_m = G_{mix} - G_1 - G_2 < 0 \tag{4}$$

In order for the mixture to be stable, ΔG_m has to reach a local minimum. A description of the free energy of mixing that takes intermolecular interactions between solvent and polymer molecules into account, is based on a lattice theory independently derived by Flory and Huggins.(Flory 1942), (Huggins 1941), (Young and Lovell 2011).

In the Flory-Huggins framework, the free energy of mixing per number of moles of solvent and polymer segments $\Delta G^*{}_m$ can be expressed as follows.

$$\Delta G^*{}_m = \frac{\Delta G_m}{n_1 + zn_2} = RT(\phi_1 \ln\phi_1 + \frac{\ln \phi_2}{z} + \chi\phi_1\phi_2) \tag{5}$$

χ is the Flory-Huggins polymer-solvent interaction parameter, $n_1 \text{and}\, n_2$ are the number of moles of solvent and polymer, $\phi_1 = \frac{n_1}{n_1+zn_2}$ represents the solvent volume fraction. $\phi_2 = \frac{zn_2}{n_1+zn_2}$ represents the volume fraction of the polymer with z segments. R is the molar gas constant.

The first two terms on the right side are entropic contributions that are always negative as $\phi_1, \phi_2 < 1$ and therefore favour mixing. The third term depends on χ and is positive. Therefore a low χ value favours mixing. (Young and Lovell 2011)

If the polymer network is entangled, an additional change in the Gibbs free energy ΔG_e deriving from the entropic network deformation of the sample has to be taken into account. An expression for this has been derived by Flory and Rehner by applying rubber elasticity theory.(Arnold 2010) $M_e \text{ and } \rho$ represent the entanglement molecular weight and the polymer density, respectively.

$$\Delta G_e = \frac{\rho RT}{2M_e}(\frac{3}{{\phi_2}^{2/3}} - 3 - \ln(\frac{1}{\phi_2})) \tag{6}$$

The Flory-Huggins polymer-solvent interaction parameter χ can be expressed as an entropic and an enthalpic component from the interaction of polymer and solvent. Its value is dimensionless. The entropic component is typically around 0.2-0.3. The enthalpic component is given as follows: (Young and Lovell 2011), (Arnold 2010)

$$\chi_{enthalpic} = \frac{V_S(\delta_S - \delta_P)^2}{RT} \tag{7}$$

V_S is the molar volume of the solvent, δ_S and δ_P are the Hildebrand solubility parameters of the solvent and the polymer, respectively. A definition of them is in the appendix A.1. (Young and Lovell 2011)

2.1.3 Spinodal decomposition

Depending on the temperature T the Gibb's free energy curve $\Delta G^*{}_m$ of a polymer-solvent-system can exhibit one (T_i) or two (T_j) (local) minima for certain polymer-solvent concentrations ϕ_u and ϕ_v (see Figure 2 & Figure 3). (Young and Lovell 2011)

The Gibb's free energy change associated with a potential phase separation process in two new concentrations ϕ_u, ϕ_v at any point A is given by the difference of the free energy of mixing ΔG_B at B and the free energy of mixing ΔG_A at A. B is derived from the cross-section of the tieline and the vertical from A (see Figure 2). (Young and Lovell 2011) $\Delta G_B - \Delta G_A$ has to be minimized for phase separation to occur.

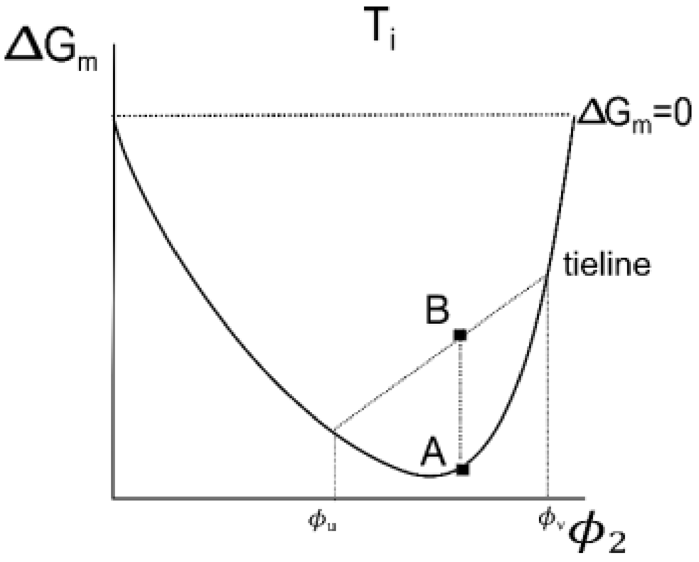

Figure 2: The free energy difference ΔG_m of mixing depending on polymer concentration ϕ_2 at Ti

For temperature T_i the free energy difference $\Delta G_B - \Delta G_A$ is always positive. Therefore, the system is a stable one phase system for these conditions. This corresponds to $\frac{\partial^2 \Delta G}{\partial^2 \phi_2} > 0$.

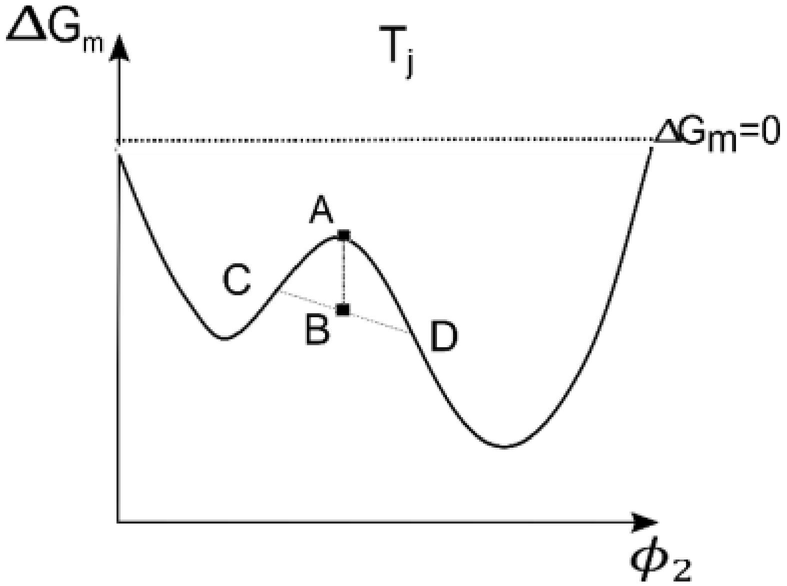

Figure 3: Free energy of mixing for the solution with a metastable concentration at Tj

For temperature T_j the difference $\Delta G_B - \Delta G_A$ is negative for concentrations between the inflection points C and D and therefore demixing is favoured. This corresponds to $\frac{\partial^2 \Delta G_m}{\partial^2 \phi_2} < 0$.

At the inflection points $\frac{\partial^2 \Delta G_m}{\partial^2 \phi_2} = 0$ and they define the boundary between a one-phase and a two-phase system for different temperatures. This boundary is called spinodal. (Young and Lovell 2011) At concentrations and temperatures below the spinodal, spinodal decomposition, but no nucleation occurs. The line resulting from the local minima is called binodal and represents the boundary between a mixed state and a demixing state. Nucleation occurs between the binodal and spinodal (detailed explanation see section 2.1.4).

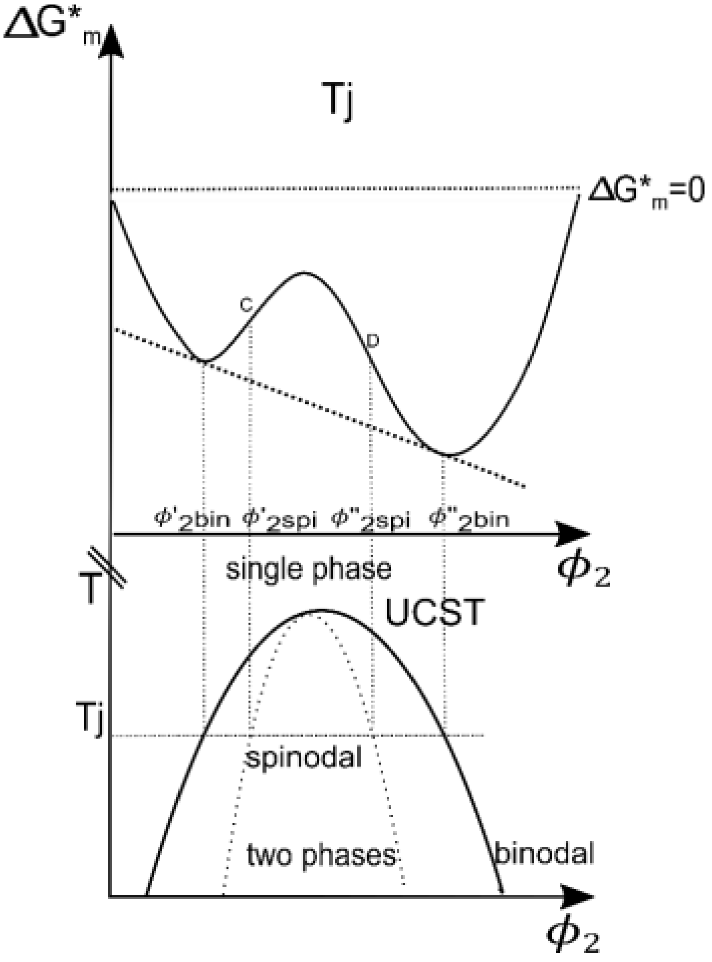

Figure 4: Derivation of spinodal and the binodal from the free energy of mixing. As in (Young and Lovell 2011)

If solubility increases with increasing temperature, the system is not stable against concentration fluctuations below the upper critical solution temperature (UCST) of the spinodal. Otherwise, this temperature is called lower critical solution temperature (LCST).

The amplitude of concentration fluctuations increases due to diffusion towards higher concentration regions of the components (“uphill diffusion”).(van de Witte et al. 1996) This leads to an interconnected solvent rich and a solvent poor phase. The dynamics description for this are provided by the Cahn-Hilliard theory (Cahn 1965) as in (Smolders, Aartsen, and Steenbergen 1971).

Once established the interconnected rich and poor solvent phase can phase separate again (secondary phase separation). (van de Witte et al. 1996)

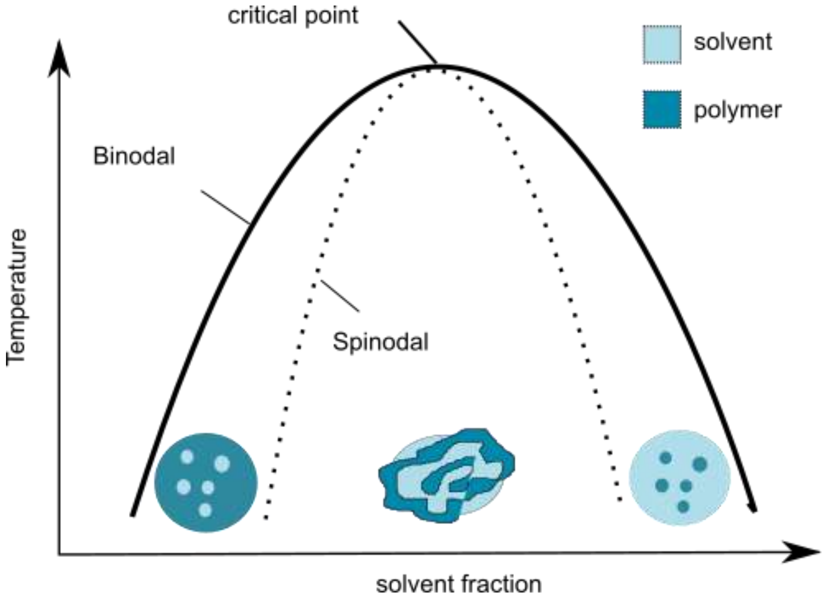

Figure 5: Schematic of a binodal and a spinodal in a polymer-solvent system. Between the binodal and the spinodal nucleation and growth of either the polymer in solvent rich concentrations or the solvent for solvent poor concentrations occurs. (Aubert and Clough 1985)

2.1.4 Nucleation

For concentrations between the two minima of $\Delta G^{*}{}_{m}$ and the inflection points, $\Delta G_A - \Delta G_B$ is positive, but has small values (see Figure 4). $\Delta G_A - \Delta G_B$ therefore represents an energy barrier that can only be overcome by larger fluctuations. (van de Witte et al. 1996) This barrier is described by classical nucleation theory.

The minima of $\Delta G^{*}{}_{m}$ for different temperatures define the binodal. The binodal and the spinodal meet at the critical point, as shown in Figure 8.

For a sufficiently high polymer concentration, nucleation of the solvent molecules is supposed to take place. For low polymer concentrations ϕ_2 the polymer is nucleated. This can result into polymer droplets. (Salvatore Iannace 2015) Nucleation can be suppressed by rapid cooling if the spinodal is reached sufficiently fast (see Figure 5). (Vonka et al)

Usually for solvent and polymer mixtures, increasing temperature increases the miscibility as χ is decreased. Therefore, in the case of most solvents, a temperature quench triggers phase separation. This is in contrast to supercritical CO_2, where an increase in temperature decreases its solubility. And therefore phase separation in this case can also be initiated by an increase in temperature. (Stéphane Costeux 2014)

It is also worth noting the difference between homogenous and heterogenous nucleation. Homogenous nucleation refers to the generation of nuclei only based on phase separation from two phases. Heterogenous nucleation refers to nucleation from nucleators such as added particles to decrease the surface energy locally to enhance nucleation. The foaming process developed in this thesis as well as the standard solid state foaming process are usually based on homogenous nucleation. Therefore, in the following nucleation theory is described for homogenous nucleation.

2.1.4.1 Classical nucleation theory

A way to describe homogenous nucleation qualitatively, is classical nucleation theory (CNT). It was first established by Volmer and Weber in 1926 based on the thermodynamic work of Gibbs.(Kashchiev 2000), (Volmer and Weber 1926) Volmer's and Weber's description of nucleation was initially based on the case of the formation of a liquid droplet from the gas phase.(Volmer and Weber 1926)

It therefore neglects some of the foaming process conditions such as e.g. depressurisation rate, which will be discussed in more detail in the next section.(Kashchiev 2000)

CNT gives a stability argument for nuclei based on the description of the free energy barrier $\Delta\mathrm{G}(R)$. For small nuclei radii R the free energy initially increases with nucleus radius until a critical nucleus volume is reached and the free energy decreases and the nuclei growth is energetically favoured. This stable growth is also referred to as post-critical state.

Nucleation can either occur within the same substance or in between two different substances. The nuclei can either be condensed (solid or liquid) or in their gas phase.

For a nucleus in the gas phase the free energy change that occurs on formation of a spherical nucleus depends on its radius R and the number of gas molecules $n(R)$ it already contains, is given by (Kashchiev 2000):

$$\Delta \mathrm{G}(R) = -n(R) * (\mu_{old} - \mu_{new}) - \frac{4\pi}{3} R^3 \Delta P + \int_{p_0}^{p} V(p)dp + 4\pi R^2 \gamma \qquad (8)$$

μ_{old} and μ_{new} describe the chemical potentials of the new nucleus phase and the old surrounding phase for a nucleus containing n molecules. ΔP is the difference between the pressure p inside the nucleus and the surrounding pressure p_0. γ is the surface tension. $V(p)$ is the cluster volume depending on pressure.

For an incompressible, condensed nucleus, like in the case of methanol, the volume $V(p)$ is independent of pressure and $V(p)$ yields $\frac{4\pi}{3} R^3$. Therefore, the two pressure related terms in equation 8 cancel and the free energy change for the formation of spherical condensed nuclei is:

$$\Delta \mathrm{G}(\mathrm{R}) = -n(R)\Delta\mu + 4\pi R^2 \gamma \qquad (9)$$

For the nucleation of a solvent from a polymer, the difference in chemical potentials $\Delta\mu$ is the difference between the chemical potential of the solvent μ_0 and the chemical potential of the solvent mixed in the polymer μ_1.(Han and Dae Han 1990) It can be expressed by Flory-Huggins theory (see equation 10).(Han and Dae Han 1990), (Young and Lovell 2011)

$$\Delta\mu = \mu_1 - \mu_0 = RT(\ln\phi_1 + \left(1 - \frac{V_1}{V_2}\right)\phi_2 + \chi{\phi_2}^2) \qquad (11)$$

This accounts for the demixing behaviour of a solvent with weight fraction ϕ_1 and molar Volume V_1 from a polymer with weight fraction ϕ_2 with molar volume V_2 and therefore also takes into account the influence of the molecular weight of the polymer. It predicts an increase in $\Delta\mu$ with an increase in molecular weight of the polymer or an increase in solvent fraction, which would both lead to a decrease of the free energy barrier and increase the nucleation density and decrease cell size.

An increase in nucleation density with increase in molecular weight of the polymer has been observed for PMMA foams made by solid state foaming. At the same time the cell size and porosity decrease with an increasing molecular weight.(Van Loock et al. 2019) Also in accordance with theory, an increase in nucleation density for higher solvent concentration has been observed for solid state foaming.(Martín-de León, Bernardo, and Rodríguez-Pérez 2017) As discussed in section 2.2.1, for foams developed with solvents that are liquid at room temperature, an increase in cell size has been observed with increase in solvent fraction, which is probably related to coalescence.

2.1.4.2 Limitations of classical nucleation theory

Classical nucleation theory is regarding to accuracy mostly a qualitative description of the nucleation process. One of the major limitations that prevents its application is that not all parameters (e.g. surface tension (Tomasko et al. 2009)) are experimentally accessible through the nucleation process.

From a theoretical perspective, in the early stages of nuclei development, the nuclei aren't spherical and when applied to polymers, viscoelastic effects can be significant that are not taken account of. (Tomasko et al. 2009), (Kashchiev 2000), (Di Maio and Kiran 2017). Generally, CNT is used to establish qualitative trends.

The viscoelastic properties of the polymer play a role when it comes to the description of stresses within the polymer. An influence of viscoelastic properties on the nucleation process can be expected for void sizes above the entanglement length between the individual polymer chains (see section 0 equation 8).

Apart from the pressure and temperature change itself, CNT does not take into account the rate of pressure or temperature changes. However, experimental evidence suggests that the rate of temperature and pressure change does influence nucleation. For example, Guo et al. experimentally observed for PS and CO_2, that nucleation density increases and cell sizes decrease with a decrease in the rate of the depressurisation.(Qingping Guo et al. 2006) However this could also be related to the fast freezing polymer that might prevent nucleation.

Despite the described shortcomings, CNT captures the main changes in the free energy state of a system and is therefore a great tool to evaluate the qualitative impact of main changes in the system.

2.1.5 Cell growth and coarsening

Within CNT a post-critical nucleus would grow infinitely given sufficient access to solvent molecules and being unrestricted to grow. In reality, solvent access is limited and the polymer viscoelastic properties restrict growth as well. Whether or not the nuclei are foamable for the given conditions also depends on their size, which can be influenced or expanded by hydrostatic tension. (Merritt and Weinhaus 1978)

The nuclei expansion is therefore described by a growth process that accounts for diffusion and the viscoelastic response of the polymer.

Various models have been developed with different ways to take into account governing parameters such as diffusion and the polymer response.

Most recently van Loock et al. developed a model in which the constitutive response of the polymer is taken into account.(Van Loock et al. 2019)

The model is based on the following relation between the pressure difference inside p and outside p_0 the nucleus upon foaming and radial expansion and depends on the von Mises effective stress σ_e.

$$p \quad - p_0 = \int_{r=b}^{r=a} \frac{2\sigma_e}{r} dr \tag{12}$$

$$\sigma_e = F\left(\varepsilon_e, \dot{\varepsilon_e}, \frac{T}{T_g}\right) \tag{13}$$

The von Mises effective stress was determined as a function F of effective strain ε_e, strain rate $\dot{\varepsilon_e}$, temperature T and glass transition T_g in the polymer of question.

This indicates how important the polymer's stress response is and indicates that a change in stress within the polymer matrix might influence void formation.

In general, there are two specific mechanisms that lead to coarsening; Oswald ripening and coalescense (Tsai and Torkelson 1990a).

Coarsening of the structure is mainly driven by minimization of the interfacial free energy. The radii of polymer poor droplets increase exponentially with time, whereas their number decreases exponentially with time. The growth rate decreases with an increasing polymer concentration. Structures formed by spinodal decomposition coarsen by the growth of the domains. (van de Witte et al. 1996), (Song and Torkelson 1994)

2.2 Foam formation processes for polymeric foams

The foaming-concept developed in this thesis is based on temperature-induced phase separation. Temperature induced phase separation processes will be discussed in the following sections before introducing the concepts for CO_2 assisted polymer-foaming.

2.2.1 Thermally induced phase separation

Historically a variety of techniques to drive phase separation of a polymer solution have been employed. An overview is given by de Witte et al. (van de Witte et al. 1996) Conceptually the simplest method is phase separation of a binary solution induced by a temperature quench referred to as thermally induced phase separation (TIPS).

Thermally induced phase separation as a porous membrane fabrication technique was first introduced by Castro in 1981.(Castro 1981), (Samitsu et al. 2013) It is applied in tissue engineering (Nam and Park 1999; Whang et al. 1995; Freyman, Yannas, and

Gibson 2001) as well as membrane development. (Song and Torkelson 1995), (Lloyd et al. 1990), (Vonka et al. 2016), (van de Witte et al. 1996)

For thermally induced phase separation a polymer and a solvent are mixed and phase separation is induced by a drop in temperature. Depending on the magnitude of the temperature drop and solvent concentration (see Figure 5) this leads to either spinodal decomposition or nucleation. The thermodynamic details on this will be explained in section 2.1. Usually, the decrease in temperature is sufficient to freeze the solvent and remove it by freeze drying so that it can sublimed from the polymer structure without any structure violation. However, if the solvent is frozen before phase separation is achieved, demixing does not take place. (Aubert and Clough 1985)

For an amorphous polymer at sufficiently high quench rates the gap between spinodal and bimodal states is traversed fast enough to suppress nucleation and growth (details in section 2.1). Therefore, at sufficiently high quench rates spinodal decomposition is assumed to take place instead of nucleation and growth.(Aubert and Clough 1985; Caneba and Soong 1985; Vonka et al. 2016) This could lead to bi-continuous structures, but it is standard to assume that interfacial tensions between the two phases lead to spherical structures. (van de Witte et al. 1996) (Koros & Fleming 1993, p. 43)

It has been observed that the void size decreases with increasing cooling rate as coarsening is prevented if the structure is below T_g faster.(Matsuyama, Berghmans, and Lloyd 1998),(Aubert and Clough 1985), (Vonka et al. 2016)

It was also reported that cell sizes decrease with increasing polymer concentrations. (Matsuyama, Berghmans, and Lloyd 1998; Reverchon, Rappo, and Cardea 2006) Matsuyama et al. explained this by the higher viscosity of a polymer-rich solution, that decreases void expansion or coarsening. However, the observation for CO_2 assisted foaming is that an increase in CO_2 uptake reduces cell size and increases porosity (see section 2.2.3). This would also be in accordance with the qualitative predictions of nucleation theory (see section 2.1.4.1). This difference in observation and theory indicates that the bigger cell size at higher solvent concentrations in TIPS foams results probably from coalescence of the nuclei. With respect to thermally induced phase separation, Hung et al. also relate reduced coarsening to a higher degree of entangled polymer concentration and therefore higher viscosity.(Hung et al. 2016)

Furthermore, solvent starts desorbing from the outer layers of the polymer. This leads to skin development upon phase separation, which refers to a solvent deprived layer of polymer. This also leads to a gradient in polymer concentration and subsequently in cell distribution normal to the surface if a temperature drop large enough to induce freezing is not applied immediately after removing the sample from the solvent as observed by Matsuyama et al.(Matsuyama, Berghmans, and Lloyd 1998)

2.2.2 Pressure-induced phase separation

The dynamics of pressure-induced phase separation have been investigated before by a light scattering-based approach.(Zhuang and Kiran 1998). Compared to thermally induced phase separation, pressure-induced phase separation has the huge advantage that a change in pressure occurs instantaneously across the sample. Therefore, any gradients in cell size distribution due to a solvent desorption gradient should be prevented. If a gas is employed, it instantly expands the nuclei if the pressure is dropped below its vapour pressure and the polymer is above its T_g. In the best case therefore, nuclei expand with a minimum of coalescence. This is why nano-foaming manufacturing processes are based on gasses as a nucleating agent.

However, it has been reported that despite the instantaneous pressure change across a sample, a skin (void-free layer) is still formed in samples that had been subject to pressure induced phase separation in particular, in the so called two-step-process (see section 2.2.3.1). (Judith Martín-de León, Bernardo, and Rodríguez-Pérez 2019) This means solvent desorption, which leads to solvent depletion in the outer layers occurs in this process as well. This indicates that solvent desorption could be an additional critical factor for foam formation and it is important to pay attention to its implication on the foam development process.

2.2.3 CO_2 assisted polymer foaming for nanofoam generation

The first microcellular polymer foams were developed based on a CO_2 assisted pressure induced batch foaming process in 1980 at MIT.(Martini 1981)(Notario, Pinto, and Rodriguez-Perez 2016a) It is also referred to as solid state foaming process, since the polymer is supposedly foamed from a solid state compared to extrusion foaming. As of today, this has proven to be the most promising technique to achieve nanocellular foams.(Stéphane Costeux 2014)

The reason for its success is often connected to supercriticality of CO_2 that occurs above 31.1 °C and 7.39 MPa.(David L. Tomasko et al. 2003) This may at first seem plausible, as supercriticality leads to the disappearance of the surface tension.(Di Maio and Kiran 2017) However, since solubility of CO_2 increases with decreasing temperature it has also been observed that nanofoams more successfully develop at lower temperatures. Several foaming processes leading to nanofoams are not conducted in the supercritical regime, but rather below 0 °C. (Stéphane Costeux 2014) E.g. the first semi-transparent nanofoam has been developed from a CO_2 saturation temperature of -32 °C at 20 MPa.(Martín-de León, Bernardo, and Rodríguez-Pérez 2017) With these observations, supercriticality no longer appears to be a major factor in the successful generation of nanofoams.

The main historical reasons for the employment of CO_2 as a gassy foaming agent are its great solubility in amorphous polymers compared to other gases (e.g. nitrogen) as well as its easy handling and environmental advantage compared to other blowing agents. (Di Maio and Kiran 2017)

The success of employing CO_2 for the generation of nanocellular polymer foams is highly dependent on the employed process conditions, in particular with regards to pressure, temperature and CO_2 concentration.

From a thermodynamic standpoint (see section 2.1.4.1), the critical energy barrier for nucleation decreases with an increase in solvent concentration and magnitude of pressure drop. This is also experimentally observed for solid state foams. So usually an increase of initial CO_2 concentration and pressure drop leads to a decrease in cell size and higher porosities. (H. Guo, Nicolae, and Kumar 2015) It has also been shown for microcellular foams that an increase in the depressurisation rate leads to a greater decrease in cell size. (Stéphane Costeux 2014) In addition, depressurisation rate is also an important parameter that influences temperature because of the Joules-Thompson-effect. This means that the sample temperature is decreased and depending on the process conditions, may bring it below T_g.(Urbanczyk et al. 2010) The temperature change during the process therefore also influences the cell development depending on its proximity to T_g.

The external pressure and temperature define the equilibrium conditions for CO_2 absorption and equilibrium concentration. However, there is so far no reliable way to experimentally determine equilibrium CO_2 uptake in a polymer in dependence of pressure and temperature. (Di Maio and Kiran 2017)

It is assumed that cell growth is stopped by the increasing viscosity of the polymer. Viscosity, glass and melt transitions are experimentally difficult to access within this process. The same applies to CO_2 concentration. (Di Maio and Kiran 2017) Furthermore, the process cannot be well observed in detail due to the high depressurisation rates of up to 100 MPa s^{-1}. As a result, little is known about these events in detail.

The most successful process for setting records in terms of cell size and porosity in nanocellular polymer foams is a batch foaming process also referred to as solid state foaming. Industrially preferential, however, would be a continuous and up-scalable process such as extrusion foaming or injection molding process. The potential and limitations of these two processes will be discussed in the following section.

2.2.3.1 Batch foaming

One of the most promising foaming techniques to reach low cell sizes is the gas dissolution batch foaming process employing CO_2. This is often referred to as solid state foaming.(Stéphane Costeux 2014) The designation “Solid State Foaming” refers to the fact that due to the proximity to T_g, a solid polymer is foamed rather than a polymer melt.(Miller, Chatchaisucha, and Kumar 2009) This process has delivered record beating foams with regards to producing low cell size and low density, but due to its low production throughput it is mainly used in academic research.(Di Maio and Kiran 2017)

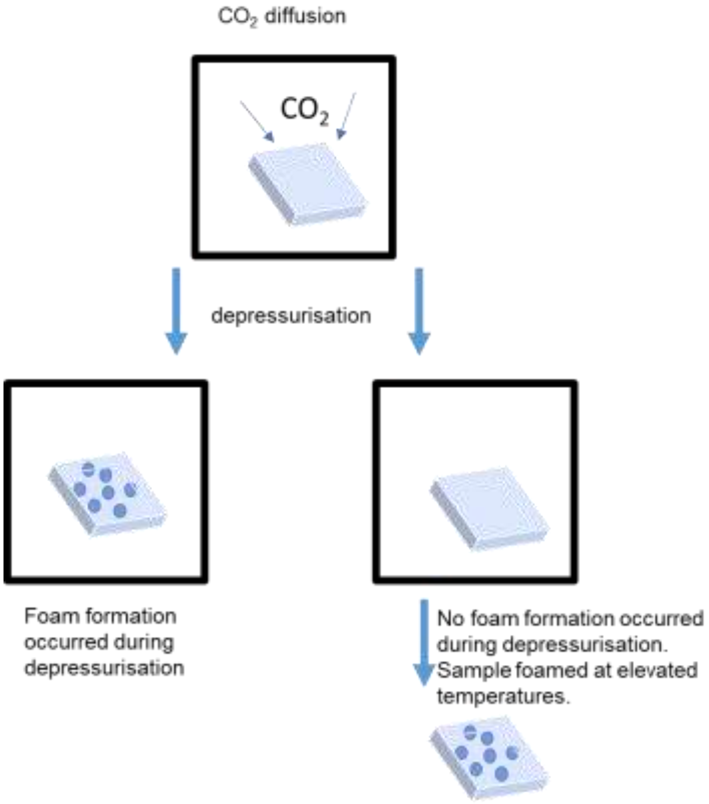

Figure 6: Left: One-step CO_2-assisted batch foaming process. Right: two-step-CO_2 assisted batch foaming process. (Di Maio and Kiran 2017)

In this process (Figure 6) a gas (usually CO_2) is dissolved in the polymer under high pressures and at low temperatures.[1] Once a sufficient gas concentration is reached[2], the pressure is released and the gas is desorbed from the polymer. This triggers nucleation and can also lead to void growth (one-step process) in particular for high saturation pressures. However, it is also possible that the void growth process has to be initiated by an increase in temperature to provide for expansion by bringing the sample above its T_g (two-step process).(Di Maio and Kiran 2017), (Stéphane Costeux 2014)

---

[1] For nanocellular foams pressures vary between ca. 1 and 100 MPa and temperatures between –5 °C and 32 °C.

[2] One of the problems with CO_2-assisted foaming is that the final gas uptake is unknown since it is difficult to measure.

If the polymer is below T_g at depressurisation the nuclei may remain unexpanded and it the polymer appears transparent from the autoclave. (Stéphane Costeux 2014) A second expansion step during which the polymer is dipped in a warm water bath to bring it above T_g and allow for nuclei expansion into foam voids. (Notario, Pinto, and Rodriguez-Perez 2016a)

This is the difference between a one-step and a two-step process. If the gas-polymer mixture is sufficiently rubbery, the nuclei expand during the pressure release (one step process).

As many polymer CO_2 systems lie in the metastable region between the spinodal and the bimodal (see 2.1), nucleation is usually assumed to be the phase separation mechanism in solid state foaming.(Stéphane Costeux 2014) But for high CO_2 concentrations and high foaming temperatures, bi-continuous structures have been observed in solid-state foaming processes and have been linked to potential spinodal decomposition. (H. Guo 2015)

2.2.3.2 Extrusion foaming

The industrially preferred process for foam production is extrusion foaming. Other than batch foaming it is a continuous and up-scalable process.

For extrusion foaming, the molten polymer is mixed with CO_2 by a screw and pushed towards the die. Due to the small diameter of the die, pressure builds up and the polymer-CO_2 mixture experiences a pressure drop upon exiting the die.(Di Maio and Kiran 2017)

One of the difficulties in extrusion foaming is to achieve the right rheological state that allows for nuclei expansion before the CO_2 is lost. But the polymer needs to be in a melted state, which requires a high melting temperature (ca. 180 °C for amorphous polymers like PS and PMMA). This limits the CO_2 solubility to below 15 w/w%, which limits homogenous mixing as well as nucleation.(Stéphane Costeux and Foether 2015) Furthermore, traditional extruders have a limitation in CO_2 intake due to pressure limits of the barrel as well as a time limit due to the continuity of the process.

One approach to achieve a better solubility of the CO_2 before foaming is to freeze the outer layers by lowering the temperature in the die. (Di Maio and Kiran 2017)

The best achievements have so far been seen in nanofoams with a cell size of around 300 nm.(Stéphane Costeux and Foether 2015) Therefore, the state-of-the-art process to achieve small cell sizes so far remains the batch foaming process.

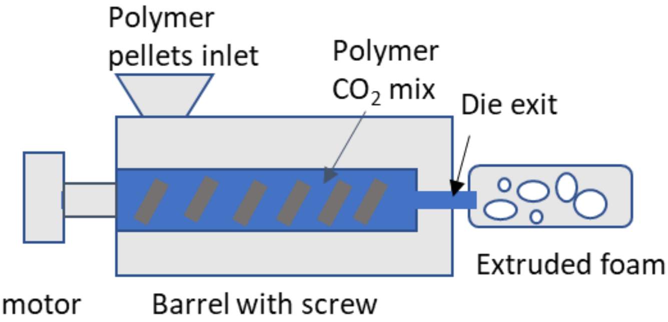

Figure 7: foam extrusion process. (Di Maio and Kiran 2017)

2.3 Influence of the polymer stress state on polymer foaming

2.3.1 Representation of a stress state

A stress state in a cubic piece of material can be described by nine components (Young and Lovell 2011):

$$\sigma = \begin{pmatrix} \sigma_{11} & \sigma_{12} & \sigma_{13} \\ \sigma_{21} & \sigma_{22} & \sigma_{21} \\ \sigma_{31} & \sigma_{32} & \sigma_{33} \end{pmatrix} \tag{14}$$

Here the first subscript identifies the normal to the plane on which the stress acts, and the second subscript defines the direction of the stress. Therefore, the diagonal elements represent normal stresses whilst the off-diagonal elements represent shear stress components. The stress tensor can be separated in two components

("DoITPoMS - TLP Library Stress Analysis and Mohr's Circle - Representing Stress as a Tensor"):

$$\sigma = \begin{pmatrix} \sigma_H & 0 & 0 \\ 0 & \sigma_H & 0 \\ 0 & 0 & \sigma_H \end{pmatrix} + \begin{pmatrix} \sigma_{11} - \sigma_H & \sigma_{12} & \sigma_{13} \\ \sigma_{21} & \sigma_{22} - \sigma_H & \sigma_{21} \\ \sigma_{31} & \sigma_{32} & \sigma_{33} - \sigma_H \end{pmatrix} \tag{15}$$

The volumetric changes a stress causes are represented by the hydrostatic component σ_H defined as the average of the normal stresses:

$$\sigma_H = \frac{1}{3}(\sigma_{11} + \sigma_{22} + \sigma_{33}) \tag{16}$$

Whereas the shape change is represented by the deviatoric stress tensor σ_D.

$$\sigma_D = \begin{pmatrix} \sigma_{11} - \sigma_H & \sigma_{12} & \sigma_{13} \\ \sigma_{21} & \sigma_{22} - \sigma_H & \sigma_{21} \\ \sigma_{31} & \sigma_{32} & \sigma_{33} - \sigma_H \end{pmatrix} \tag{17}$$

2.3.2 Role of hydrostatic tension on nuclei development

The previously discussed classical nucleation theory changes if one assumes stresses do play a role for nucleation since the hydrostatic contribution of the stress would change the polymer volume and potentially contribute to nuclei expansion. Therefore, volume and pressure (stress) cannot be considered independently and the integral term in equation 8 has to be taken into account.

The integral was derived to be close to zero (see appendix A.6). Therefore, the free energy turns out to be dependent on the pressure difference ΔP inside and outside of the nuclei. For a polymer-solvent system in which the solvent is a liquid, this difference is zero in equilibrium. But if a stress state develops, a hydrostatic tension can be assumed to provide for an effective expansive stress p_H.

$$\Delta \mathrm{G}(\mathrm{R}) = -n(R) * (\mu_{old} - \mu_{new}) - \frac{4\pi}{3} R^3 p_H + 4\pi R^2 \gamma \tag{18}$$

CNT is a stability argument for nuclei. When (effective) hydrostatic tension is taken into account, it predicts that more stable (post-critical) nuclei could arise with increasing hydrostatic tension.

Technically hydrostatic tension arises in the polymer matrix. CNT does not take into account viscoelastic properties that would represent hydrostatic tension explicitly.

The direct influence of hydrostatic tension within the polymer matrix would probably also have to be described in a nuclei growth concept that explicitly takes viscoelasticity into account. This is also important from the point of view that a stable nucleus is not necessarily an foamable nucleus within the foaming conditions. (Merritt and Weinhaus 1978)

2.3.3 Studies on the influence of stress state in polymer foaming

The influence of stress in polymer foaming has been discussed in several studies., but mostly in terms of a shear stress contribution in extrusion foaming. The discussions about the potential influence of hydrostatic tensions in batch foaming focus mostly on void formation in the polymer in the sense of crazing.(Holl et al. 1999b)

2.3.3.1 Influence of shear stress

Stress as a property that is important in polymer foaming is mostly discussed in terms of shear stress in extrusion foaming. A number of reviews of this topic can be found in: (Favelukis, Tadmor, and Semiat 1999) and (M. . Guo and Peng 2003).

The effect of shear stress on nucleation was first described by Lee and Biesenberger. They described the effect of shear stress based on a cavity model, which had been introduced by Harvey et al. to describe nucleation in blood vessels.(Harvey et al. 1944) They then experimentally found that at low solvent levels, additional shear is necessary to introduce nucleation. (S. T. Lee and Biesenberger 1989) Chen et al. experimentally found that an increase in shear stress leads to an increase in nucleation density.(Chen et al. 2002)

Lee proposed that shear force highly contributes to reduce the free energy barrier for the case of extrusion foaming. This hypothesis is based on the assumption of heterogenous nucleation from a clump of nucleating agent that leaves cavities from which the gas bubbles grow. It is suggested that the shear force helps to pull out the bubble from the cavity. (S.-T. Lee 1994)

For the homogenous case, Favelukis et al. developed a cell stretch model to explain the influence of shear on homogenous nucleation in the case of a Newtonian fluid.(Favelukis, Tadmor, and Semiat 1999)

This model was further expanded by Chen et al. for foam extrusion from PS and CO_2. (Chen et al. 2002) They argued that shear causes the nuclei to stretch. They made the assumption that because of the energy donation that increases the surface area, a stretched nucleus would have the same potential to grow like a spherical nucleus with a radius of half the length of the stretched nucleus. And therefore, an originally smaller but streched nucleus has the same potential to grow as a bigger spherical nucleus.

This can only be assumed if the shear keeps the nuclei stretched, because the surface to volume ratio of a stretched cell is energetically less favourable than that of a spherical nucleus. Unless the nuclei are kept stretched, they would relax back into a spherical state.

Since shear stresses are inserted when the polymer is pushed through the die and cells immediately expanded, this might be a relevant model for extrusion foaming. Furthermore, Guo et al. developed a theoretical model to explain how the increase of screw speed leads to an increase of shear energy which leads to an increase in nucleation density.(M. . Guo and Peng 2003)

Cell stretch models that account for shear stress only explain the impact of permanent stress on nucleation. The question remains what occurs for an elastic stress event.

2.3.3.2 Influence of hydrostatic stress

In addition to the cavitation model Albalak at el. suggested that tensile stresses lead to a local increase of ΔP (which they refer to as superheat) and therefore a decrease of the free energy barrier and an increase in nucleation rate.(Albalak, Tadmor, and Talmon 1990)

This idea was further developed by Wong et al. in order to describe a positive effect of tensile stress on nucleation while compressive stress has the opposite effect.(Leung et al. 2012; Wang, Zhao, Yu, et al. 2017)

Wang et al. further developed the idea of tensile stresses and differentiated between the influence of deviatoric and hydrostatic components of stress and implemented this into nucleation theory.(Wang, Zhao, Yu, et al. 2017) They researched the influence of uniaxial stress and compression during batch foaming of thermoplastic polyurethane and CO_2. In the case of uniaxial tensile stress, the stress was applied throughout the absorption and desorption process, whereas the compressive stress was applied via a hot compression machine after depressurisation. In both cases they observed an increase in cell nucleation density. This is unexpected for the compression and is contradictory to the results presented later in this thesis (see section 6.6). They concluded that in the case of uniaxial stress, the distortional as well as dilatational stress contribute to a decrease of the energy barrier. They argue that in the case of compression the dilatational stress component increases the free energy barrier, but the distortional contribution is high enough to achieve an increase in nucleation density. (Wang, Zhao, Mark, et al. 2017) Another explanation for the observation of expansion despite the theoretic expectation that compressive stress should suppress nucleation, could be based on the results in chapter 7 of this thesis, that indicate that a temperature increase leads to stress-induced nucleation. Therefore, the here cited observed increase in nucleation density might be based on the temperature increase induced by the hot compression machine.

Handa and Zhang also found that compressive stress increases the cell nucleation density in the case of a two-step batch foaming process from PMMA and CO_2. They applied pressure of magnitudes between 2 and 50 MPa to slowly depressurized PMMA, that had previously been in equilibrium with CO_2. They found faster foaming and lower density foams can be achieved with increasing pressure. This seems to contradict the hypothesis that hydrostatic tensile stresses increase the nucleation density. However, they also argue that the applied pressure forces a higher amount of CO_2 into the polymer, which then leads to a higher supersaturation and a faster and better foamability. The effect is limited above pressures of 35 MPa. No explanation is given for this limitation. (Handa and Zhang 2000) It seems likely that at these pressures nucleation is destroyed.

Furthermore, Elder et al. studied nanovoid nucleation dynamics with the help of MD simulations employing a sampling method that makes the timescales of nucleation events accessible with MD simulations. They found that the nanovoid nucleation rate in dicyclopentadiene (DCPD) is highly dependent on hydrostatic tension. (Elder et al. 2018)

Holl et al. addressed the issue in how far hydrostatic tension resulting from depressurisation could lead to crack formation. They suggested that hydrostatic tension resulting from depressurisation combined with a decrease in mixture strength leads to cracks resulting from fracture in the polymer matrix.(Holl et al. 1999a) For a batch foaming process with polycarbonate and CO_2 they showed that cracks develop in particular for higher foaming temperatures. They concluded that because of the decrease of mixture strength with higher temperatures the hydrostatic tension increases and therefore more cracks are observed.

Adams and Kweeder suggested that nucleation occurs heterogeneously at defects in the polymer. These defects are an artefact of the polymer production process. (Adams, Balyuzi, and Burge 1978), (Holl et al. 1999a), (Ramesh, Rasmussen, and Campbell 1994). Ramesh et al. followed this hypothesis and developed a cell growth model based on the heterogenous nucleation within a rubber particle taking into account stresses. They suggest that the pre-existing voids need to have a critical size.(Ramesh, Rasmussen, and Campbell 1994)

All of these studies reveal that the polymer response to stresses in the course of the foaming process and its influence on nucleation is an important parameter for nucleation, which has not been fully understood to date. To our best knowledge there is no study which experimentally examines the stress response in the polymer during desorption and to the temperature changes that are associated with depressurisation and its potential contribution to nuclei development.

2.4 Polymer foam characteristics

A foam is usually characterized by its porosity ϕ and average cell size with radius r. Another parameter is the nucleation density ND (see equations (19) and (20)). It is deduced from the total amount of foamed cells per unfoamed polymer volume $V_{polymer}$. This neglects any coalesced voids.(Stéphane Costeux 2014)

$$\phi = 1 - \frac{V_{polymer}}{V_{foam}} \tag{19}$$

$$ND = \frac{6 * 10^{12} * \phi}{\pi r^3 (1-\phi)} \frac{1}{cm^3} \tag{20}$$

A notable difference for polymeric foams in general is that between closed and open cell structures (see Figure 8). Closed cell foams are more interesting for thermal insulation as the cells block the heat flow. Open cells allow for a flow of e.g. nutrients and are therefore more interesting for tissue engineering. (Di Maio and Kiran 2017)

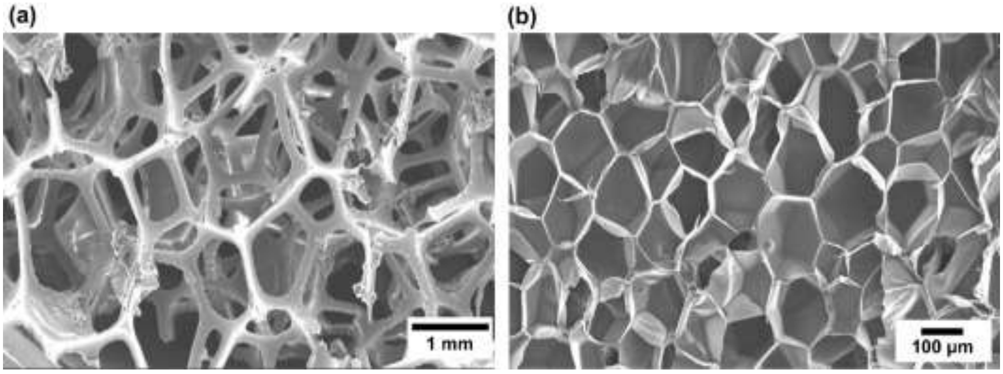

Figure 8: a) open cell polymer foam; b) closed cell polymer foam. Images taken from: (Okolieocha et al. 2015)

For polymer foam production mainly three types of polymer are used; composites, amorphous or semi-crystalline single-phase polymers. Composites are usually specifically designed to increase nucleation density e.g. by increasing the CO_2 content in parts of the polymer to facilitate nucleation there. In general, it is an option to optimize materials for nuclei development by adding nucleating particles such as silica or clay particles to enhance nucleation. Semi-crystallinity is problematic as it adds the crystal phase as an additional parameter that needs to be controlled. (Stéphane Costeux 2014), (Bernardo et al. 2017) Otherwise crystal structures can lead to inhomogeneities within the foam.

2.5 Benefits of nanocellular polymer foams and industrial aims

For microcellular foams, it has been proven that mechanical properties in terms of tensile strength and impact properties can improve compared to conventional foams. Therefore it is expected that nanocellular foams will possess even better mechanical properties.(Notario, Pinto, and Rodriguez-Perez 2016b)

It is also expected that the thermal conductivity in nanofoams decreases by a factor of 2-3 compared to conventional foams below a cell size of around 70 nm.(Martín-de León, Bernardo, and Rodríguez-Pérez 2019) The decrease in thermal conductivity with decrease in cell size to the nanoscale is attributed to the Knudsen effect, which states that thermal conductivity decreases once the cell size is smaller than the mean free path of the gas molecules (70 nm for air at room temperature), because the gas molecules are then rather colliding with the pore walls than with each other and therefore energy transfer is reduced.(Notario et al. 2015)

Below 40 nm foams it has been proven by León et al. that PMMA foams become semi-transparent. In addition to their low thermal conductivity, this makes nanofoams a very attractive insulation material for building applications.(Martín-de León, Bernardo, and Rodríguez-Pérez 2017)

Aside from the anticipated properties above, it is also expected that the confinement of the polymer on the nanoscale will further enhance properties regarding filtration, sensing and catalysis.(Notario, Pinto, and Rodriguez-Perez 2016a) Therefore, it is of great industrial interest to be able to reach a significant decrease in cell size (Notario, Pinto, and Rodriguez-Perez 2016a)

To achieve these properties, it is not only important to decrease the cell size, but also to reach a high level of porosity of about 80%, which means a nucleation density around 10^{17} nuclei/cm^3 is required to reach a cell size of 70 nm (see Figure 9). (Stéphane Costeux 2014)

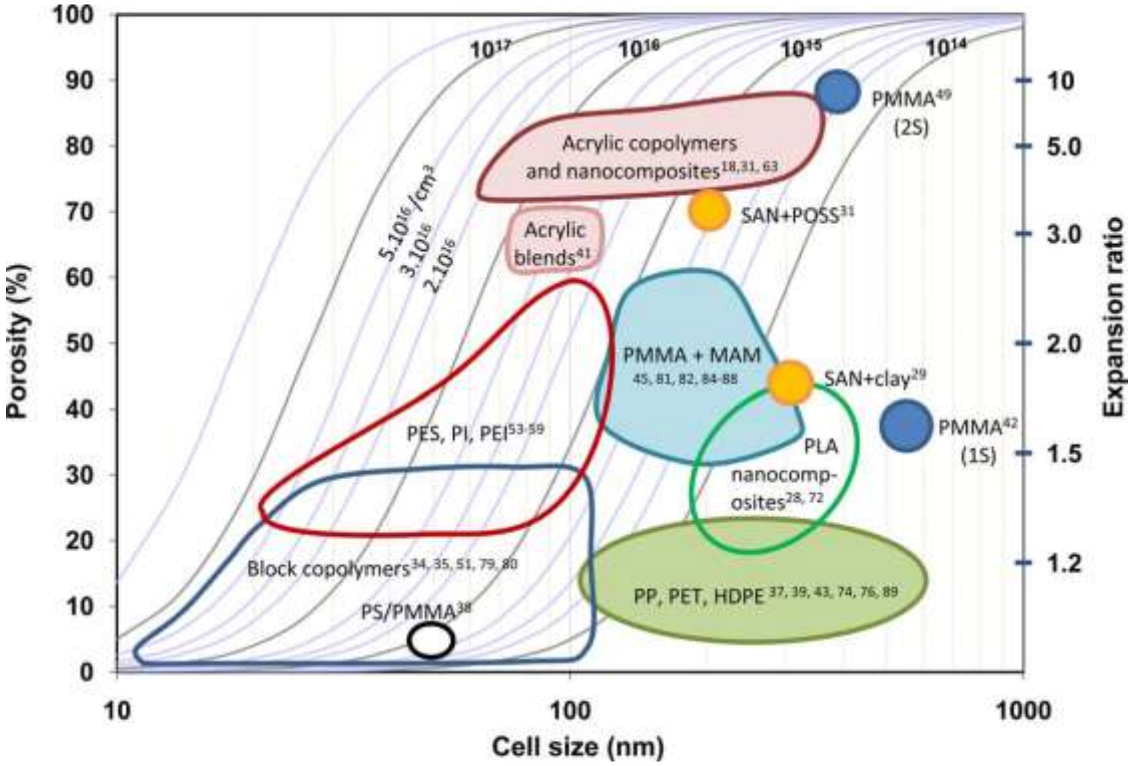

Figure 9: The interdependencies cell size, porosity and cell nucleation density (sinusoidal lines). For high porosities and small cell sizes, a high number of nuclei have to be generated. (Stéphane Costeux 2014)

Regarding a potential lower limit to the decrease of cell size, it was found by van Loock et al. that the minimum reachable cell size is probably dependent on the molecular weight of the polymer in terms of the wall thickness, which needs to be on the scale of the entanglement length of the polymer to prevent collapse of the foam cell. (Van Loock et al. 2019)

3. Materials and methods

3.1 Materials

3.1.1 PMMA characterization

Clear-cast Perspex® PMMA sheet with width of 2 mm from Lucite International was acquired and laser cut into the sizes of either 2×20×20 mm^3 pieces or 2×20×140 mm^3 strips. All samples were annealed at 120 °C to decrease the water content of ca. 1 w/w% right before methanol absorption.

Unfortunately, the number of samples needed for experiments was underestimated, because the demand for strips for tensile testing and liquid nitrogen quenching led to an unforeseen sevenfold demand of sample area needed (strip 140 × 20 × 2 mm^3 compared to square 20 × 20 × 2 mm^3). Therefore, the samples employed, were from two different batches 1 and 2. Batch 1 has been exclusively employed for the foam characterization in chapters 4 and 8 as well as all birefringence and geometry characterization. All other foaming experiments that include tensile testing and liquid nitrogen quench are exclusively based on batch 2.

As will be discussed in chapter 0 there was a difference in cell size between foams from these two batches. Therefore, molecular weight analysis as well as TGA and DSC was performed on the two different batches to identify the reason for this difference.

3.1.1.1 Molecular weight analysis

Molecular weight analysis was conducted by the *Polymer Characterization Research Technology Platform* laboratory at the University of Warwick.

Gel Permeation Chromatography was employed to determine the molecular weight. Therefore, PMMA was dissolved in tetrahydrofuran. Two samples of each batch were measured. The column set used are rated up to 10 million g mol^{-1}.

Table 1: Molcular weights (number M_n and weight average M_w and dispersity **Đ**) of batch 1 and 2

Sample	M_n [g mol^{-1}]	M_w [g mol^{-1}]	Đ
Batch 1	420,000	1,961,000	4.67
Batch 1	425,000	1,976,000	4.65
Batch 2 **Peak 1**	573,000	1,915,000	3.34
Batch 2 **Peak 1**	582,000	1,908,000	3.26
Batch 2 **Peak 2**	7,000	23,000	3.28
Batch 2 **Peak 2**	8,000	24,000	2.98

The molecular weight distribution of batch 2 exhibited a second distribution, which is very low and can most likely be neglected.

A difference in dispersity indicates that there is a difference in molecular weight distribution.

Batch 1 has a lower number average molecular weight by 155.000 g mol^{-1}. However, it has a higher weight average molecular weight by 57.000 g mol^{-1} compared to batch 2. That indicates as reflected in the dispersity there is a bigger variation in chain length and potentially a higher fraction of longer chains. This might contribute to a higher viscosity in batch 1 and the observed difference in cell size. This issue is more closely discussed in section 4.5.

3.1.1.2 TGA analysis

TGA was conducted in order to evaluate potential differences in composition of the two PMMA batches such as differences in additives.(Gałka, Kowalonek, and Kaczmarek 2014) The weight loss rate of at least 5 samples of 5 mg from each batch was measured. For better data readability only two weight loss rate curves of batch 1 and 4 curves from batch 2 are depicted in Figure 10. The weight loss curves do not reveal any characteristic differences between samples of batch 1 and batch 2. Moreover, the weight loss behaviour varies quite significantly within the same batch. Which is very surprising given the assumption that macroscopically the PMMA samples should not be too different.

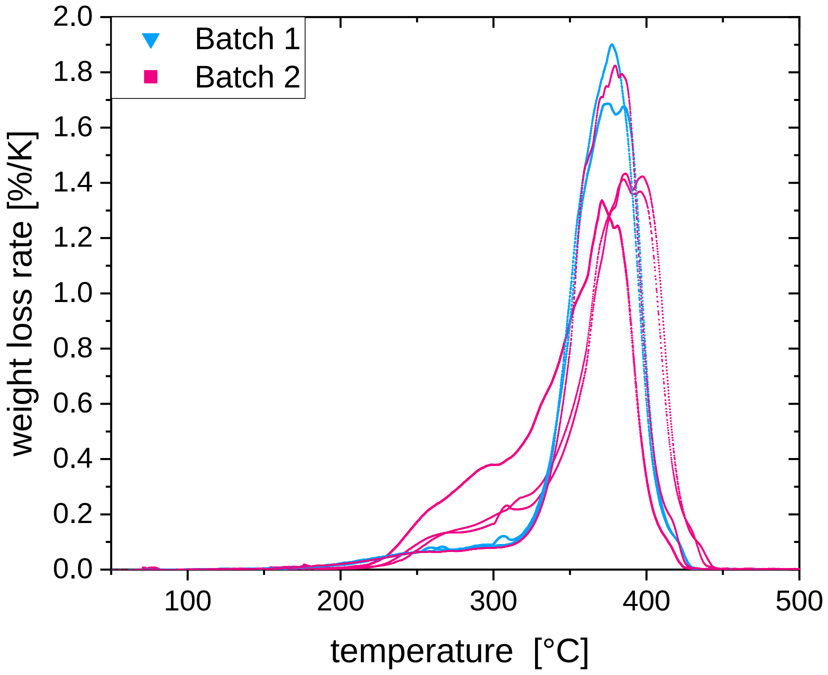

Figure 10: TGA analysis of the two different batches

These measurements have been repeated within 6 months with the same result that the decomposition behavior varies in between samples of the same batch.

The underlying reason for this is not fully understood. As reported in (Ferriol et al. 2003) and (Gałka, Kowalonek, and Kaczmarek 2014), changes in decomposition behavior can be attributed to either changes in molecular weight or additive composition. However, it is surprising that these effects occur on a macroscopic level as it would indicate heterogeneities on a macroscopic level. This is more plausible for additive agglomerations.

But as TGA does not reveal systematic differences in decomposition behaviour between the two batches, it does not reveal the root course for the systematic differences in foaming behavior between the batches.

3.1.1.3 DSC analysis

Dynamic Scanning Calorimetry (DSC) was performed on *TA Instruments Q500*. In order to determine T_g, two samples with sample size of 5 mg were scanned by two cycles with 10 K/min between 25 °C and 150 °C. The first cycle was for conditioning while T_g was determined from the second cycle.

The calorimetric response from both batches (batch 1: 118.0 °C, batch 2: 118.5 °C) is the same within the accuracy of glass transition determination with the DSC on the scale of several Kelvin.(Strobl 1997, p. 238) Therefore, the glass transition seems to be the same for both batches.

3.2 Further materials

3.2.1 Methanol

Methanol of HPCL grade was acquired from Fisher Scientific.

3.2.2 Silicone oil

Silicone oil with a temperature range -50 °C – 200 °C was acquired from Fisher Scientific.

3.3 Methods

3.3.1 Birefringence mesurements

Birefringence is a difference in refractive indices, Δn, that results from a change in polarization caused by the molecular order in an anisotropic material, such a polymer matrix. Depending how the molecular order is caused one differentiates between orientational and photoelastic stress birefringence.

Orientational birefringence is caused by permanent chain orientation, often induced during processing of the polymer above T_g, resulting in a frozen order in the polymer matrix below T_g. Orientational birefringence is usually irreversible below T_g.

In case of photoelastic birefringence, the orientation causing the change in polarization results from an elastic strain of up to 1% applied below the T_g of the polymer. It is reversible if the strain is released. (Shafiee et al. 2015)

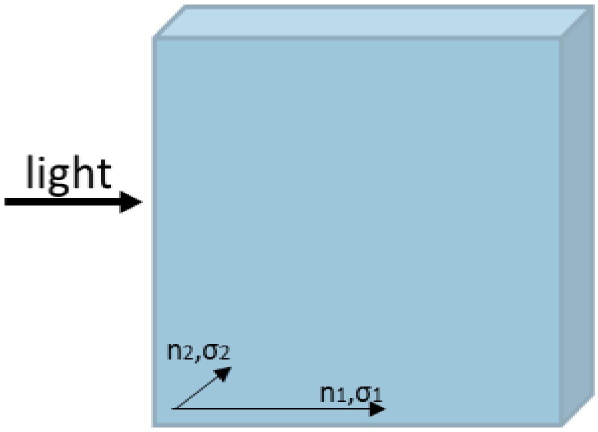

Figure 11: Incoming white light through the sample width. Refractive indices along the principal stress σ_1, σ_2 axis are changing in dependence of applied stress state.

In the case of photoelastic birefringence, the difference in indices of refraction changes linearly with the difference in principal stresses σ_1, σ_2 along the principal stress axis depending on the stress optical coefficient ς. For the case of plane strain, this leads to the expression:

$$\Delta n = n_2 - n_1 = \varsigma \cdot (\sigma_1 - \sigma_2) = \varsigma \cdot \Delta\sigma \qquad (21)$$

where $\Delta\sigma$ is the difference in principal stresses $\sigma_1 \geq \sigma_2$. The two optical axis with $n_1 < n_2$ are refered to as the “fast” and “slow” transmission axes, respectively.

If light enters a birefringent sample along the principal axis σ_1, it is transmitted with the two different indices of refraction n_1 and n_2 within the sample. For linearly polarized white light, this can be described by two perpendicular waves with different amplitudes propagating with different speeds. Depending on wavelength and sample thickness t, this leads to an accumulated retardation $\Delta\Gamma$ between the two waves.

$$\Delta\Gamma = t \cdot \frac{\Delta\lambda}{\lambda} = t \cdot \Delta n = t \cdot \varsigma \cdot \Delta\sigma \tag{22}$$

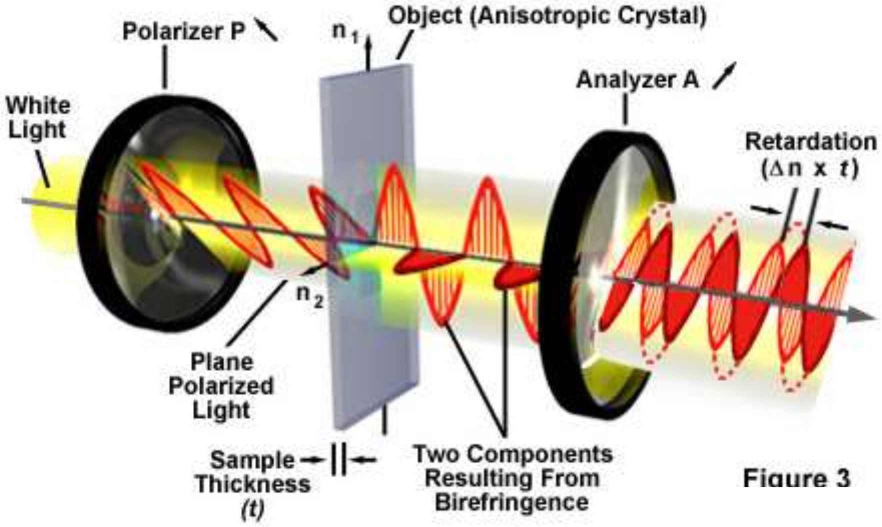

Figure 12: Depending on the thickness of the specimen, t, a retardation $\Delta\Gamma$ is accumulated between the light transmitted along the two principal axis which causes a change in polarization. Between crossed polars this results in different colours as components of polychromatic light polarized perpendicular to the analyzer are removed from the spectrum. (image from “Light and Color - Optical Birefringence | Olympus Life Science”)

The retardation causes a phase shift φ and therefore a change in polarization of the recombined rays. Between crossed polars the change in polarization leads to a change in colour of transmitted light (see Appendix). This can be measured in comparison to a sample of known retardation.

3.3.1.1 Birefringcence measurement with a quartz wedge

Since methanol desorbtion and birefringence changes significantly on the time scale of 60 s in the initial desorption stages, a method was needed with which birefringence measurements can be performed within a short time span. Most measurment methods employ a microsope and are based on compensation of the retardation. This makes them accurate, but time costly in preparation.

A quartz wedge is not a very accurate measurement tool to measure birefringence. But measurements can be taken very quickly (ca. 10 – 20 s). As compared to other techniques no microscope or complicated compensation techniques are needed. Therefore, a quartz wedge was chosen to quantify the birefringence and its accuracy was increased as described below.

A quartz wedge has a known gradient of retardation. If it is placed behind the specimen of interest between crossed polarizers, the sample retardation is then added and can be read out as the relative shift in retardation between the wedge and the sample.

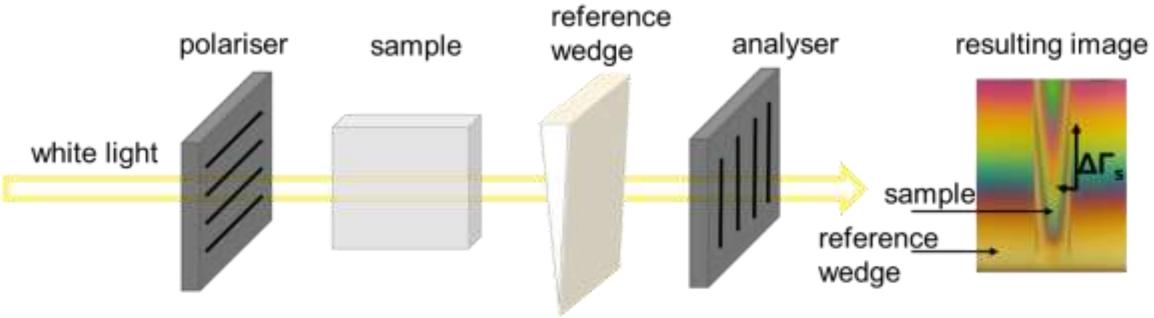

Figure 13: Measurement of birefringence with a quartz wedge between crossed polarizers. The incoming polarized light is retarded by the sample by $\Delta\Gamma$. This retardation is added to the retardation of the quartz wedge, which is dependent on its thickness. The sample retardation can be read out as the relative retardation between wedge and sample.

The sample retardation was measured along the 20 mm long sides of the samples. The faces through which retardation was measured had been polished with sand paper before methanol absorption. A picture of the sample retardation was taken in a light box in which the wedge was fixed. So that all pictures were taken at the same sample to camera distance and magnification. The camera employed was a Samsung S5 mobile phone camera (resolution: 16 MP, 5312x2933 pixels).

3.3.1.2 Increasing the accuracy of quartz wedge method

The usual accuracy for reading out retardation with a quartz plate is between 100 and 200 nm if retardation is read out on the Michael Levy chart. The inaccuracy is on such a large scale as the bands are quite broad and therefore retardation cannot be read out accurately based on eyesight.

Therefore, the retardation was not read out by eyesight, but the difference in RGB values was taken with the help of a python script[3] (see A.5). The Python code went through the following steps:

- Coarsening the image scaling down to a 10th of the image size using LANCZOS scaling method
- Normalizing the image for intensiy
- Taking the RGB values of a reference pixel on the quartz wedge.
- Search along the sample pixel by pixel horizontally until the RGB values match within a tolerance of 50 units in RGB space (values for each channel in RGB go from 0 to 255).
- Once the RGB values of each are all within a tolerance of 50 units of the reference pixel, the distance in pixels between this was taken as retardation (see **Error! Reference source not found.**).

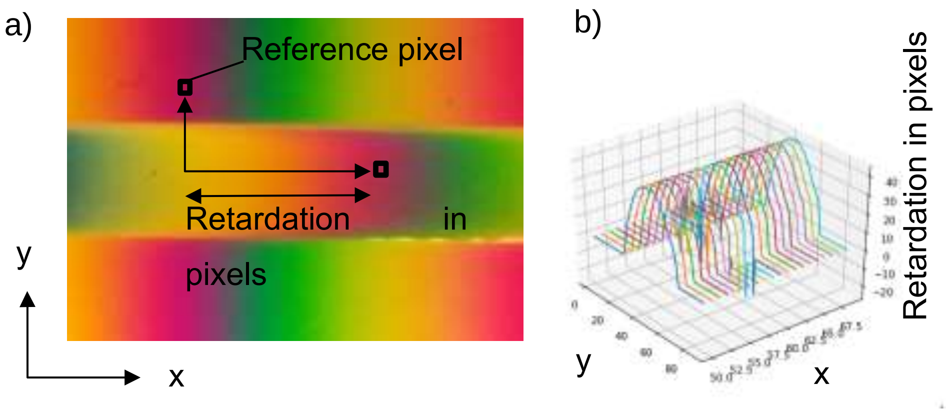

Figure 14: a) retardation of sample with reference to glass wegde and b) resulting distribution of retardation across the sample (right).

---

[3] The idea for reading out the retardation computationally based on RGB space was developed between Prof James Elliott and Angelika Beinert. Most of the coding for the Python script was developed by Dr Jerónimo Terrones with a contribution of Andrew Fowler.

The pixel to wavelength scale factor of the picture was calibrated with the help of the analysis module “Colour profiler” in ImageJ. With Colour profiler, the difference in pixels between minima of green light was measured to be 1515.5±10 pixels. The obtained value was taken from 5 pictures with 3 minima. So the value was taken from 10 distance measurements between minima. It is assumed that the minima of green light equal magenta which results from the retardation of 530 nm as verified with a full lambda waveplate. Therefore the scale factor for calculating the retardation from the distance in pixels, obtained from the python code is 10*530/1515.5 with an accuracy of 3.5 nm.

The accuracy of the entire measurement employing the script to read out the retardation was estimated by measuring the retardation of a λ/4 waveplate with a known retardation of 137 nm. The standard deviation of retardation of ten individual measurements of the retardation of the λ/4 waveplate was 20 nm. This is the total assumed accuracy of this technique taking into account repeatability of the measurement and accuracy of the retardation read-out. Therefore, the method itself is considerably more accurate than by eyesight.

The major influence on the accuracy of the measurement seems to be the temperature. Despite being stored in an incubator the samples are subject to temperature variations of a few Kelvin, which can have an effect on the stress development (see section 8.1). The error on the birefringence of methanol desorbing samples is therefore higher. The scattering for desorption at 25 °C suggests that the accuracy is within ca. 160 nm. Major other influences on the retardation measurements are the variation in sample sizes which will lead to slightly different stress distributions.

3.3.1.3 Choice of stress optical coefficient

The molecular causes of anisotropy in polymers that cause elastic birefringence have been originally described by Kuhn and Gruen based on polymer chain segment statistics. The anisotropy can also be influenced by solvents as they influence the rigidity of the polymer chains.(Kuhn and Grün 1942), (Student 2007) Which is why in the case of PMMA and methanol different stress optical coefficients are reported depending on methanol sorption state. Similarly, the temperature influences the resulting anisotropy.(N. Thomas 1978)

Values between $4\cdot10^{-12}$ m^2 N^{-1} for pure PMMA and $8\cdot10^{-12}$ m^2 N^{-1} for fully methanol swollen PMMA have been reported.(N. Thomas 1978) The exact dependence of the stress optical coefficient on desorbing methanol content has not been found in literature. A linear dependence from methanol concentration was assumed since it had been found that elastic properties in terms of Young's modulus change linearly with methanol content (see 6.2).

In order to measure the concentration dependent stress optical coefficient it would be necessary to measure the birefringence in dependence of applied stress for different concentrations and correct for the desorption induced birefringence. This is a problem in the light of the high scattering of birefringence data (see Figure 31). Furthermore, at higher methanol concentrations, concentration changes quite fast upon desorption and it would be difficult to obtain a meaningful tensile stress induced retardation measurement on a short time scale. Since the interest was predominantly on the stress development as a phenomenon not on the exact magnitudes, a closer determination of the stress optical coefficient has therefore not been undertaken.

3.3.2 Pore size analysis

X-ray-microtomography was performed with Bruker SkyScan 1176. With this technique cross sections of a material acquired by x-ray scans are joint to a 3 D model. The pixel size is here on the micronscale. In this particular case scans were acquired with a pixel size of 3 µm, at an operating voltage of 45 kV and 0.2° step size. From the resulting projections 1000 layers were reconstructed with Bruker NRecon v. 1.6.10.2. The average pore diameter was obtained from every 100th layer. In total an average was taken from 3000-10,000 pores depending on cell size. For this analysis ImageJ 2.0.0-rc-671/1.52g was employed. For this the images were first binarized (see Figure 15) with "trainable Weka Segmentation V3.2.27", which is a plugin of Image J and processed with "Analyze particles" after pre-processing the image with despeckling, outlier removal, and completing broken strut lines with a watershed algorithm.

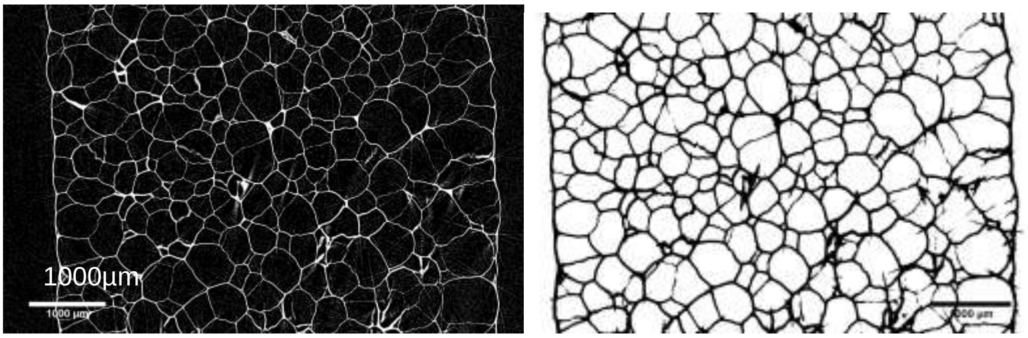

Figure 15: Left: MicroCT image crossection of a foam. Right: Binarized image.

Since the pore size analysis is only conducted in 2D, not the exact diameter of pores will be measured, but it will be underestimated, since in the majority of cases the layer does not represent the equator of a cell, but slices above or below it. There are ways to correct for this.(YH and HC 2003) However, they are relatively time consuming, since several correction factors have to be calculated. Since this study is only interested in trends in cell size changes no correction was performed.

3.3.3 Porosity determination

Porosity is determined from the polymer $V_{polymer}$ and foam volume V_{foam} as follows:

$$p = 1 - \frac{V_{polymer}}{V_{foam}} \tag{23}$$

The volumes were measured with the help of a caliper by obtaining 5 measurements of thickness, one from each corner and on from the middle and one measurement for each of the side lengths.

Since the foams are not fully even and have some variations in thickness, they contribute mostly to the inaccuracy of the measurements. Therefore, the accuracy also depends on the foaming temperature as will be seen in section 4.3.1. Therefore, the accuracy on porosity is determined from the standard deviations of foams foamed at the same foaming temperature.

3.3.4 Nucleation density and definitions regarding nuclei development

Nucleation density per cm^3 from cell with an average diameter of d in µm and porosity p can be determined as follows:

$$ND = \frac{6 \times 10^{12} p}{\pi d^3 (1 - p)} \qquad (24)$$

It should be noted that nucleation density in this case refers to nuclei resulting in a foam cell. The real nucleation density is potentially higher.

During the course of carrying out the work for this thesis, a difference between nucleus states was identified. The following definitions were assigned:

- **Post-critical nucleus:** nucleus in a post-critical state according to classical nucleation theory (see 2.1.4.1). This means the free energy barrier is overcome and a stable nucleus is developed. This nucleus is not necessarily in a foamable state, which means it cannot be expanded into a foam cell by the available foaming conditions (in this case expansive force resulting from the evaporating methanol in the oil bath at a chosen foaming temperature).
- **Foamable nucleus:** a post-critical nucleus that is in a foamable state, which means it is big enough to be expanded to a foam cell by the available foaming conditions. It is hypothesized in section 6.7 that post-critical nuclei are expanded into a foamable state by hydrostatic tensions that are either applied externally or develop within the polymer matrix due to desorption.

3.3.5 FE modelling

In order to obtain the hydrostatic component of the desorption-induced stress, the stress state of a methanol desorbing slab of PMMA was modelled by FE simulations using the software package COMSOL v. 5.3a Structural mechanics as well as heat transfer packages were employed. The model setup is described in chapter 9.

3.3.6 Analysis of glass transition temperature with DMA

The glass transition in samples with methanol content could not be determined with DSC due to the methanol weight change resulting from methanol loss. Therefore, DMA was employed for determination of the glass transition for samples containing methanol.

Dynamic mechanical analysis (DMA) was performed with a *TA instruments Q800*. 1.5×35×10 mm^3 samples were clamped in a dual cantilever sample holder. Measurements were taken at frequency of 1 Hz with a temperature rate of 4 K min^{-1} between 25 and 130 °C.

The glass transition is determined as the midpoint temperature between the intercepts of the tangents of the sections above and below the glass transition step of the storage modulus and an inflectional tangent to the glass transition step (see Figure 16). This method is further described in (Ehrenstein, Riedel, and Trawiel 2004).

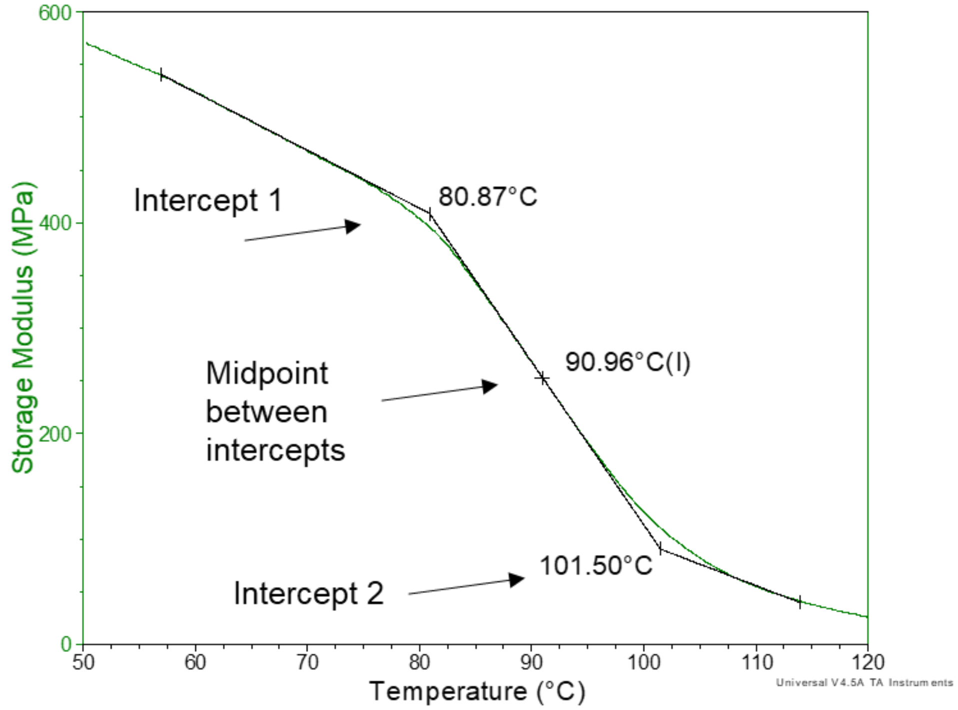

Figure 16: Determination of T_g from Storage Modulus.

3.3.7 Weight measurements

Sartorius SE2-F microbalance with tolerance of 0.001 mg was used to measure the methanol take up in PMMA. The methanol uptake was measured as weight fraction %w/w from the swollen weight w and the unswollen weight w_0 as follows:

$$\%\mathrm{w/w} = \frac{w - w_0}{w} \tag{25}$$

3.3.8 Geometry measurements

The widths of the sample were determined with a digital caliper (accuracy 0.01 mm). The thickness was determined with a digital thickness gauge (*Mitutoyo*, resolution 0.01 mm) separately in the middle as well as at each of the four corners.

The change in sample geometry (geometry t means width or thickness here) upon desorption was calculated either as:

1. The changes compared to the unswollen sample geometry $t_{\mathbf{0}}$, relative to the current geometry t:

$$\frac{t - t_{\mathbf{0}}}{t} \tag{26}$$

2. The changes compared to equilibrium swelling t_e, relative to the current sample geometry t:

$$\frac{t - t_{\boldsymbol{e}}}{t} \tag{27}$$

The changes in swelling geometry were therefore calculated relative to the current state. This is also in analogy to the convention of determining weight fraction.

3.3.9 Tensile testing

Tensile testing was performed on a *Tinius Olsen 5 ST* with a constant strain rate of 5 mm min^{-1}. Pressure is applied on the same machine via circular discs (d = 1 cm) at a constant rate of 1 mm min^{-1}.

3.4 Instruments

3.4.1 Laser Cutter

The laser cutter *Laserscript LS3060* was employed to cut the PMMA samples to size.

3.4.2 Silicone Oil bath

Two identical Silicone oil baths from *Büchi B-490* with a temperature range from 25 °C -180 °C were employed. The accuracy of the temperature is 3 °C.

3.4.3 Ovens

All of the absorption and desorption measurements were conducted in *Carbolite NR30F*.

All annealing was conducted in *MTI OV-DZF 6050*

3.4.4 Incubator

An incubator *Stuart Scientific 60D* of was used to keep the samples at 25 °C. The accuracy of the temperature is estimated to be around 2 K.

3.4.5 SEM

SEM samples were prepared by freeze-fracturing them in liquid Nitrogen and cutting them open with a side cutter. A similar method is described in (Song and Torkelson 1994). Afterwards they were coated with Palladium.

SEM micrographs were obtained from *FEI Nova NanoSEM FEG*.

4. Foam formation from PMMA and methanol

In order to get a better insight in nanofoam development, which is experimentally difficult to access within the solid-state foaming process, a similar, but experimentally more accessible foaming process was developed with PMMA and methanol. The process, which was partly derived from early-stage experiments with polystyrene (PS) and acetone is briefly described in the first section of this chapter.

The resulting model foam process from methanol and PMMA is then described and the foam is characterized.

4.1 Method development

The idea for the foaming process from PMMA and methanol is partly based on observations from early stage freeze drying experiments conducted with polystyrene and acetone as well as PMMA and methanol. The idea behind the freeze-drying experiments was to sublimate the solvent out in order to achieve a porous structure resulting from the sublimated solvent. The problem with this idea was, to find access to a local and frequently usable freeze dryer that would go below the freezing point of methanol (–98 °C) or acetone (–95 °C).

But the observations from these early stage experiments led to the idea for manufacturing a foam based on temperature induced phase separation (TIPS).(Matsuyama, Berghmans, and Lloyd 1998)

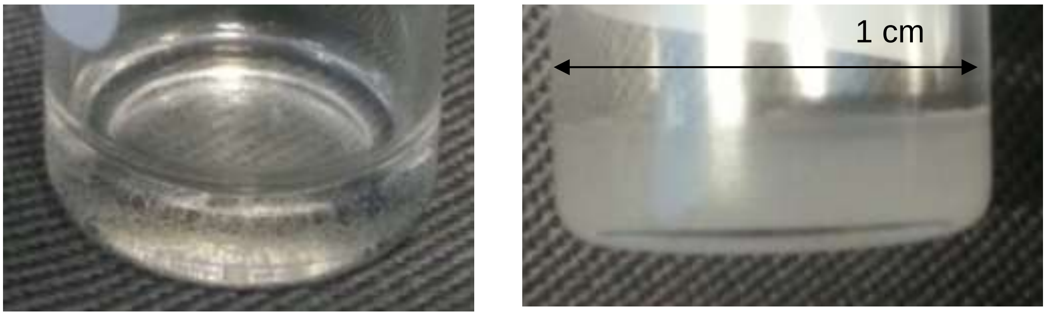

Figure 17: swollen PS sample before (left) and after (right) acetone evaporation.

It could be very well observed in PS (granules or also plates) and acetone that after being fully mixed and taken out of acetone, the mixture becomes opaque (see Figure 17). This means phase separation occurred and a porous structure developed. If the mixture is additionally dipped into liquid nitrogen it also becomes untransparent and white. The opaqueness and whitening was assumed to result from nucleation and void development, which could be confirmed by SEM images (see Figure 18). The whitening after a liquid nitrogen quench was interpreted to result from a greater amount of nuclei development.

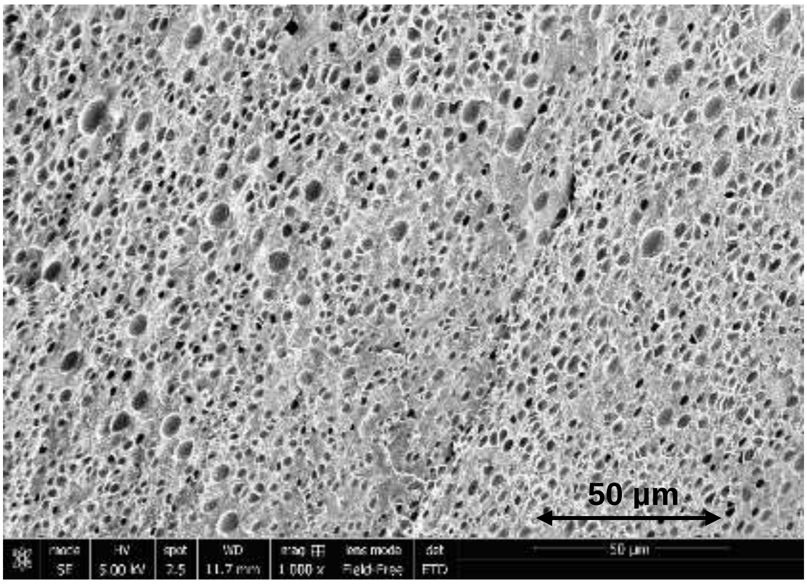

Figure 18: SEM image of voids within a LN quenched PC and Acetone mixture.

Since acetone swells PS by around 70 w/w% it is difficult to handle the highly viscous material. Methanol only swells PMMA by ca. 20 w/w%, but no nucleation event could be observed after taking the equilibrated methanol charged PMMA out of methanol in the sense of developing opaqueness or void formation in SEM images. The reason is most likely that the nuclei are far too small or too few to be observable.

Since a liquid nitrogen quench seemed to increase the amount of nuclei, the methanol charged PMMA was put into liquid nitrogen in the hope of achieving phase separation in PMMA and methanol resulting from the larger drop in temperature.

And indeed, after the liquid nitrogen quench bubble formation could be observed (see Figure 19) when the sample was put in a silicone oil bath at 170 °C post-quench compared to an unquenched sample. It has to be noted that most of these experiments were performed with extruded PMMA (Perspex®, extruded acrylic), which has presumably a lower molecular weight. The impact of the liquid nitrogen quench is less pronounced with higher molecular weight cast material.

Figure 19: Left: foam formation of fully methanol charged extruded PMMA after a liquid nitrogen quench and transfer to a 170 °C silicone oil bath. Right: foam formation of a fully methanol charged extruded material without a liquid nitrogen quench and transfer to a 170 °C silicone oil bath.

Initially, it was assumed that the liquid nitrogen (LN) quench had increased the nucleation density due to temperature induced phase separation. But later it was suspected that the quench might have contributed to a higher nucleation density because it induces stresses that facilitate nucleation. The influence of a liquid nitrogen quench on foam formation will be more closely discussed in chapter 7.

As stress development is also accompanying methanol desorption from PMMA (N. Thomas 1978), it was considered that desorption-induced stress development could also lead to post-critical nucleation. And indeed, methanol-desorbed samples resulted in a homogenous foam after foaming in a silicone oil bath above 150 °C (see 4.2). This way a foam formation process was developed that resembled the solid state foaming process and could be employed to study foam formation. It also appeared that the stress state development plays a larger role in it and could be a key parameter to gain a better understanding of foam development in this case.

Therefore, in order to gain a deeper knowledge about foam formation within PMMA and methanol and potentially beyond, at first the best foaming parameters for the methanol desorbed samples were looked for as described in chapter 4.

In a next step the qualitative and quantitative stress state development was characterised in chapter 5. In chapter 6 and 7 the impact of application of additional stress on foam development was investigated. In how far stress development depends on the desorption conditions was looked at in chapter 8 and in chapter 9 the magnitude of stress development is discussed with the help of FE modelling.

4.2 Method description

The developed standard method of creating a foam from PMMA and methanol consists of three steps. Methanol absorption into PMMA to equilibrium, desorption to below 8.5 w/w% remaining methanol content and expansion at 170 °C for 1 min in a silicone oil bath followed by stabilization at 115 °C for 8 min in another silicone oil bath. In this section the details of this procedure are more closely described. The parameter choice experiments leading to this standard procedure are discussed thereafter in the sections 4.3.1 and 4.3.2..

As can be seen in Figure 20, homogenous foam formation only becomes possible once the methanol concentration decreases below a value of 8.5 w/w% (closer analysis of onset of foamability in section 6.4). An attempt to understand the necessity for desorption will be made in chapter 5.

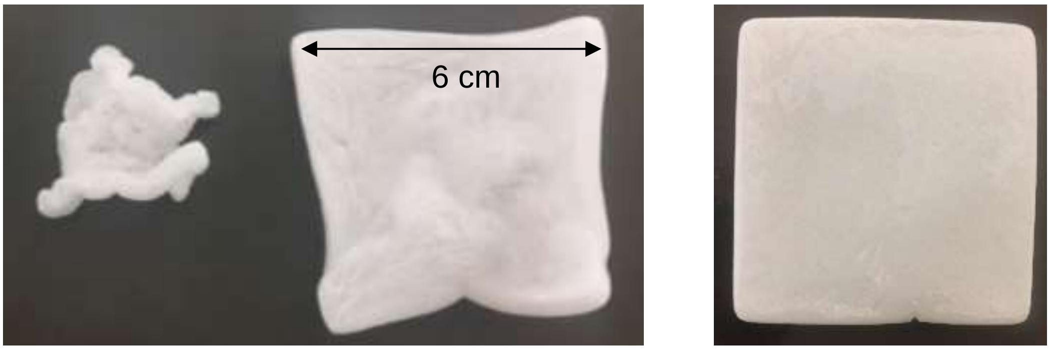

Figure 20: Foam formation after desorption to 10.3, 9.1, 8.0 w/w% methanol content (from left to right).

***Methanol absorption*:**

PMMA specimens were annealed for at least 72 hours at 120 °C in order to minimize the water content. After cooling down, the samples were weighted, their thickness and length measured and they were immediately put into individual glass jars containing methanol. Methanol was absorbed into PMMA in an incubator kept at 25 °C until an equilibrium concentration was reached at 18 ± 0.3 w/w% (batch 1) and 18.5 ± 0.3 w/w% (batch 2). Reaching equilibrium concentrations takes around 168 h. The error is resulting from weighing error, but also from slight temperature differences (see chapter 8)

It is important to mention that any pre-stresses in the PMMA are erased due to the nature of the Case II methanol absorption process.(N. . Thomas and Windle 1981)

***Methanol desorption*:**

Subsequently, the fully swollen PMMA was taken out of the jars, the surfaces cleaned of excess methanol and placed in a grid, so it was almost freestanding and left desorbing to below 8.5 w/w% remaining methanol concentration in an incubator at 25 °C. This remaining methanol concentration is reached within about 168 hours desorption time.

***Foaming*:**

The foaming process consists of two steps (see Figure 21). The first step is the actual foam formation in a silicon oil bath with a temperature T_1 for a time t_1 (for standard procedure: T_1 = 170 °C for t_1 = 1 min). The second step is a stabilizing step in a second silicone oil bath with a temperature T_2 for a time t_2 (standard procedure: T_2 = 115 °C for t_2 = 8 mins). The standard choice of temperatures and times in the oil baths will be discussed in section 4.3.

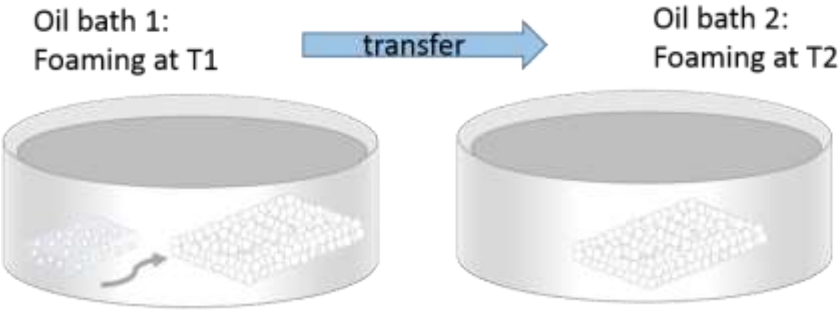

Figure 21: Foaming procedure: The methanol desorbing PMMA is inserted in a silicone oil bath with a temperature T_1 for a time t_1 (standard: 170 °C for 1 minute). Afterwards it is stabilized in a second silicone oil bath at temperature T_2 for time t_2 (standard: 115 °C for 8 minutes).

For the first step, the methanol desorbed PMMA is put into a silicone oil bath at T_1 for t_1. It is left sinking to the bottom of the oil bath in order to minimize contact with tweezers, which led to marks. This leads to direct contact with the silicone oil bath base for one side of the sample. Therefore, heat transfer should be slightly different for the sample face touching the base. But no inhomogeneity in cell sizes across the sample diameter could be observed (see Figure 22). Therefore, this method was continued to be employed.

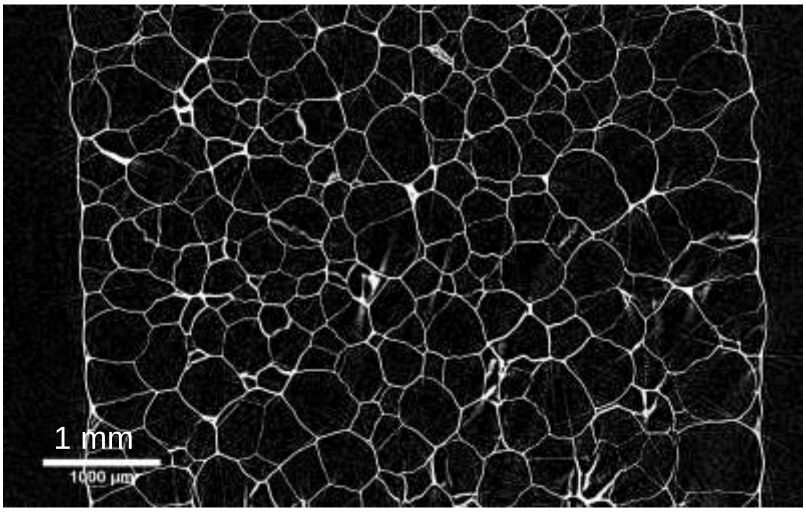

Figure 22: MicroCT image of a cross section of a typical foam resulting from the described procedure.

Once the first foam cells develop and therefore the foam sample density drops below the silicone density, the sample floats upwards and is kept within the silicone oil bath by a glass cylinder with a weight inside.

After T_1, t_1 the sample needs to be transferred to another silicone oil bath, in order to further decrease its methanol content. Otherwise it would desorb back into the cell walls if the sample was already taken out of the silicon oil bath. This leads to the breakdown of cell walls and subsequent sample deflation. On the other hand e.g. 170 °C proved too high to keep the sample desorbing at this temperature since it is high above T_g (118 °C) and would therefore also lead to sample shrinkage (see section 4.3.1).

Therefore, for the second desorption step, the foam is put into another silicone oil bath at $T_2 < T_1$ for $t_2 > t_1$ to decrease the remaining methanol content. In order to prevent floating on top of the silicone oil, the foam is held below the surface of the silicone oil by putting it in a glass cylinder with a weight inside. The foam will shrink a little in the stabilizing oil bath. Since the expanded state after the first oil bath is collapsing quite fast, it is difficult to exactly measure the amount of shrinkage in the second oil bath. However, based on the observed shrinkage of the sample dimensions in the oil bath, it was estimated that the sample shrinkage is around 20% in volume for 8 min desorption at 115 °C (standard).

The stabilizing techniques that are employed in CO_2-assisted foaming in which the expanded foams are immediately frozen in liquid nitrogen or ice water is not applicable in this process. The reason for this is that unlike the CO_2, methanol is not in a gas state and therefore stays as a liquid within the cells. Upon a liquid nitrogen quench the methanol freezes and shrinks since its thermal expansion coefficient is positive.(Dortmund Data Bank) This results in immediate sample shrinkage. In the case of ice water, methanol stays in a liquid state and also re-enters the cell walls, leading to shrinkage.

4.3 Choice of parameters and foam characterization

In order to understand the impact of the foaming temperatures T_1 and T_2 and times t_1 and t_2 and to choose standard process parameters, a study was conducted in which these parameters were varied.

4.3.1 Choice of foaming time t_1 and foaming temperature T_1

For the foaming time t_1, the time needed to fully expand the foam was chosen. This was in most cases ca. 60 s.

In order to understand the impact of foaming temperature T_1, it was varied between 150 and 180 °C. T_2, t_1 and t_2 were kept at their standard values (115 °C, 1 min and 8 min respectively, details on how T_2, t_2 were chosen see section 4.3.2) and foam properties determined. For each data point of foam properties resulting from these foams at least 3 samples were employed. The indicated errors are the standard deviation.

Figure 23 shows what foams formed at different foaming temperatures T_1 look like. Below T_1=150 °C the sample does not fully expand. The expanded state slightly decreases above T_1=180 °C. This is reflected in the porosity measurement (see Figure 24).

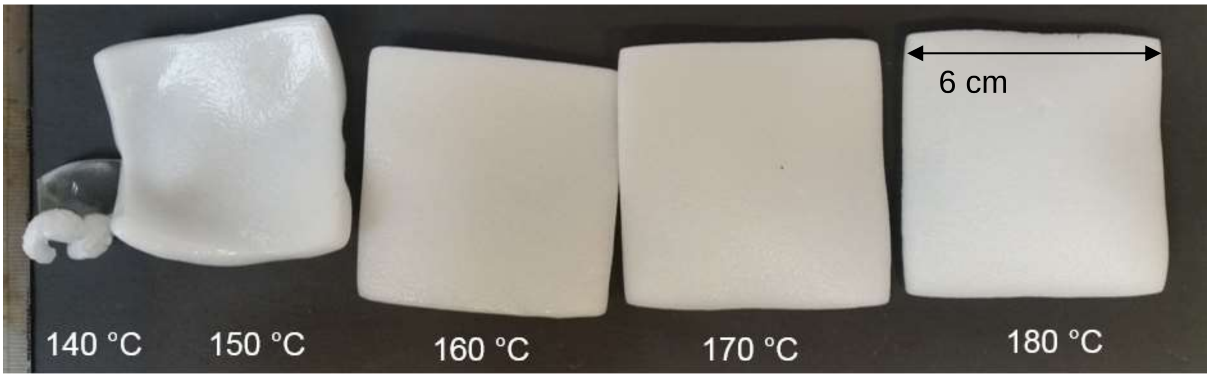

Figure 23: Foam formation for different T_1. At lower T_1 the foams are not homogenously expanded as the vapour pressure does not provide for the necessary expansion.

Figure 24 shows that porosity and nucleation density increase with foaming temperature T_1 until they reach a plateau at T_1 =175 °C (T_2 = 115 °C) with an indicated decrease at 180 °C. This fits to the fact that for foaming at 175 °C and at 180 °C bursting bubbles could be heard as popping noises. Therefore, the plateau indicates that a balance is reached between the increase of expanded nuclei and shrinkage or damage to the cells close to the thermal degradation of PMMA.

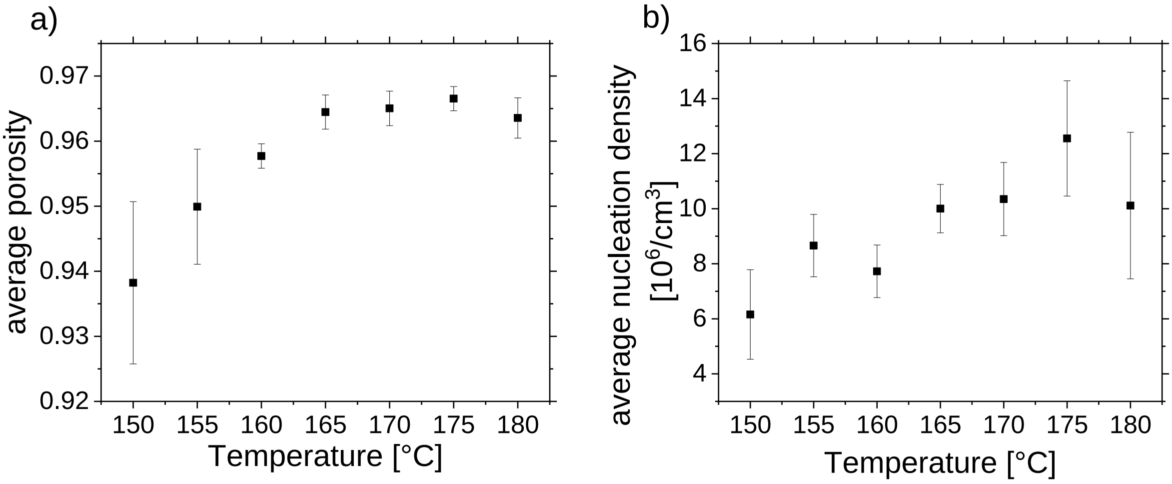

Figure 24: a): Porosity development in dependence of foaming temperature T_1. The highest porosity is reached around 170 °C, which was therefore chosen as foaming temperature. b): Nucleation density depending on foaming temperature T_1. T_2 was set at 115 °C for t_2=8 min

The quite large standard distributions of porosity at lower temperatures T_1, reflect the fact that the foams are less homogenously expanded at lower temperatures (see Figure 23). Therefore, 170 °C was chosen as standard foaming temperature T_1 in order to choose a foaming temperature at which the most expanded state is reached, but at the same time cells are conserved and reproducibility is ensured.

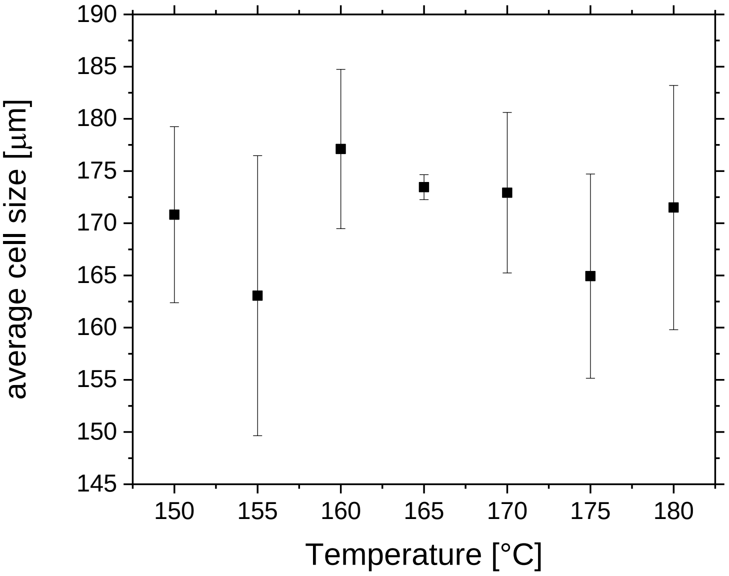

Figure 25: Cell size dependending on foaming temperature in the first oil bath. All foams were left in the second oil bath at 115 °C for 8 min.

As can be seen in Figure 25, the cell size development is independent of foaming temperature, while porosity and nucleation density increase (see Figure 24). This indicates that at higher foaming temperatures more nuclei expand and grow to the same cell size and contribute towards a higher porosity. It seems the change in nucleation density is not high enough to change cell size in this regime.

An independence of cell size on foaming temperature is also observed in solid state foaming processes (see (Martín-de León, Bernardo, and Rodríguez-Pérez 2016)). It indicates that once nuclei are expanded by the vapour pressure their growth is limited by the polymer unless there are major changes in nucleation density. This would explain, why the average cell size resulting from the two employed PMMA manufacturing batches of different molecular weights is different. This will be further discussed in section 4.5.

4.3.2 Choice of stabilisation time t_2 and temperature T_2

In order to choose stabilisation time t_2 and stabilisation temperature T_2 for the stabilising oil bath, they were varied between 6 and 20 min and 90 °C and 150 °C, respectively. In this case only one sample was employed per data point.

As can be seen in Figure 27, cell size reaches a maximum around T_2 = 115 °C, which is just below the T_g of the glassy polymer (118°C). Therefore, the polymer filled with methanol is presumably above T_g in the oil bath and as long as a substantial amount of methanol is evaporating, the vapour pressure keeps the voids expanded without too much shrinkage. And once a substantial amount of methanol evaporated, the sample is approaching T_g and is therefore mostly stable. This also explains why the cell size and porosity (see Figure 27) are largely independent of foaming time t_2 up to stabilisation temperature T_2 = 130 °C.

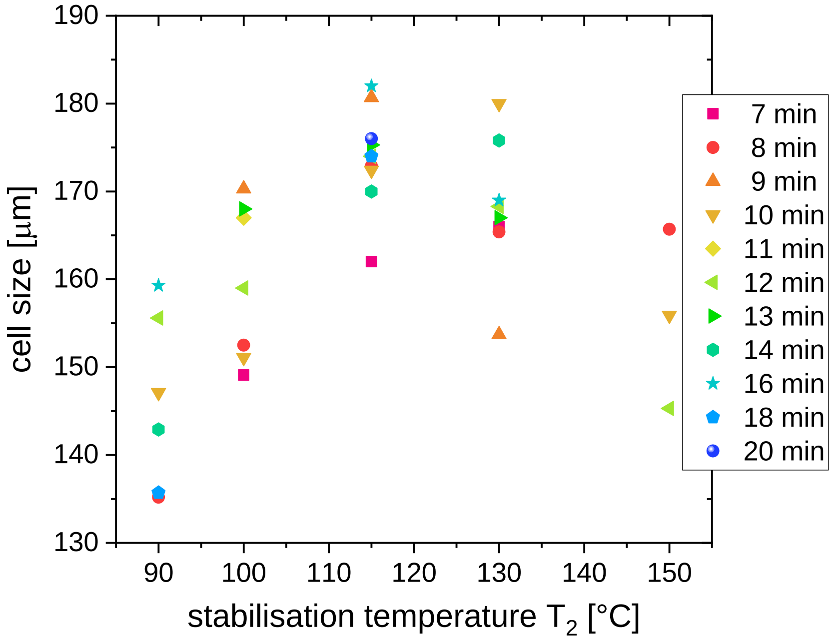

Figure 26: cell size depending on stabilisation time t_2 and temperature T_2.

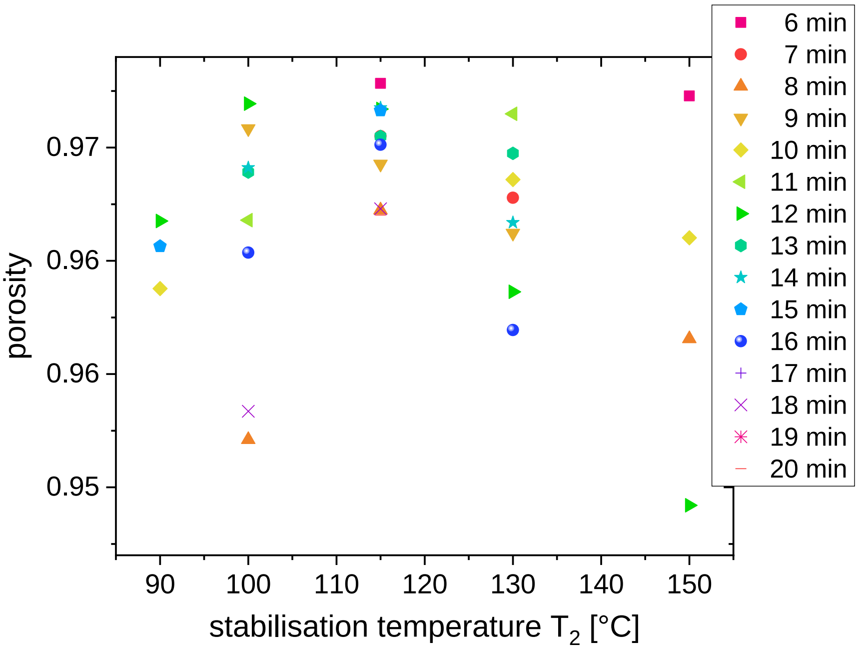

Figure 27: porosity depending on stabilisation time t_2 and temperature T_2.

As can be seen from Figure 27, a maximum in porosity is also reached around T_2 = 115 °C (Figure 27). 115 °C was therefore chosen as stabilisation temperature T_2 for the second oil bath.

The time t_2 was chosen as 8 min as it is minimum time at which foams are almost always stable at 115 °C desorption temperature. Below 8 min they often collapse, because of the remaining methanol content.

The standard process was therefore chosen as: T_1 = 170 °C, t_1 = 1 min, T_2 = 115 °C, t_2 = 8 min.

4.3.3 Resulting foam properties

As can be seen from Figure 28, the standard process results in a foam with an average cell size of 175 ± 13 µm for manufacturing batch 1 and 250 ± 15 µm for manufacturing batch 2 (see Figure 28 a)).

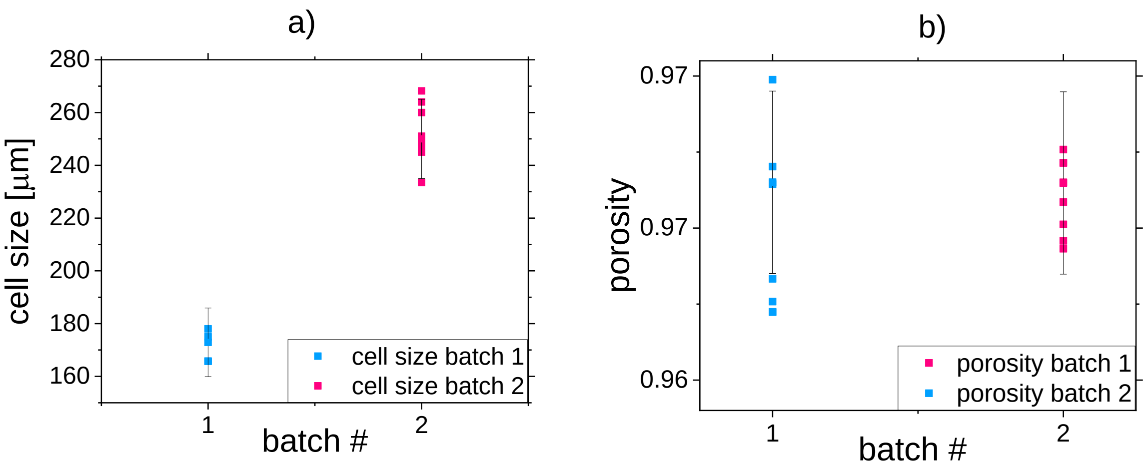

Figure 28: Cell size and porosity difference between the two batches of PMMA for standard foaming conditions at 8 w/w% remaining methanol content.

There is no major difference in porosity between the two batches (see Figure 28 b)). But the nucleation density also differs significantly (see Figure 29). The reason will be discussed in 4.5.

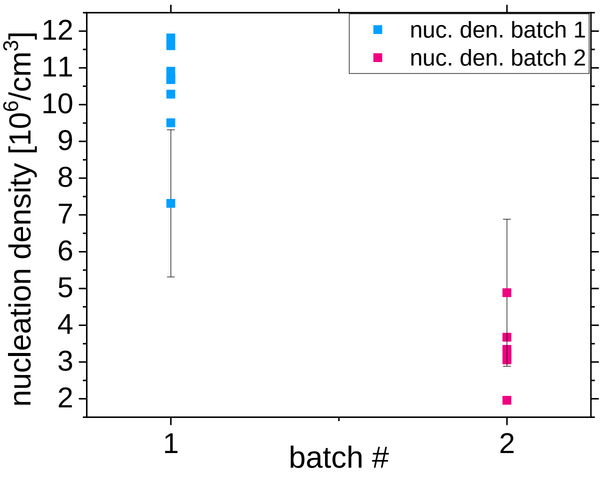

Figure 29: Difference in nucleation density between the PMMA batches.1 and 2 for standard foaming conditions at 8 w/w% remaining methanol content.

4.4 Discussion: influence of T_g on foam formation

As discussed in section 4.1, the process was developed based on the observation that desorption-induced stress development might play a role for the generation of post-critical nuclei. And that the desorption step is necessary for the stress-development.

However, another consideration was that desorption is necessary to increase the T_g of the polymer-solvent mixture. Since in order to achieve nuclei expansion, the T_g of the polymer-solvent mixture might need to be higher than the boiling point of methanol (65 °C). As this would ensure that methanol starts evaporating and its vapour pressure expands nuclei before they collapse above T_g.

As can be seen from Figure 30, the T_g of the methanol desorbing PMMA sample at 8 w/w% is around 65 °C, which is the boiling point of methanol. This would match the consideration that desorption is necessary to reach a T_g below the boiling point of methanol.

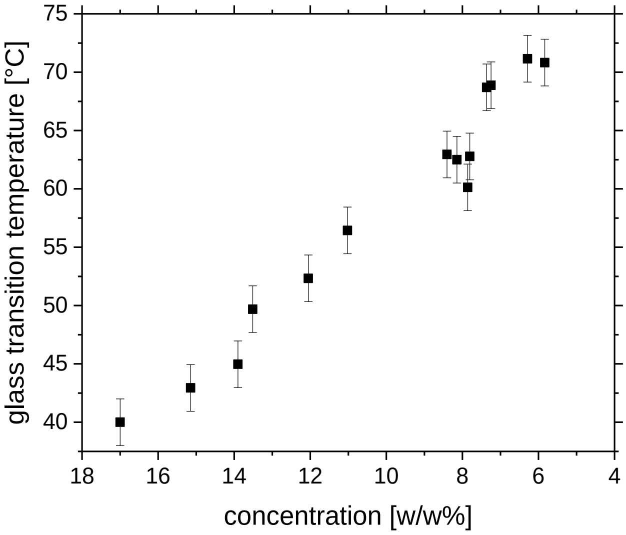

Figure 30: Glass transition development of PMMA during desorption of methanol measured by DMA as described in 3.3.6.

On the other hand, one of the key observations for this work was that a fully charged sample of extruded PMMA, would foam with big bubbles after a dip in liquid nitrogen (see section 4.1).

It seemed that in this case foamable nuclei were developed that did not collapse despite the T_g in a fully equilibrated PMMA-methanol mixture is most likely far below 65 °C according to Figure 30. It is therefore most likely that nuclei collapse is not immediately occurring upon reaching T_g. Depending on the nucleus size, nuclei shrinkage might take long enough to reach the boiling point of methanol before total collapse so that nuclei can expand into voids even if the T_g of the PMMA-methanol mixture is lower than the boiling point of methanol.

Therefore, it is very likely that reaching a T_g above the boiling point of methanol is not the main reason for the necessity of desorption. The theoretical reason why stresses could play a role for nucleation is discussed in the following chapter 5.

4.5 Discussion: Molecular weight influence on foam formation

The independence of cell size (see Figure 25) from the actual foaming temperature T_1, has also been observed for polymer nanofoams from PMMA manufactured by solid state foaming.(Judith Martín-de León et al. 2020), (Martín-de León, Bernardo, and Rodríguez-Pérez 2016) It seems that in order to change the cell size a more severe change in nucleation density needs to occur that can be achieved with a change in foaming conditions. It seems the polymer molecular weight could be an influencing factor on cell size.

It has also been observed for nanofoams generated from PMMA of different molecular weights by CO_2 assisted solid state foaming, that the cell size decreases with increase in molecular weight and nucleation density at the same time increases. (Judith Martín-de León et al. 2020) , (Van Loock et al. 2019)

One reason could be that that differences in molecular weight cause differences in demixing behaviour, which is dependent on molecular weight (see section 2.1.2). The potential to mix decreases with increasing molecular weight. Therefore, the free energy barrier decreases with an increase in molecular weight (see section 2.1.4).

Furthermore, the viscosity increases with molecular weight (see (Carter, Walter C., Robert L. Scott 1946)) and nuclei are inhibited in their growth.

These two reasons could explain the differences in foam properties, which are observed for the two different manufacturing batches (see Figure 28). Though the number average weight is smaller for batch 1, its weight average is higher compared to batch 2 as well as its dispersity (see section 3.1.1.1). This indicates that it might contain partly higher molecular weight parts compared to batch 2, which might contribute to the observed higher nucleation density in batch 1 (see Figure 29). However, more data would be needed to prove this.

All in all, it seems that in the case of the PMMA-methanol system, cell size is independent of foaming conditions, but potentially dependent on the polymer molecular weight.

4.6 Summary

A foam was made from PMMA and methanol in a process that is analogue to solid state foaming except for the depressurisation step that is replaced with a desorption step.

It was found that in order to achieve a homogenous foam, methanol desorption from a fully charged PMMA sample to below 8.5 w/w remaining methanol concentration at 25 °C is necessary before foaming and stabilization in a silicone oil bath. The standard foaming procedure comprises an expansion step for 1 min at foaming temperature T_1 = 170 °C in a silicone oil bath and a stabilization step of 8 min in another silicone oil bath at T_2 = 115 °C.

Desorption induced stress development that influences nuclei development is considered as a reason for the necessity of the desorption step. Reaching a glass transition temperature above the boiling point of methanol seems not to be the major reason for the necessity of the desorption step.

It was found that cell size is almost independent of foaming temperature T_1 for desorption at 25 °C. It was concluded that the changes in nucleation density caused by different foaming temperatures are not high enough to change cell size.

A significant difference in cell size between the two manufacturing batches was found and correlated to their differences in molecular weight. It hints that higher molecular weight proportions in a polymer might be beneficial for decreasing the cell size. However, the data is not substantial enough to give clear indications.

5. Skin-induced stress state development

The foamability of methanol swollen PMMA was observed to be dependent on sufficient methanol desorption after equilibrium swelling. The necessity of methanol desorption for homogenous foamability was linked to desorption-induced stress development that contributes to nuclei generation. The qualitative reason for desorption-induced stress development as well as the magnitude of the stress development and geometric changes that are related to stress development will be discussed in the following chapter.

5.1 Qualitative description of skin-induced stress development

In the initial stages of desorption, methanol is depleted from the outer layers (skin) of the PMMA slab. The skin consequently contracts and becomes glassy. As the sample core is still swollen with methanol, it is set under compression by the contracting skin (see Figure 31, 1b)). In turn the skin is set under tension. The sample core therefore exhibits a positive retardation Δr corrosponding to a compressive stress state in the beginning of desorption.

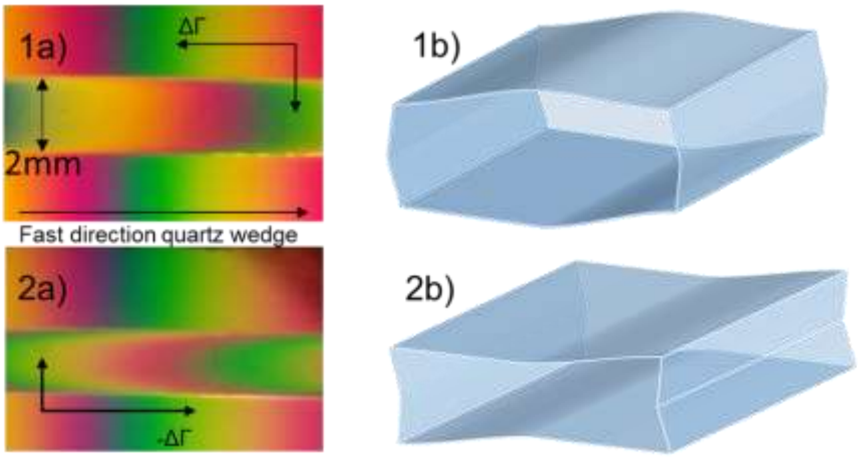

Figure 31: Birefringence development during the methanol desorption and the related geometric changes. 1a) and 1b): Because of skin contraction, the sample core is set under pressure. 2a) and b): At later desorption stages the core layers contract and are set under tension by the rigid skin.

With further desorption, the core layers lose methanol and shrink as well. They are constrained from shrinking by the glassy skin layer which had become glassy in an extended state (see Figure 31 2a)). Therefore, the core layers are now set under tension by the skin, while the skin is set under compression by the core layers. In this state, the core layers show a negative birefringence which translates in a tensile stress state (see Figure 31 2b)).

Since it was assumed that the stress development is also closely connected to geometric changes, the following sections quantify the geometric changes during desorption as well as the resulting stress development.

5.2 Quantitative geometric changes

In order to quantify geometry changes and stress state development, a fully methanol charged PMMA slap ($2 \times 20 \times 20$ mm^3, batch 1) is taken out of methanol. Surplus methanol on the sample faces is removed, it's weight and geometry is determined with a microscale, a caliper and a thickness gauge and subsequently its birefringence is measured with the quartz wedge method described in section 3.3.1.1.

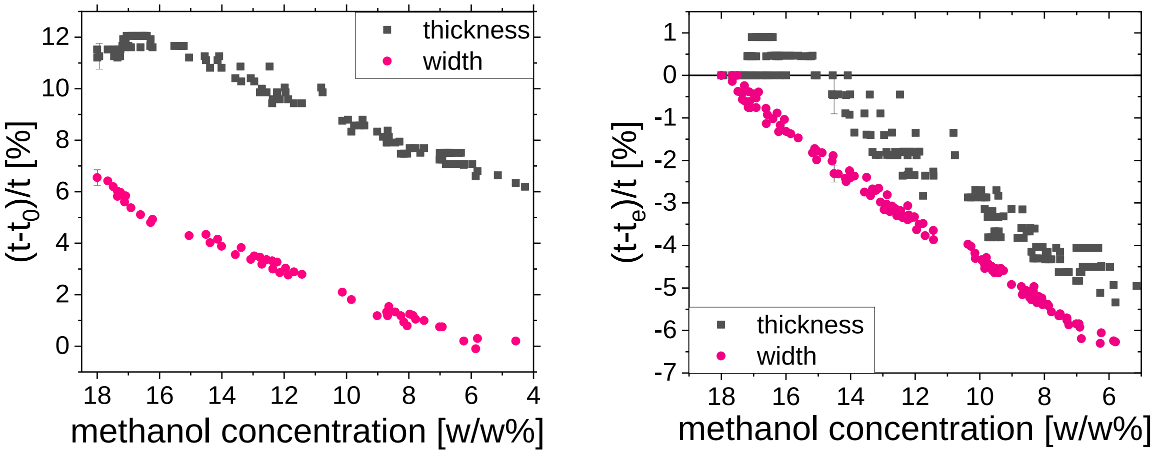

Figure 32: Left changes relativ to t_0. Right changes relative to t_e.The data is taken from desorption of seven individual samples.

Figure 32 shows the changes in width and thickness (t means width or thickness) here upon desorption at 25 °C with reference to unswollen state t_0 and equilibrium swelling t_e (see 3.3.8).

The uncertainty on the data derives from the inaccuracy of the caliper and inhomogeneities in sample geometry. The error bars were derived from the standard deviation of 5 data points taken at the same concentration. For the purpose of readability only one data point has been assigned with an error bar. Since the error of the thickness gauge (0.01 mm) is quite big compared to the thickness (2 mm), it imposes a bigger uncertainty to the thickness than the error of the caliper (0.01 mm) imposes to the larger width (20 mm).

The equilibrium thickness increase relative to the unswollen sample geometry is larger than for the width. This has already been observed by Thomas in her PhD thesis. (N. Thomas 1978) The reason is discussed in section 0. However, this initial anisotropy seems not to be related to an initial stress state that might affect foam formation since in the swollen state the stresses are measured to be zero by birefringence (see Figure 36). It was ruled out that this effect is a desorption related effect. For this, the dimensions were measured when the equilibrated sample was still immersed in methanol. The result was still the same anisotropy. Therefore, desorption induced shape change could be ruled out as a reason for this swelling anisotropy and was not investigated more closely.

The thickness initially increases during desorption, which is in particularly visible from the geometry changes relative to equilibrium thickness. The effect is subtle for 25 °C desorption temperature. But the trend can be confirmed for measurements at higher desorption temperatures (see 8.1.2). To double check that the change is not hidden due to the greater width, the geometric changes were also plotted in Figure 33 relative to $(t_e - t_\mathbf{0})$, which also only shows an initial increase in thickness not in width upon desorption.

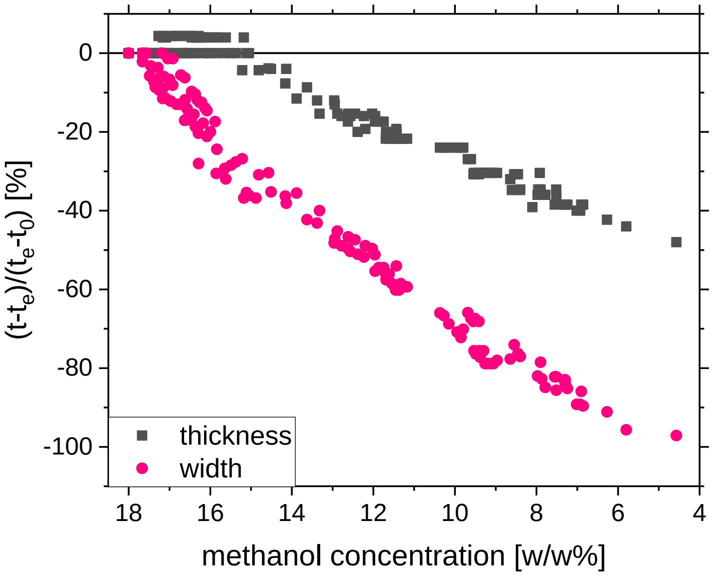

Figure 33:Geometry changes upon desorption at 25 °C relative to t_e-t_0. The difference in slopes in this case results from the differences in equilibrium swelling for thickness and width.

Figure 33 confirms that the width decreases with the start of desorption. The increase in sample thickness most likely results from the constraints that are imposed on the sample by the skin in the early stages of desorption. This can be explained as follows:

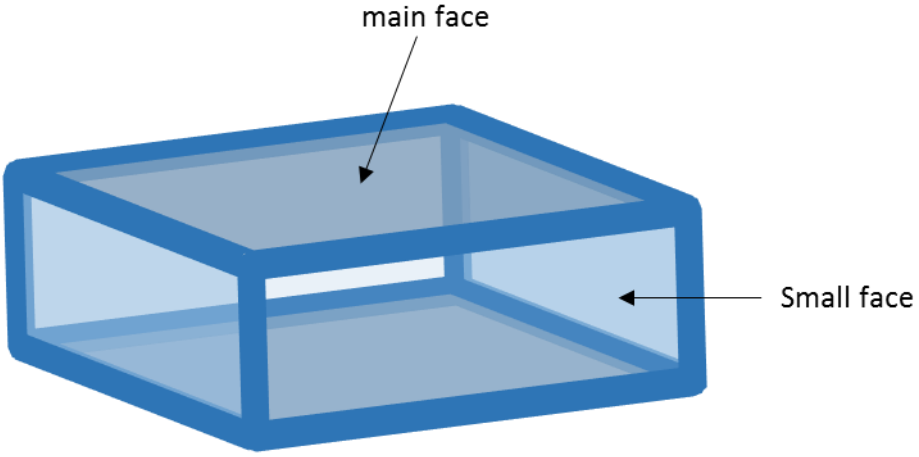

Figure 34: The skin forming a three dimensional bar at the sample edges that imposes a geometric constraint upon desorption.

In the early stages of desorption, desorption from two sides at the edges leads to a stiff three-dimensional frame that has a higher constraining effect than the two-dimensional skin on the faces. The ratio of solidified edge to face is much higher for the small faces. Therefore, the small faces are more constrained than the sample main faces that are initially pushed outside. This results in the observed increase in sample thickness, whereas the side faces do not show a measurable increase in dimensions.

The initial thickness increase upon desorption leads to an advanced decrease in swelling ratio of width compared to swelling ratio of thickness. Therefore, geometry changes upon desorption are not isotropic. This indicates that stresses might develop.

However, it must also be stated that changes in particular in the tensile stress state stress state would not necessarily be reflected in changes in geometry. The reason is that the stress state derives from the strain imposed by the skin on the contracting core layers, which is not necessarily reflected in geometry changes.

5.3 Quantitative skin-induced stress development

5.3.1 Verification of elastic stress state

As discussed in section 3.3.1.3, birefringence can be of either elastic or orientational origin. Only if it is of elastic origin, it can be linked to its originating stress state by the stress optical law. Therefore, it is necessary to evaluate whether the desorption-induced stress state is elastic in origin.

Elastic birefringence vanishes once the stress that is causing it is taken away. Therefore, in order to check for the nature of birefringence, the sample was sawn in the middle in order to eliminate the skin as source of stress.

As can be seen from Figure 35, the birefringence vanishes if the skin is sawn off and the imposed stress is released. This indicates that the birefringence is caused by an elastic stress state.

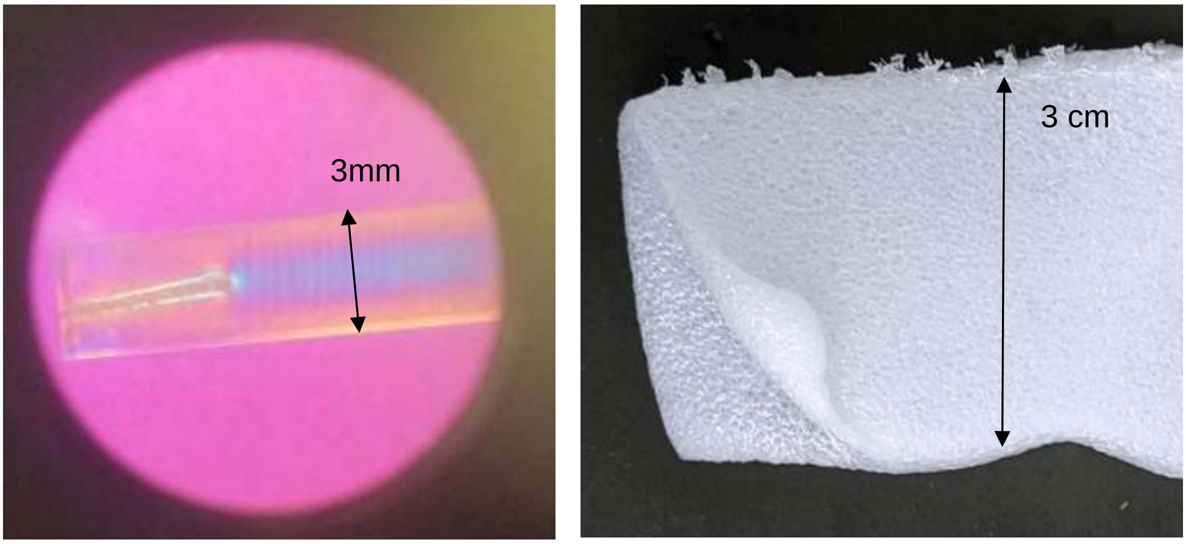

Figure 35: Left: Birefringence vanishes if the constraint of the skin is released by sawing in the cross-section. Right: Sample foamed after sectioning. Foam fully develops on both sides despite the stress release caused by the release of the skin.

A sample for which the stress had been released like that still fully develops into a foam. This strongly indicates that it is the stress history that is relevant for nucleation and foam development rather than the stress imminent at foaming. Stress-state measurements

Figure 36 a) shows the stress development during desorption that was obtained from birefringence measurements with and without correction of the stress optical coefficient as described in 3.3.1.3. A close up of the corrected data is shown in Figure 36 b).The data results from desorption curves of 10 different samples for which birefringence had been measured during desorption to determine the stress like described in section 3.3.1.1. Without correction means that the stress optical coefficient has been kept at $4 \cdot 10^{-12}$ m^2 N^{-1}, which is the value for pure PMMA.

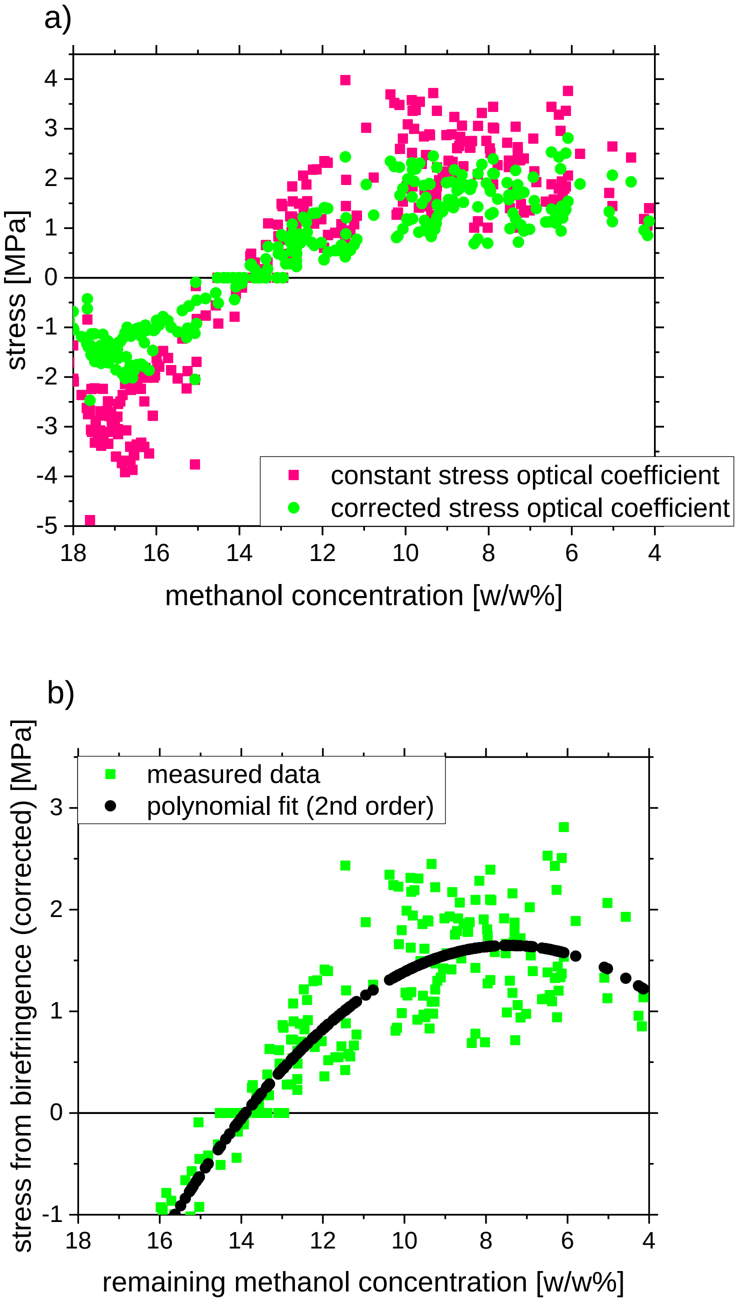

Figure 36: a): Stress development resulting from methanol desorption at 25 °C in a 2×20×20 mm^3 slab of PMMA.
b): Polynomic (2nd order) fit of the corrected stress data in dependence of methanol concentration.

As discussed in section 3.3.1.3 the stress optical coefficient changes with methanol concentration. Therefore, a linear dependence between concentrations between remaining methanol concentration and and stress optical coefficient between 8 and 4 $\cdot 10^{-12}$ m^2 N^{-1} has been assumed. This makes sense in the light that the measured retardation is essentially a measure of strain reflected in a change in the orientation of the polymer structure.(Pick, Lovell, and Windle 1979) Since the Young's modulus increases linearly with decrease in methanol concentration (see 6.2), it makes sense that the stress optical coefficient also decreases linearly with a decrease in methanol concentration.

There is quite strong scattering in the data. It is suspected that the scattering is mostly related to the fact that the temperature has a strong impact on the birefringence development (see discussion 3.3.1.1). No error bars for the stress resulting from the method are depicted since in this case, they would be significantly smaller than the scattering on the data resulting most likely from temperature variations.

The error on methanol concentration varies with desorption. For high methanol concentrations between 18 and 16 w/w%, desorption is so fast that the time between weight and birefingence measurement results in an offset between real concentration at birefringence and measured concentration. At later stages, desorption is sufficiently slow and the main uncertainty results from weight measurements. The uncertainty on concentration is estimated from the impact of weight changes within 30 s of desorption, which is the time needed for weight and birefringence measurement. This would lead to an uncertainty of 0.1 w/w% initially. At later stages, the error is estimated to result mostly from weighing errors which is derived by weighing the same sample 10 times. It was found to be 0.03 w/w%. However, variations in initial weight were observed to be higher and up to 0.3 w/w% which is most likely resulting from variations of temperature (see chapter 8).

In the beginning of desorption the stress state is compressive as can also be seen from the geometry changes in Figure 37. The compressive stress state reaches a maximum and then decreases. The decrease of the compressive stress state coincides with the reverse of the increase in sample thickness. The stress state switches from compressive to tensile, when the sample dimensions are back to equilibrium swelling dimensions after the expansion during the beginning of desorption. This indicates that the thickness increase results from the compressive force resulting from the contracting skin.

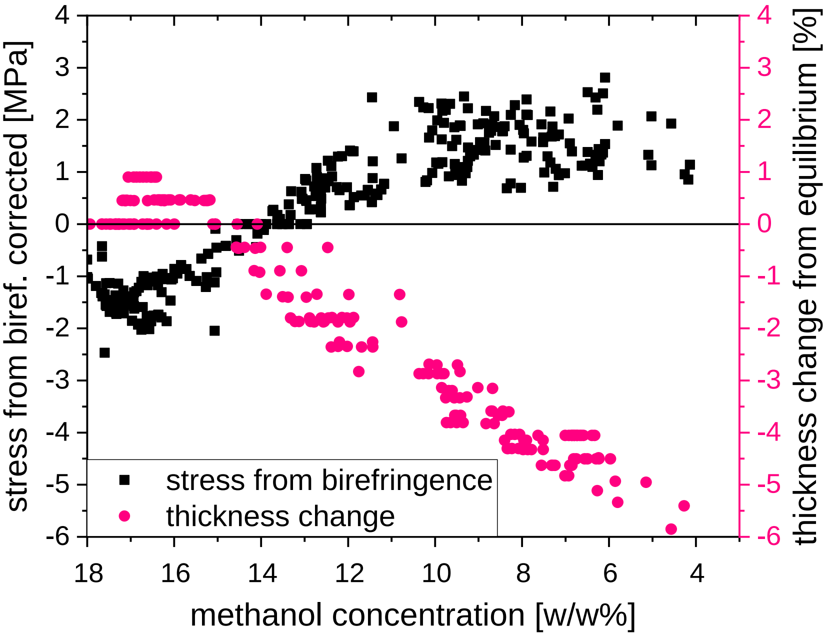

Figure 37: The correlation between tensile stress state measured by birefringence (concentration corrected stress optical coefficient) and changes in sample thickness.

The stress state becomes tensile at around 14 w/w% remaining methanol concentration. Below 10 w/w% remaining methanol concentration the rate of stress increase with methanol desorption is leveling off and the stress state reaches its maximum of 1.75 MPa around 8 w/w% remaining methanol concentration (derived from curve with corrected stress optical coefficient with polynomial fit (second order)). This is in accordance with the consideration that a certain stress state must be reached before foaming becomes possible below 8.5 w/w% methanol content.

5.4 Summary

The stress state resulting from methanol desorption in fully charged PMMA was characterized with the help of birefringence measurements and geometry changes. The measurements reveal that methanol desorption from fully equilibrated PMMA initially leads to a compressive stress state, presumably caused by the methanol-deprived glassy skin layer that compresses the sample in particular along the width so that the main faces are pushed out during the initial stages of desorption, which can be measured as a thickness increase. At later desorption stages the skin layer constrains the inner layers from contracting and sets them under tension which can be measured by birefringence. The geometry measurements indicate an unisotropic geometry change, but it is difficult to say whether this is directly correlated with the birefringence development that results from the restraining impact of stiff glassy skin layer on the core layers and is not necessary measurable in terms of geometry change.

It was shown that the birefringence is of elastic origin and vanishes once the skin is removed, which excludes occurrence of permanent chain alignment. A sample would also foam even if the stress is released. It is therefore concluded that it is the stress history which is important for foaming rather than the stress present at foam formation.

It was found that the maximum of the tensile stress state derived from birefringence measurements is reached at 8 w/w% remaining methanol content, which is when homogenous foam formation becomes possible. This strongly indicates that for the foaming process employed here, the stress state development is a necessary condition for foam development.

6. Influence of additional tensile stress on foam formation

Since stress development seems to contribute towards the development of foamable nuclei, the question was in how far additionally applied stress as well as pressure would influence the development of foamable nuclei and subsequent foam formation. Therefore, first the strain response of additionally applied tensile stress on methanol desorbing PMMA was characterized.

To understand the limits of the stress application on void formation, the impact of yield stress on void formation at high and low methanol concentrations was investigated.

The impact of the magnitude of different tensile stresses on foam formation at different methanol concentrations is discussed thereafter.

Since the application of tensile stress seems only to have a significant influence on foam development if it is applied after desorption to lower methanol concentrations, mainly this case is discussed.

6.1 Method for application of tensile stress

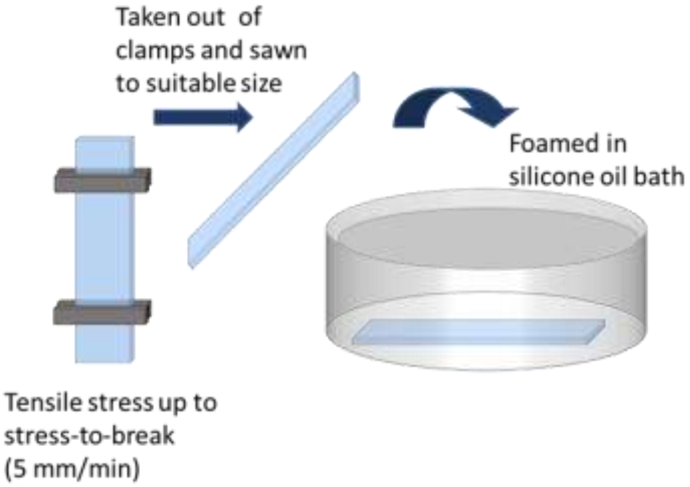

Figure 38: Procedure for application of biaxial stress prior to the foaming step on a methanol desorbing sample that had previously been equilibrated with methanol.

Strips of 2×20×140 mm^3 PMMA from batch 2 were desorbed to different concentrations of remaining methanol after full equilibrium absorption in methanol. Thereafter, a tensile stress between 10 MPa and stress-to-break was applied with a strain rate of 5 mm/min. Gauge length was chosen to be 100 mm. The stress was immediately released and the sample taken out of the clamps of the tensile tester. The sample was sawn to a suitable size for foaming (see Figure 38). The part of the sample that had been outside the clamps serves as unstressed reference sample and is foamed jointly with the stressed part so that variations in the foaming procedure are insignificant.

6.2 Stress-strain response of PMMA desorbing methanol

In order to understand how the Young's modulus is affected by methanol desorption, it was derived from the stress-strain curves taken at different methanol concentrations that had been reached by desorption. The resulting values (see Figure 39) suggest that the Young's modulus linearly increases with decrease in remaining methanol concentration. The uncertainty was deduced from the standard deviation of three measurements of methanol free samples.

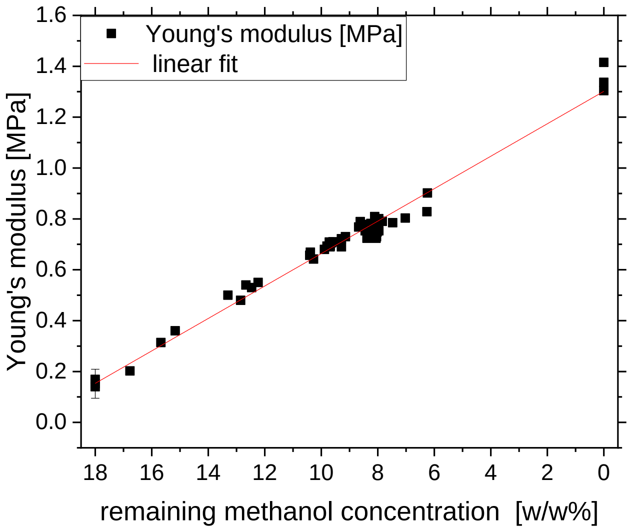

Figure 39: Young's modulus depending on methanol concentration. The measurements were based on determination of the gradient of stress-strain curves.

As can be seen in Figure 40, pure PMMA exhibits a linear stress-strain curve. Methanol acts as a lubricant and leads to plastic deformation and yielding.

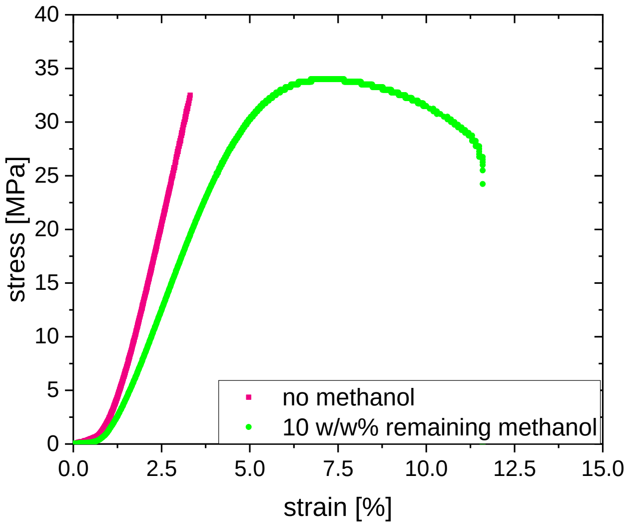

Figure 40: Stress-strain curve for PMMA with and without methanol content.

As can be seen in Figure 41 the applicable yield stress increases with decreasing remaining methanol concentration.

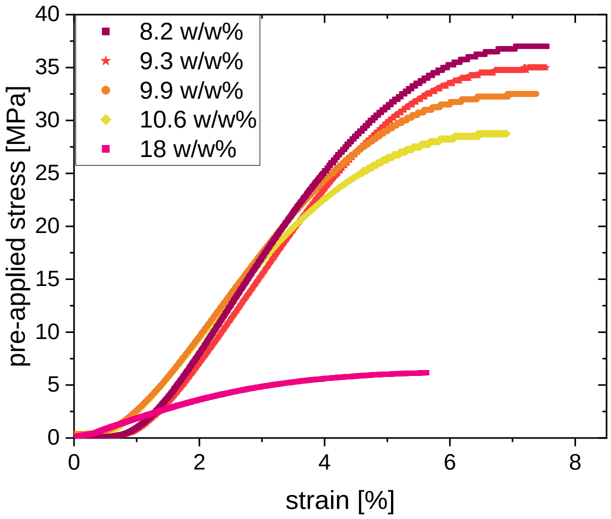

Figure 41: Application of tensile stress on samples of different methanol concentrations reached by desorption.

6.3 Influence of tensile stress on foam formation depending on methanol concentration

In order to see how the maximum applicable tensile stress influences void formation at different concentrations, yield stress was applied after desorption to different methanol concentrations and then the sample was foamed for 1 min at 170 °C. Figure 42 shows the void development of samples that have been subject to yield stress after desorption to methanol concentrations between 17 and 13 w/w% before foaming.

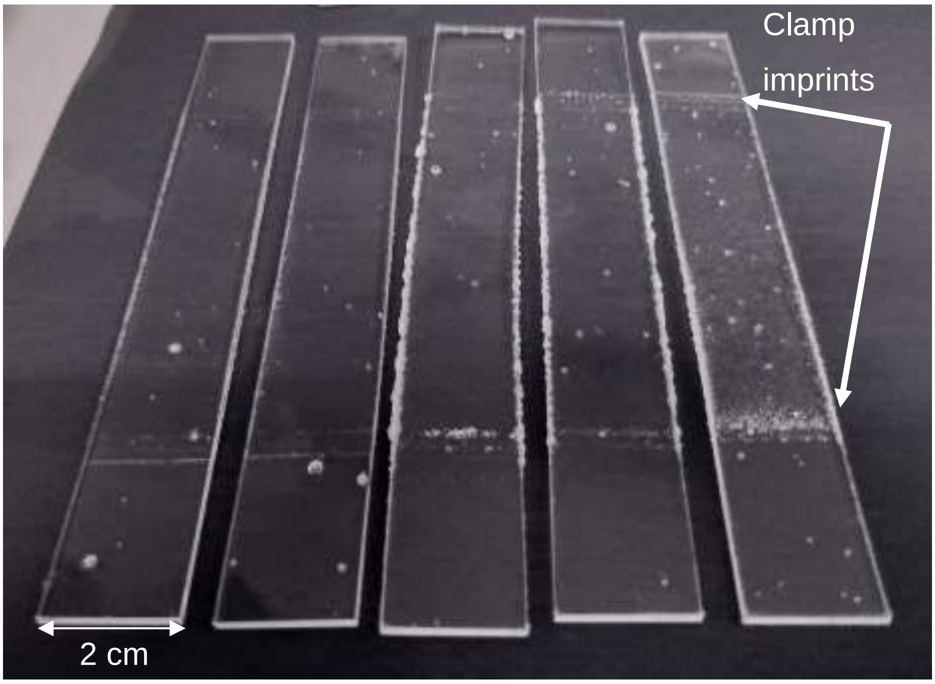

Figure 42: Foam development after application of tensile stress to yield stress (18.6, 19.8, 21.6, 22.2, 25 MPa) for concentrations of 16.7, 15.7, 15.2, 13.3, 12.7 w/w%. residual methanol concentration.

As can be seen from Figure 42, additional void development, as a consequence of stress application, is only very subtle at higher methanol concentrations. However, there is a clear indication that the application of tensile stress or its hydrostatic component are beneficial for void development.

In section 7.3.2 it will be discussed that if higher hydrostatic stresses from other sources can be applied, more visible voids can be achieved at these high concentrations as well. This indicates that a major limitation for the development of additional voids at high methanol concentrations is the magnitude of applicable hydrostatic tension via application of tensile stress.

Interestingly, the amount of additional void development resulting from the tensile stress application seems to increase with desorption. This is a hint that the additional stresses potentially further expand desorption-expanded not yet foamable nuclei, which should become more with desorption, into foamable nuclei. This also indicates that nuclei development of foamable nuclei is a gradual process depending on available expansive stresses. This hypothesis will be discussed in more detail based on the results in chapters 7 and 8.

Figure 43 shows samples foamed at more advanced desorption stages (10.6, 9.9, 9.3, 8.2 w/w% remaining methanol concentration) that had been subject to yield stress (28.8, 32.5, 35, 37 MPa) after desorption right before foaming (see Figure 41).

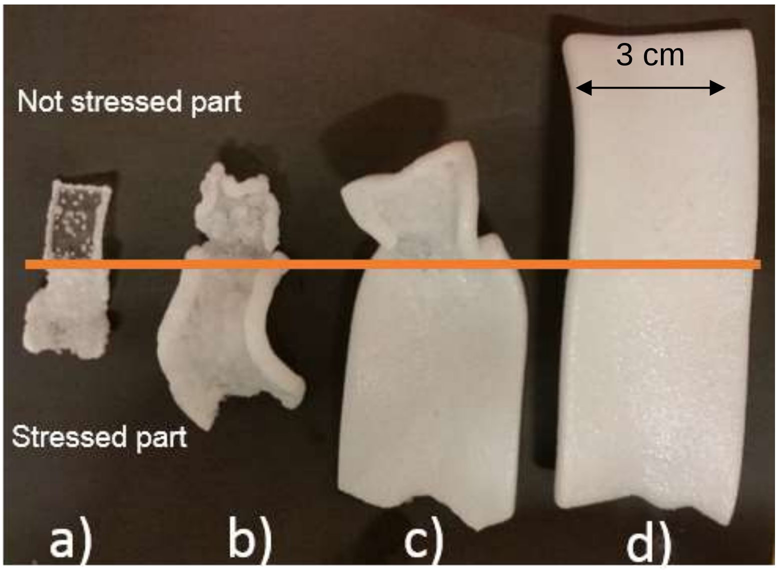

Figure 43: PMMA strips at different desorption stages (a: 10.6 w/w%, b: 9.9 w/w%, c: 9.3 w/w%, d: 8.2 w/w%) that had been subjected to a short tensile stress until yield stress (a): 28.8 MPa, b): 32.5 MPa, c): 35 MPa, d): 37 MPa) after desorption right before foaming. A clear increase in foamability can be observed for the previously stressed parts for a), b) and c). In the case of c) the stressed part is homogenously foamed compared to the unstressed part.

As can be seen in Figure 43, the pre-stressed part of the samples clearly develop a higher degree of foam formation. In particular, from c) it can be seen that application of additional stress prior to foaming leads to homogenous foam formation in a sample that would otherwise not homogenously foam, because it has not reached a sufficient desorption state yet. It seems the additional tensile stress adds to the stress state that has been achieved by the desorption induced stress and this results into development of sufficient foamable nuclei.

If tensile stress is applied before desorption to lower methanol concentrations, it does not lead to any significant additional void formation as shown in Figure 44.

Figure 44: Left: sample subject to yield stress (6 MPa) before desorption to 11.4 w/w%. Right: sample subject to yield stress (25 MPa) after desorption to 11.6 w/w% remaining methanol content.

However, additional void formation is observed for stress application before desorption if higher stresses are applied via another method as will be shown in section 7.3.3. This means, applied-stress-induced nuclei would survive at high methanol concentrations. Therefore, the most likely reason for the lack of significant additional nuclei development in case of application of tensile stresses before desorption, is the limitation of applying sufficiently high tensile stresses at high methanol concentration to achieve nuclei development.

6.4 Influence of magnitude of pre-foaming applied stress on foam formation

So far it has been established that yield stress has an impact on void development if applied after desorption to lower methanol concentrations above concentrations at which homogenous foaming is achieved (8.5 w/w%). The question remains in how far the magnitude of stress influences foamability. Therefore, the impact of different tensile stresses of 10, 20 and 30 MPa on samples with the same methanol concentration was investigated.

Figure 45 shows that increasing the tensile stress before foaming visibly increases the amount of void formation on samples with the same remaining methanol concentration. It also follows that application of tensile stress has an effect on void development even for stresses in the elastic regime (also see section 6.5). This supports the hypothesis that it is the hydrostatic component of stress that enhances void development and not cavity formation in the sense of crazing, which would happen above the elastic regime at yield stresses. (Ehrenstein, Riedel, and Trawiel 2004)

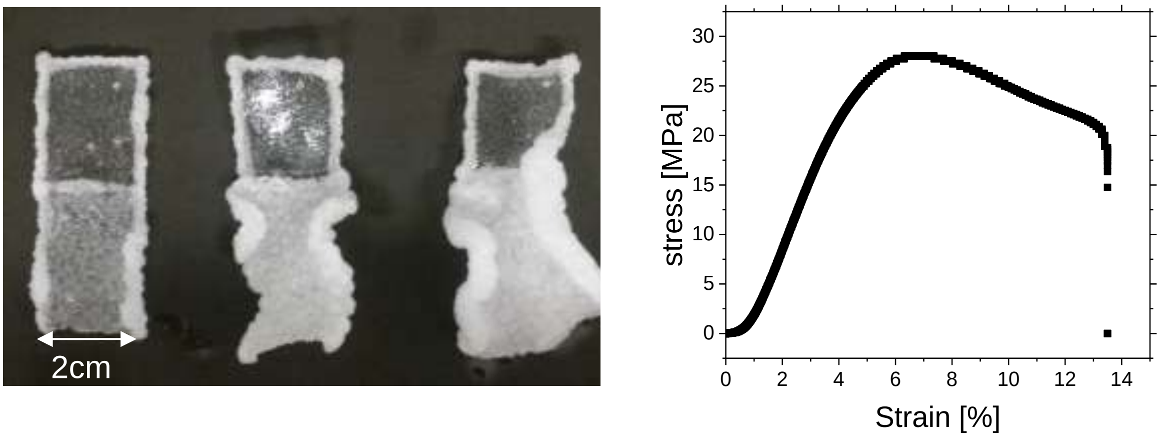

Figure 45: Left: Foam development at (left to right) 10.1, 10.2, 10.1 w/w% remaining methanol concentration in dependence of pre-applied stress (from left to right) 10, 20, 30 MPa. Right: stress-strain curve for 10.2 w/w% remaining methanol concentration. 10 MPa are clearly within the elastic regime.

It was then established for which tensile stresses homogenous foamability can be reached at different remaining methanol concentrations. Figure 46 shows how the concentration at which homogenous foam formation becomes possible increases with an increase in pre-applied stress. Homogenous foam formation means a foam without any collapsed bubbles.

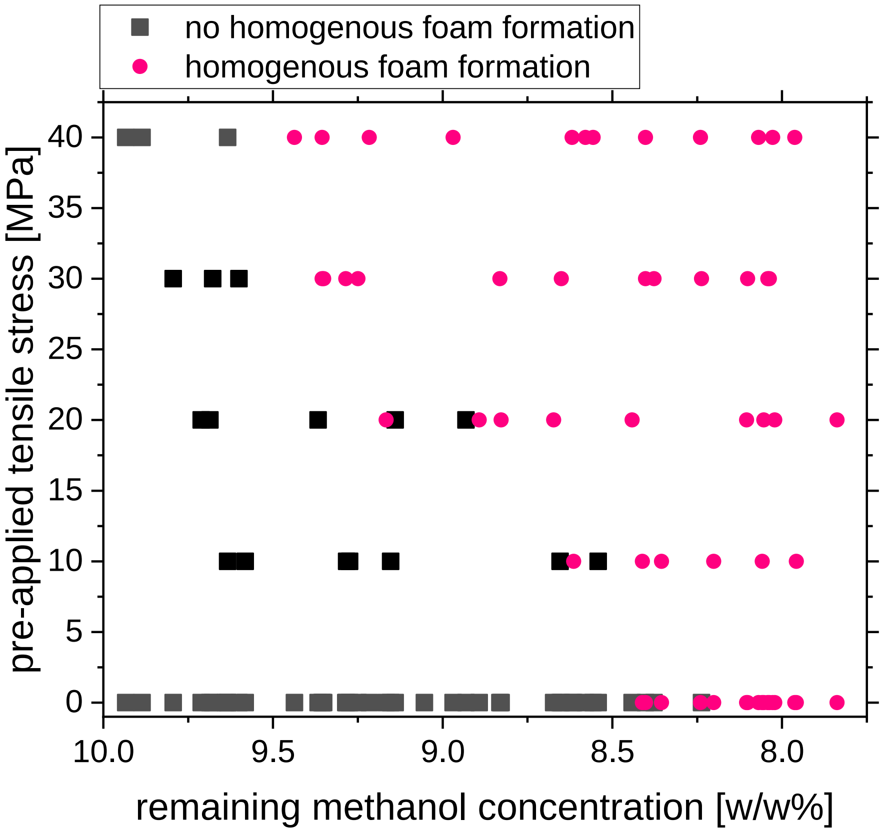

Figure 46: Homogenous foam formation depending on pre-applied stress. Black squares: no homogenous foam formation. Red dots: homogenous foam formation. Above 8.5 w/w% additional stress is necessary to achieve a homogenous foam. The higher the stress the higher the remaining methanol concentration at which full foam formation is achieved. Please, note that methanol concentration has been assigned in the direction of desorption: from high to low concentration on the x-axis.

40 MPa refers to either application of 40 MPa or stress-to-break. Above 40 MPa stresses are close to stress-to-break or are not applicable at high methanol concentrations and low viscosities.

9.43 w/w% was the highest methanol concentration at which homogenous foam formation could be achieved after application of 40 MPa tensile stress before foaming. Without application of stress before foaming, at least 8.5 w/w% remaining methanol content have to be reached by desorption. Below 8.5 w/w%, there is a transition in which foams might or might not foam homogenously. So technically, foamability is reached at 8.27 ∓ 0.13 w/w% residual methanol concentration derived from the average concentration and standard deviation of foamable samples within the transition. However, since 8.5 w/w% is the beginning of the transition phase and foaming is certain below 8 w/w%, these two values are usually referred to. The error derives from weighting errors as well as temperature variations which lead to slight differences within the samples' initial methanol take-up as well as desorption behaviour (see chapter 8).

Figure 46 also shows that for the same amount of stress application the foamability increases with desorption. At advanced desorption stages a higher stress-induced nuclei development is expected to which the effect of applied stress presumably adds. This also indicates that the effect of desorption induced stress and additional stress overlay.

In the following the foam properties resulting from samples that had been subject to additional stress before foaming compared to their unstressed control is discussed.

Figure 49 shows porosity, cell size and nucleation density depending on pre-applied stress. The major contributions to the error apart from the instrument error, are the unevenness of the foamed structure as well as differences in foam morphology that derive from deviations in the foaming procedure. Above 8 w/w% remaining methanol content, the increase in scattering results from the difficulty to take data before samples are collapsing because of the high methanol content remaining after foaming. Therefore, errors on porosity were taken from the standard deviation of five samples at both 8 w/w% for samples foamed below 8 w/w% remaining methanol concentration and the error for samples with a concentration higher than 8 w/w% was derived from five samples at 8.7 w/w% remaining methanol concentration.

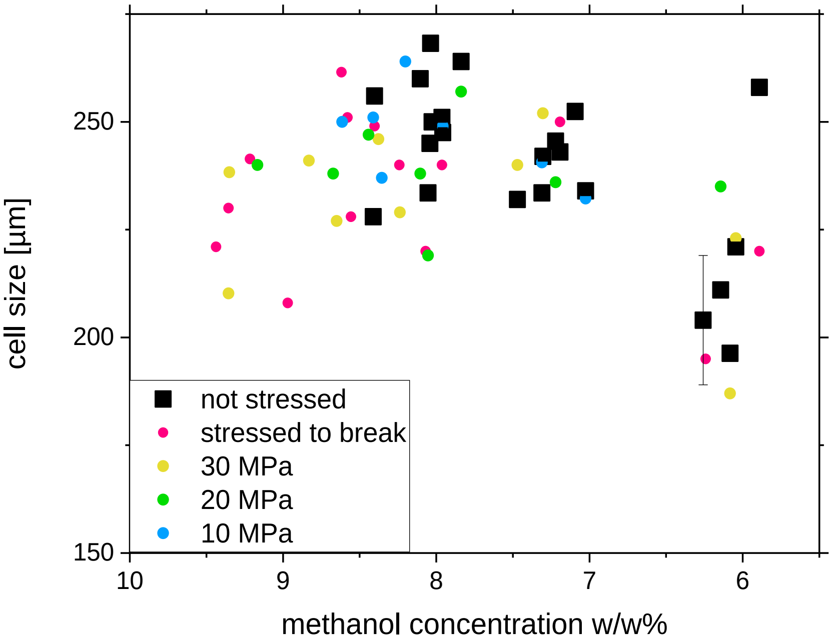

Figure 47: Porosity depending on pre-applied stress. The error on porosity increases with methanol content since samples are more likely to collapse.

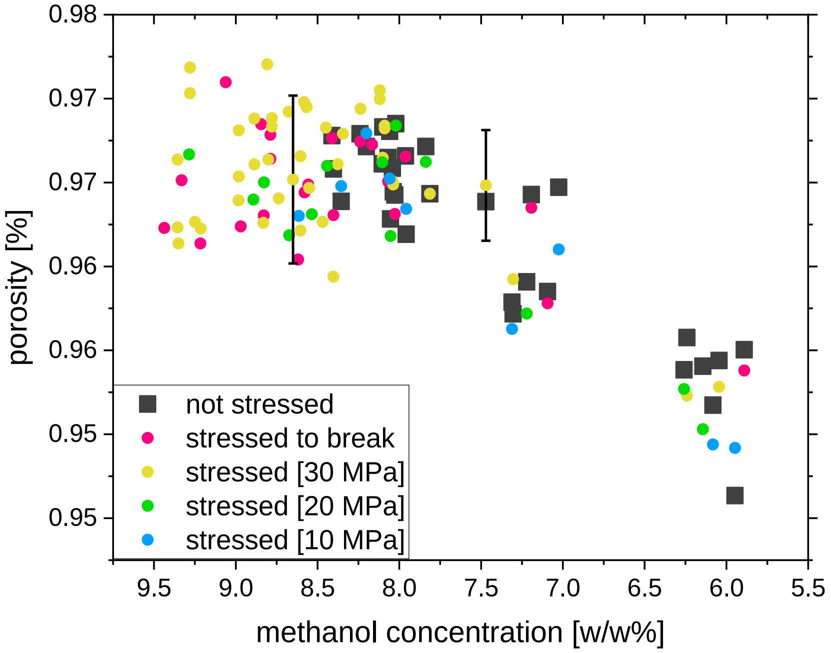

Figure 48: cell size depending on pre-applied stress. Error bars have only been inserted for only one data point to support readability of the data.

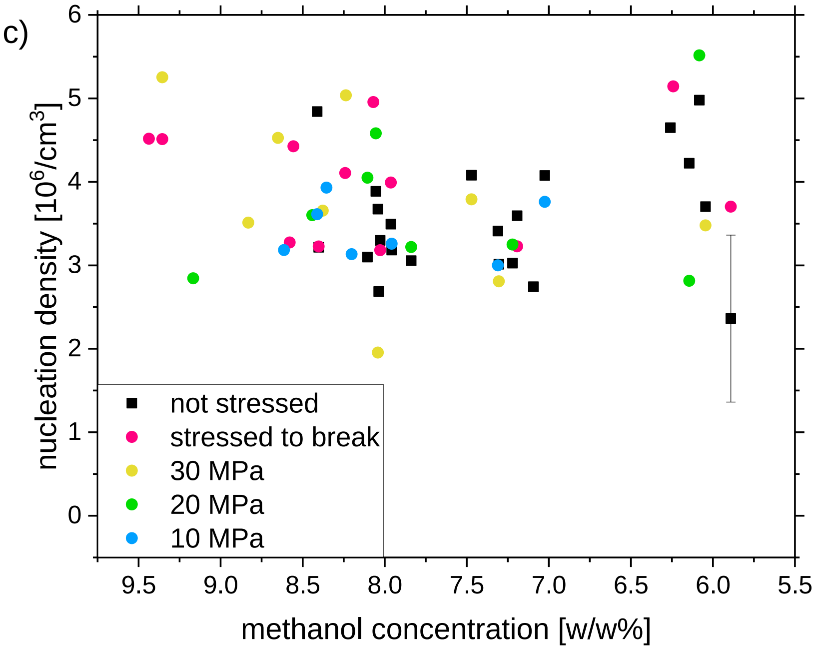

Figure 49: Nucelation density depending on pre-stress.

The error on cell size was similarly taken as the standard deviation from 5 samples foamed without pre-stress at 8 w/w%. At higher concentrations, not enough samples from one concentration were obtained to derive a meaningful standard deviation.

Above 8.5 w/w%, samples only foam homogenously after application of tensile stress. Porosity and cell size display a greater scattering. This reflects the difficulty to measure these values after foaming from higher methanol concentrations. Since the samples with higher methanol content also contain more methanol after foaming, they often collapse before cell size measurements can be taken. This could have been prevented by leaving the samples in the second oil bath for longer. But that change in procedure would have denied comparability to data from the established procedure.

Within these limitations, no firm statement can be made about any differences in foam properties between the standard foaming process and foam samples developed from precursors with a remaining methanol concentration above 8.5 w/w% after additional stress application. Cell size seems to decrease slightly for the latter, but in the light of the discussed difficulties to obtain stable samples this is likely a result of void shrinkage or collapse resulting from the surplus methanol rather than additional stress-induced nucleation. Porosity seems not to change drastically in foams foamed from above 8.5

w/w% remaining methanol concentration, when additional stress is necessary to achieve homogenous foam formation.

Below 8.5 w/w% remaining methanol content, there is no difference in cell size and porosity between the pre-stressed part of a foam and the unstressed part of the foam. This is surprising since it would have been expected that more nuclei are developing due to the additional stress. It therefore seems that the applied tensile stresses are not sufficient to develop significantly more nuclei than developed during desorption.

Below 8.5 w/w%, cell size of all foams decreases with decreasing methanol concentration. The nucleation density remains constant across the concentration range and independent of pre-stresses. This indicates that the nuclei developed during desorption are conserved. But since the methanol content further decreases, the cells supposedly expand less and turn out smaller.

6.5 Influence of additional tensile stress on birefringence

It has already been established in 5.3.1 that stresses in the elastic regime affect nuclei development. This is a strong hint that no permanent stress state is necessary to reach an increase in nucleation density.

In order to understand the influence of the additional biaxial stress, the sample stress state was measured in terms of birefringence (method employed see section 3.3.1) before and after tensile stress was applied. The measurements after tensile stress were taken after the stress release. Such measurements were conducted for different remaining methanol concentrations and at different magnitudes with a strain rate of 5 mm/min.

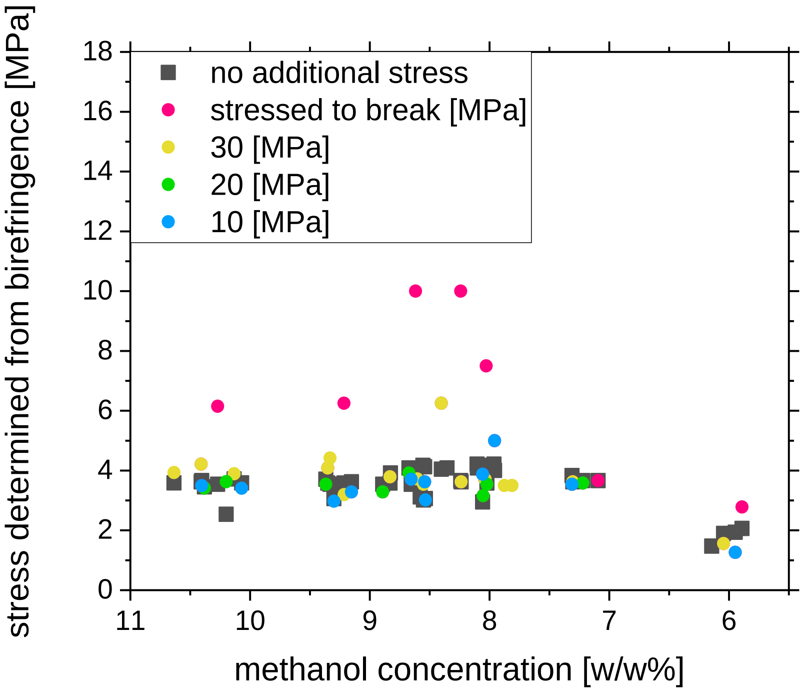

Figure 50: Stress derived from birefringence depending on concentration and pre-applied stress. As can be seen, the stress state only remains increased after stress-release at higher methanol concentrations and high pre-applied stresses. Stress to break was between 30 and 40 MPa.

Figure 50 shows the stress state in terms of birefringence before and after application of different magnitudes of tensile stress at different methanol concentrations. A permanent change in stress state after the release of the biaxial tensile stress only occurs for stresses above yield stress at methanol concentrations above 8 w/w%. A remaining change in stress state indicates that the origin of birefringence is orientational (see section 3.3.1).

Orientational birefringence cannot be translated into stress via the stress optical law (see section 3.3.1.3). Therefore, theoretically the stress state measurement for cases in which there is a difference to the unstressed state and therefore orientational is not accurate. But it shows whether the birefringence is orientational or elastic and therefore it shows whether the applied stress had an elastic or a permanent impact, which is of interest in this study.

It follows that in most cases, the impact of stress is of elastic nature, but still has an effect on nucleation (see Figure 46). This confirms the observation that it is an elastic stress that leads to a nucleation event (see section 6.3) and that post-critical nuclei growth itself is independent of the actual stress at foaming, but depends on the stress history.

6.6 Influence of pre-foaming applied pressure on foam formation

In order to see whether post-critical nuclei could also be erased, pressures between 64 and 108 MPa were applied to samples (batch 2, thickness 2 mm) with a speed of 1 mm/min via a circular disc with the radius of 0.5 cm. The samples had been previously desorped to 8 w/w% methanol content after full equilibrium absortion before foaming.

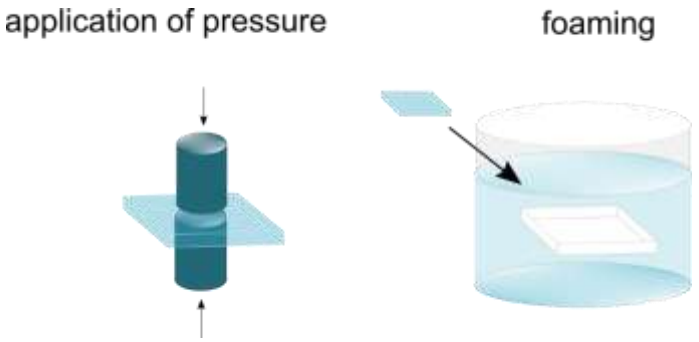

Figure 51: Application of pressure via a circular disc (r = 0.5 cm) before foaming.

Figure 52 shows the effect on foam formation of application the different pressures on the sample at 8 w/w% remaining methanol concentration before foaming.

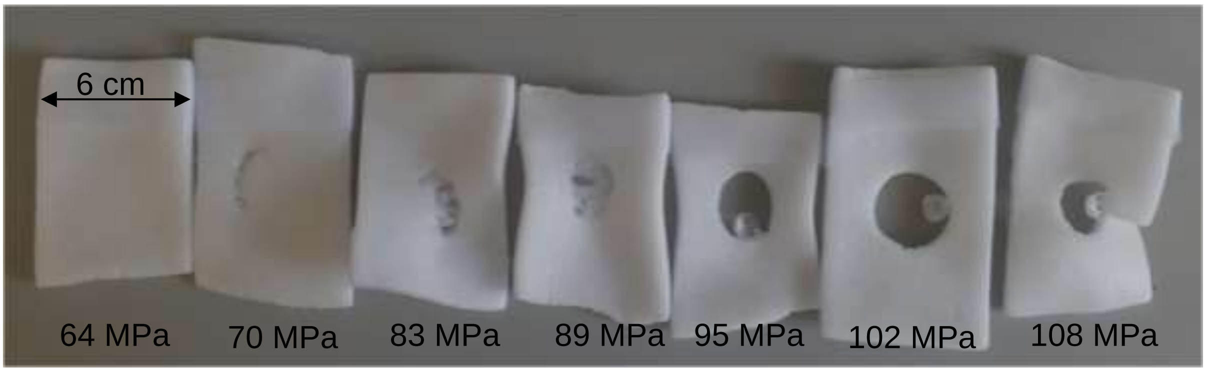

Figure 52: Effect of pre-applied pressure on foaming. From left to right: 64, 70, 76, 83, 89, 95, 102 and 108 MPa of pressure were applied after desorption to under 8 w/w% methanol content. Above 83 MPa almost no voids are created where the pressure was applied.

As can be seen above 108 MPa the sample usually cracks. Above pressures of 83 MPa almost no voids are developing after pressure application. So it seems all previously established nuclei are destroyed above this pressure and therefore foam formation is prevented. This emphasizes that nuclei are developed before foam formation and can be destroyed as well.

The pressure needed to destroy the established nuclei is about one order of magnitude higher than the stress needed to expand nuclei towards a foamable state.

Other than in the findings of Wang et al., it was not observed that pressure had any positive influence on nucleation. (Wang, Zhao, Yu, et al. 2017)

6.7 Discussion

It is somewhat surprising that additional stress treatment does lead to homogenous foam development at methanol concentrations above 8.5 w/w%, but does not affect foam properties in this case. The magnitude of applied stress affects the progress of foamable nuclei development, but not the absolute amount. The effect of applied stress on progress of nuclei development also seems to add to the progress of desorption induced stress.

It is therefore hypothesised that desorption-induced stress as well as additional stress probably contribute to the expansion of the same nuclei from a limited reservoir of post-critical nuclei towards a foamable state rather than generate new post-critical nuclei. This also means that there is a difference between post-critical and foamable nuclei and post-critical nuclei need to be brought into a foamable state (see section 2.3.2). Post-critical nuclei potentially develop upon phase separation when the polymer is taken out of methanol. Evidence for this will be discussed in section 8.2.4.

The fact that post-nuclei are rather expanded and not generated by additional stresses is also plausible in the light that nuclei generation in particular at higher viscosities at later desorption stages is most likely subject to much higher energy consumption compared to expansion of already existing nuclei. As discussed, there is no fully quantifying approach about its exact magnitude since nucleation theory is no fully quantitative theory (see section 2.1.4). However, an approach by Estravis et al. to quantify the stress needed to form a nucleus within a polymer was described by the polymer's internal pressure.(Estravis et al. 2020) In the case of PMMA it was calculated to be 41 MPa whereas the stress needed to expand an already developed small nucleus was calculated to be around 10 MPa by van Loock et al., which is much closer to the here applied hydrostatic stress of around 1 MPa (see section 9.4). (Van Loock and Fleck 2018) This supports the claim that the here applied additional stresses lead to nuclei expansion rather than nuclei development.

In this specific case, it seems the reservoir of post-critical nuclei is already exploited by the impact of desorption induced stresses. Therefore, further stresses only accelerate nuclei development towards foamable nuclei, but do not increase their number. That would explain why, the impact of desorption-induced stress and additional stress initially seems to combine during the course of desorption, but once the reservoir is used up, no additional nuclei can be expanded and no further change in foam structure or nucleation density is observed. This hypothesis will be further discussed based on the results in chapters 7 and 8.

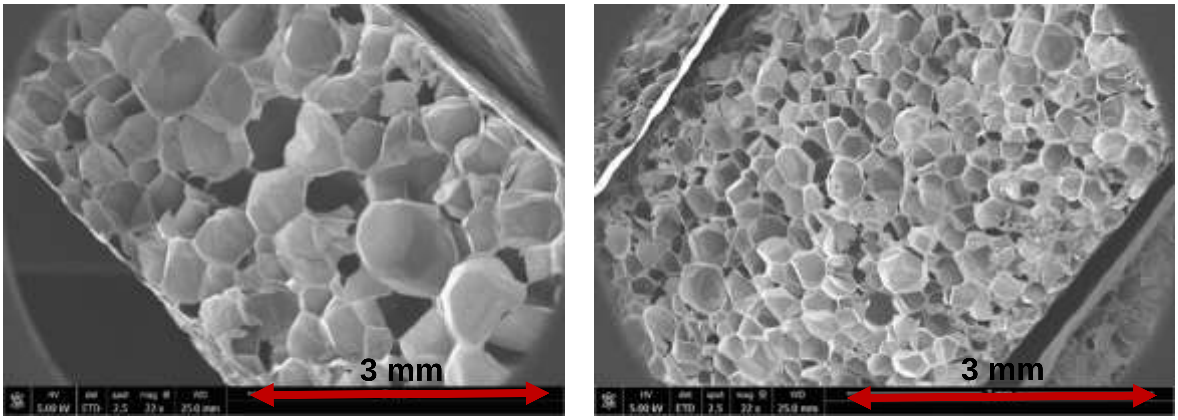

Figure 53: Left: SEM of foam from another PMMA (Perspex® 1.5 mm) resulting from the standard procedure. Average cell size: 430 µm. Right: Foam resulting from the stressed part (25 MPa) of the sample. Average cell size: 230 µm.

However, it had been observed for cast PMMA of the same commercial brand and type, but of a different thickness (cast Perspex® 1.5 mm thickness) that application of additional stress leads to a decrease in cell size (see Figure 53). It seems in this case the nucleation density increased and therefore cell size decreased after application of tensile stress. An explanation within the so far hypothesized theory about nuclei development would be that for this type of PMMA the reservoir of developed post-critical nuclei is not already emptied by desorption induced stresses. And therefore, additional tensile stress can develop more post-critical nuclei towards foamable nuclei and therefore the nucleation density is increased and cell size decreased. Another reason could be that for this PMMA the tensile stress also achieves additional post-critical nuclei that also turn into foamable nuclei, which would also increase nucleation density and decrease cell size.

Since the PMMA for which these observations had been made was difficult to obtain it has not been further employed for experiments and its properties have not been determined. However, it seems highly possible that it also has slightly different properties that play a major role for the development of the amount of post-critical nuclei. It is not certain whether this is also connected to the molecular weight as it seems to be the case for the different batches 1 and 2 (see section 4.3.3 and 4.5) For this the PMMA would have had to be analysed more rigorously.

6.8 Summary

Additional tensile stress was applied to methanol desorbing PMMA samples by a tensile testing machine before foaming at different remaining methanol concentrations with different magnitudes. The stress was only briefly applied and released before foaming.

It was found that application of such applied additional tensile stress leads to an increase in void formation in the stressed part of the sample compared to the unstressed part above 8.5 w/w% remaining methanol concentration. The number of voids increases with magnitude of applied stress at remaining methanol concentrations above 8.5 w/w%, but does not exceed the amount of voids reached after desorption to 8 w/w% remaining methanol concentration. Homogenous foamability can already be reached at 9.43 w/w% remaining methanol concentration. Once homogenous foamability is achieved, no difference in foam properties between stressed and not stressed sample is observed.

It was concluded and hypothesized that there is a reservoir of post-critical nuclei resulting from phase separation, which are expanded towards a foamable state by hydrostatic tension until the reservoir is empty. Generation of post-critical nuclei is potentially subject to higher stresses than necessary for nuclei expansion. Desorption induced stresses seem to be sufficient to empty the reservoir and additional tensile stresses do not seem to be high enough to generate new post-critical nuclei within the here employed PMMA (see section 3.1.1). Therefore, additional stresses only advance post-critical nuclei expansion, but do not lead to significantly more void formation once the reservoir is emptied.

For a different PMMA (1.5 mm cast Perspex®), foam property differences following tensile stress application have been observed. Therefore, there might be cases in which additional post-critical nuclei either develop or expand from the reservoir as a result of additional stress application.

It was found with the help of birefringence measurements that the applied tensile stress has an influence on void formation within the elastic regime in which the birefringence is of elastic nature. It can therefore be assumed that the main impact of additional stresses is not resulting from void formation in the sense of crazing.

Regarding the application of additional pressure, it was found that it most likely erases nucleation if applied above 64 MPa before foaming. This indicates that nuclei can also be destroyed before foaming.

7. Stress and foam development following a liquid nitrogen quench

The initial plan to produce void formation in methanol-filled PMMA was to generate temperature-induced phase-separation (TIPS) by a liquid nitrogen quench. While carrying out these initial experiments, it had been observed that a liquid nitrogen quench leads to a stress state and void development corresponding to an advanced desorption state compared to an unquenched sample. We refer to this as “advanced void development” in the rest of the chapter (see section 4.1). Following the observations from the previous chapters (see sections 5.4 and 6.8) that suggest that stresses contribute to void development, the question arose as to how far stress-development might also be a factor in the case of void formation following a liquid nitrogen quench.

Therefore, the stress development following a liquid nitrogen quench and its consequences for void formation are discussed in this chapter.

Unfortunately, the foam characterization for this chapter had been interrupted by the outbreak of SARS-CoV-2 and only small data sets could be collected for cell size and nucleation densities in this chapter.

7.1 Method

In order to study the influence of a liquid nitrogen quench (to boiling point −196 °C), half of a strip PMMA (batch 2, 140×20×2 mm^3) (see section 3.1.1) was quenched in liquid nitrogen for 10 s either after (section 7.3.2) or before (section 7.3.4) desorption to lower methanol concentrations. The samples were then put in a silicone oil bath at 170 °C for 60 s to expand any voids which may have formed. For most experiments there was primarily an interest in the amount of foamed voids in a not yet homogenously foamable sample. At these higher methanol concentrations the stabilization step at 115 °C wouldn’t be sufficient to stabilize the voids. Therefore, a stabilization process was only applied in cases in which a homogenous foam was made. To have a control, only half of the sample strips were inserted into liquid nitrogen in order to be able to compare them directly to the strips in an untreated state.

7.2 Initial stress development resulting from liquid nitrogen quench

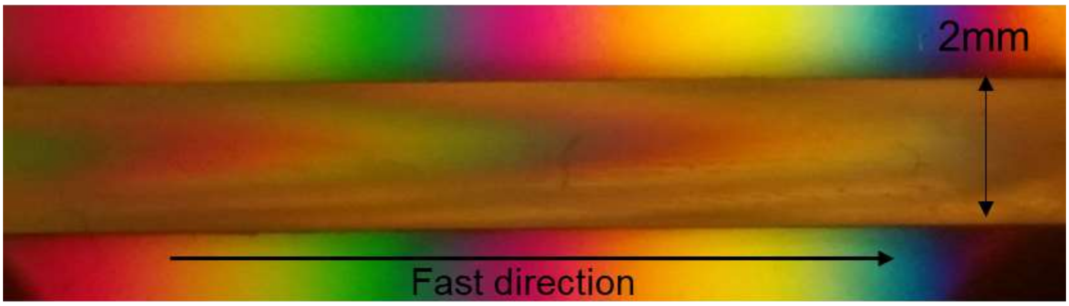

Figure 54: Birefringence colours from sample core under stress during warming up following the liquid nitrogen quench. The opacity results from water vapour.

In order to determine the stress state after a liquid nitrogen quench, birefringence measurements were taken after the liquid nitrogen quench. Due to quickly developing water vapour on the sample surfaces, it was difficult to quantify the magnitude of birefringence precisely. However, a tensile stress state in the sample core (see Figure 54) was unambiguously observed. It seems to result from the warming up of the sample after the quench as will be explained below.

The thermal expansion coefficient for PMMA and methanol is positive. Therefore, it contracts for a temperature decrease and expands with a temperature increase. (Dortmund Data Bank) Therefore, it is supposed that a liquid nitrogen quench initially induces a compressive state in the sample core since the outer layer contracts first. Once the sample warms up from the edges, it expands and sets the core under tension. Differences in layer density are therefore essentially an analogue source of stress compared to desorption-induced stresses.

Therefore, it seems likely that the density differences resulting from the temperature increase after the liquid nitrogen quench are the source of the observed tensile stress state. This hypothesis will be discussed along the observations made for foam formation associated with a liquid nitrogen treatment.

7.3 Void development

7.3.1 Effect of temperature increase following a liquid nitrogen quench

If a liquid nitrogen quench is applied at high methanol concentrations and the sample is immersed into a silicone oil bath after a short desorption time (30-60 s, necessity discussed in the next section 7.3.2) at 170 °C, it was observed (see Figure 49) that voids only develop on the side of sample which was in contact with the bottom of the silicone oil bath whilst foaming.

Figure 55: Void development at high concentrations only appearing on the face of the sample that had been in contact with the bottom of the silicone oil bath.

The reason is most likely that the bottom of the oil bath, from which the oil bath is heated is at a higher temperature and therefore induces a larger temperature difference to the sample than the surrounding oil bath. This presumably results into a higher thermal expansion of the outer sample layers in touch with the bottom of the oil bath and higher stresses that are sufficient for nuclei expansion. This is a strong hint that it is the temperature increase after a liquid nitrogen quench that provides for a tensile stress state that enables nuclei expansion.

In order to see whether a temperature increase following a liquid nitrogen dip would be beneficial for nuclei expansion, a fully equilibrated sample was partially immersed into an oil bath at 115 °C for 10 s without touching the bottom following the liquid nitrogen quench in order to generate a fast temperature increase. Afterwards, the sample was directly taken into the silicone oil bath at 170 °C for 60 s with contact to the bottom. No voids are visible after the dip at 115 °C. But voids appear on all sample faces for the consequent dip at 170 °C (one face touching bottom). This confirms the suspicion that the additional heat input at 115 °C leads to thermal expansion and therefore tensile stresses on the sample surfaces that lead to foamable nuclei. This then leads to foamable nuclei on all faces of the sample, when the sample is immersed into the oil bath at 170°C (Figure 56). This strongly suggests that in the case of a liquid nitrogen dip, the subsequent increase in temperature is contributing to foamable nuclei development.

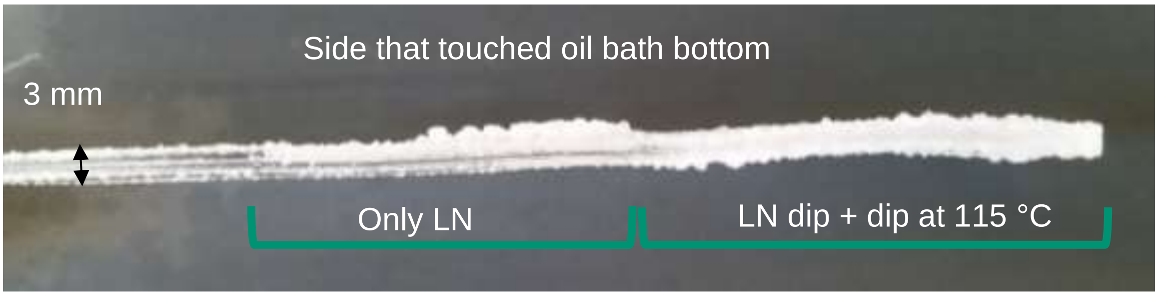

Figure 56: Sample subjected to liquid nitrogen quench after methanol absorption to equilibrium and subsequently foamed at 170 °C. The tip of the sample had additionally been subject to warming up at 115 °C before foaming at 170 °C following the quench. As can be seen, the additional warming up leads to bubble formation on all faces.

It is a bit surprising that this thermal pre-treatment is necessary to achieve homogenous void formation across the sample, as theoretically the silicone oil bath at 170 °C already provides a temperature increase itself. But it seems that the stress development is compensated by the sample becoming rubbery at these high temperatures before stresses develop. At the bottom of the silicone oil bath however, the heat transfer is faster and stresses and therefore voids might develop before the sample becomes fully rubbery.

7.3.2 Void development following a liquid nitrogen quench after methanol desorption

As can be seen in Figure 57, if a liquid nitrogen quench is applied after methanol desorption to lower methanol concentrations, the onset of void development in the previously quenched part occurs at almost equilibrium methanol concentration and is much more pronounced than after the application of additional tensile stress (see

Figure 42). It seems therefore that a liquid nitrogen quench leads to higher hydrostatic tensions than maximum applicable tensile stress at high methanol concentrations.

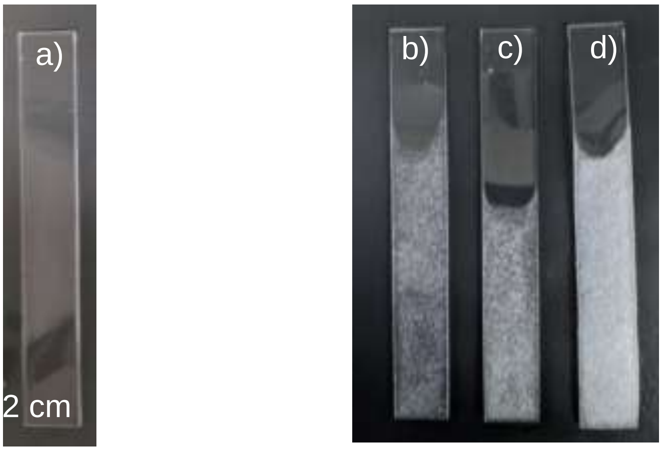

Figure 57: a): liquid nitrogen quench at full equilibrium concentration and immediate insertion into oil bath at 170 °C. b),c),d) : liquid nitrogen quench imposed after desorption at 25 °C to 18.4, 18.3, 17.8 w/w% which equals desorption times of 40 s, 3 min and 5 min.

However, a small desorption time (30-60 s) before the quench is necessary to achieve void formation. The reason could be that the skin itself, which would develop on that time scale, provides a tensile stress state to which the stress deriving from the liquid nitrogen quench can add to. The combined impact is probably necessary to achieve a high enough stress state for void development.

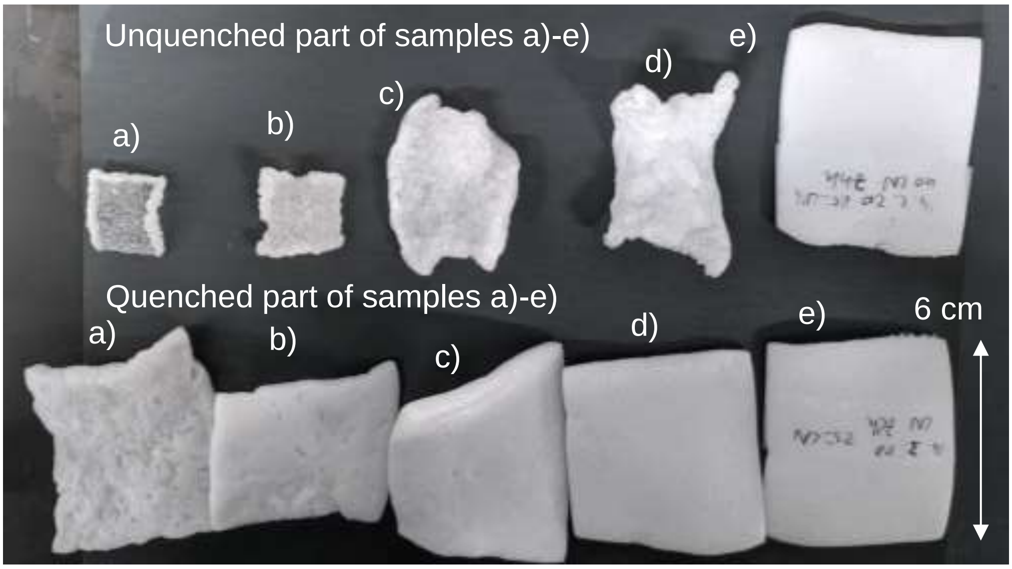

Figure 58: Top row: Part of samples a)-e) that had been subject to liquid nitrogen quench after desorption to lower methanol concentrations; bottom row: corresponding piece of the same samples a)-e) that had not been subject to a liquid nitrogen quench. Concentration at liquid nitrogen quench and foaming from left to right: 11.1, 10.1, 9.1, 8.6, 8.2 w/w%.

Figure 58 shows samples that had been subject to a liquid nitrogen quench after desorption to lower methanol concentrations and the unquenched counterparts. Similar to the application of tensile stress, the void development is initially advanced in the quenched part depending on the desorption state. This confirms the claim made in section 6.7 that the impact of stresses on nuclei expansion superimpose.

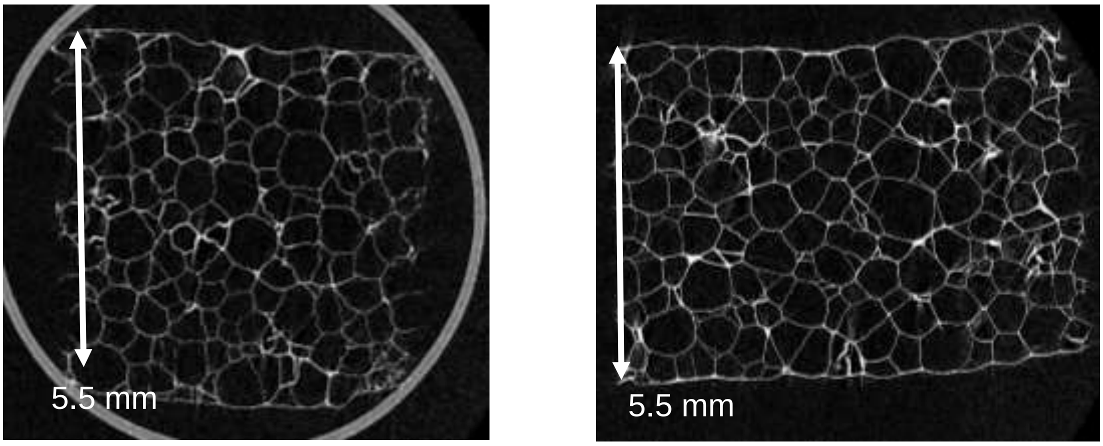

Figure 59: X-ray microtomographic images of foams. Left: foam structure of sample subject to no liquid nitrogen quench before foaming at 8.2 w/w% after desorption at 25 °C. Right: Foam structure after a quench at 8.2 w/w% remaining methanol concentration.

Once homogenous foaming in the untreated part is possible below 8.5 w/w% remaining methanol concentration, cell size, porosity and nucleation density as well as general foam structure seem not to be significantly different from the unquenched part (see Figure 59 and Figure 60, data points taken from batch 2 samples). This is in accordance with the hypothesis (see section 6.7) that there is a reservoir of post-critical nuclei from which nuclei are gradually expanded towards foamable nuclei. But even a quench is not generating sufficiently high hydrostatic tensions to develop significantly more post-critical nuclei to induce a change in foam properties.

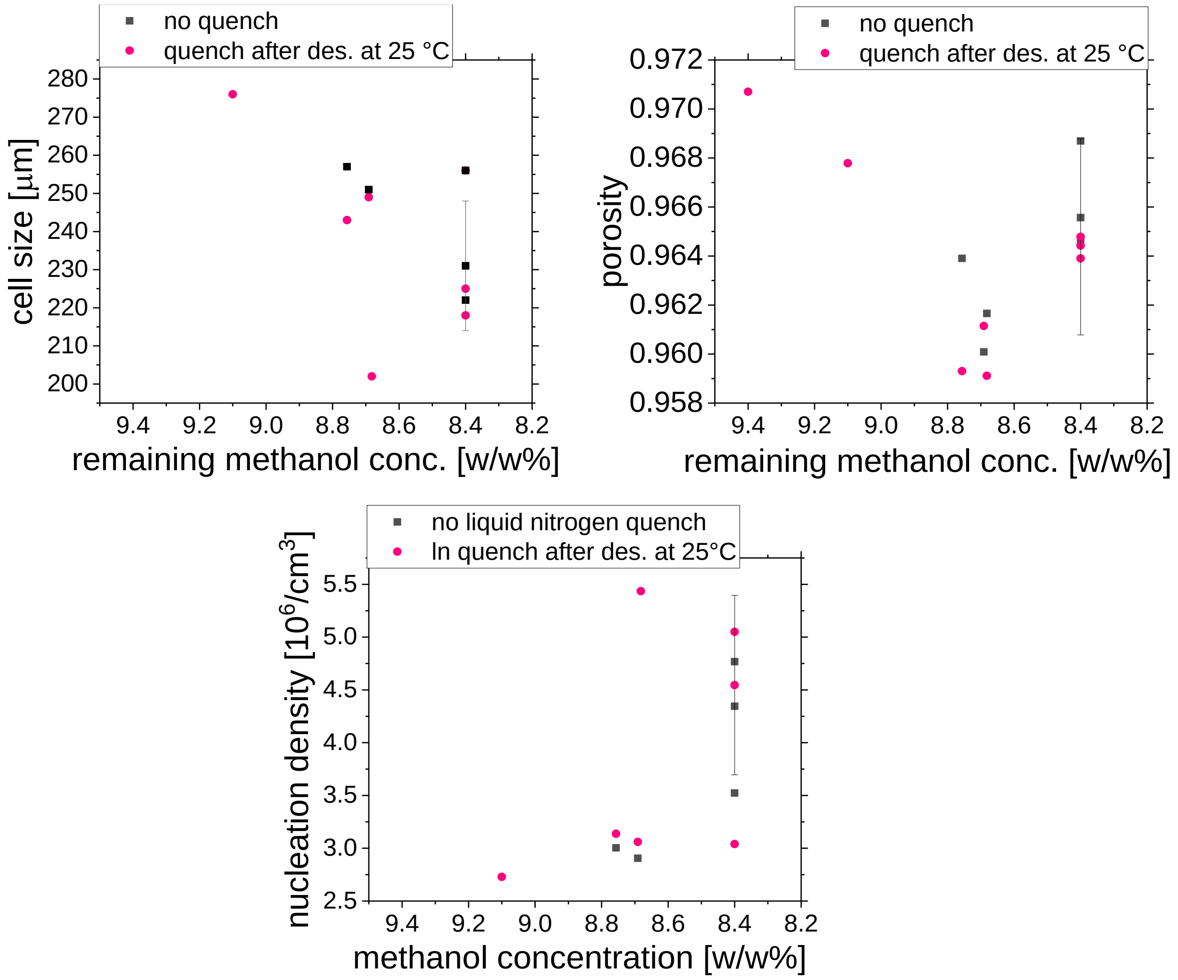

Figure 60: Comparison of cell size, porosity and nucleation density of foams resulting with or without a liquid nitrogen quench after methanol desorption at 25 °C.

The data collection for the foam properties of a foam resulting after a liquid nitrogen quench in dependence of concentration (Figure 60) was interrupted by the lab closure due to SARS-CoV-2. Therefore, there are not enough data points to fully exclude differences in foam properties of foams foamed after a quench above 8.5 w/w% remaining methanol concentration. Furthermore, it could not be determined up to which methanol concentration homogenous foaming is possible in the case of a liquid nitrogen quench after desorption to lower methanol concentrations. The liquid nitrogen quench seems to have a more significant impact compared to the application of tensile stress. Therefore, it can be expected that the remaining methanol content at which homogenous foam formation can be reached is higher in the case of a liquid nitrogen quench compared applied tensile stress in which case homogenous foaming can be reached up to 9.43 w/w% remaining methanol content. These questions could not be fully resolved.

7.3.3 Void development following a liquid nitrogen quench before desorption at 25 °C

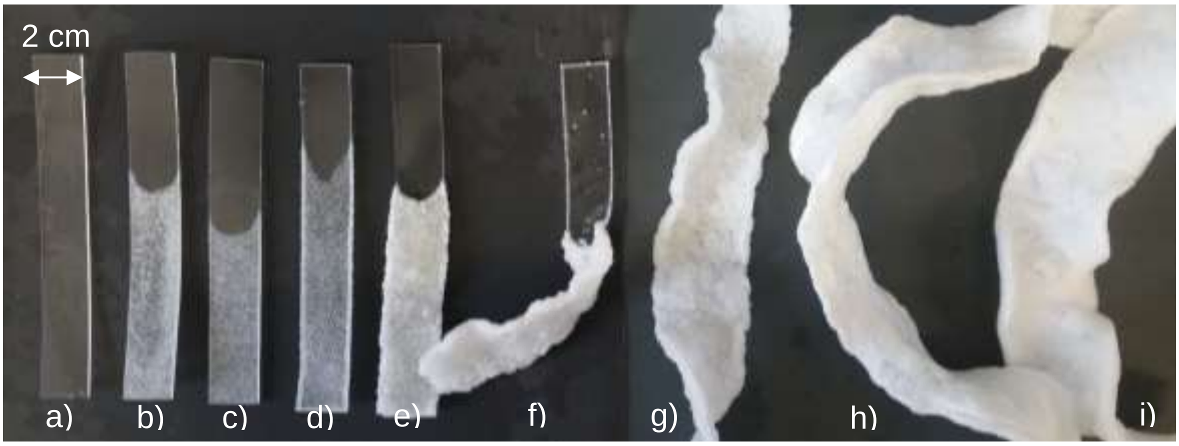

Figure 61: Foaming at 170 °C for 60 s after a liquid nitrogen quench followed by desorption at 25 °C. From left to right the samples contained a) 18.5, b) 17.9, c) 16.9, d) 15.4, e) 13.4, f) 10.4, g) 9.7, h) 9.0, i) 8.7 w/w%. The bottom part is the quenched part.

Figure 61 shows samples foamed at 170 °C for 60 s of which one part had been subject to a liquid nitrogen quench before desorption to different methanol concentrations. Unless in the case when no desorption after the quench was allowed (left sample in Figure 61), the quenched parts developed void formation in advance of the unquenched part after desorption to lower methanol concentrations.

A short desorption desorption time (30-60 s) after the liquid nitrogen quench is necessary to achieve nucleation. Most likely it is necessary for a sufficient increase in temperature to induce stress-development. This is particularly confirmed by the fact that if the sample is put on a sample holder with a grid pattern, voids are formed were the sample was in contact with the grid and the heat transfer is higher compared to where the grid holes were (see Figure 62).

Void development occurs homogenously across the quenched part of the sample with exception of the early stages of desorption (e.g. second strip from left in Figure 61). In these cases, the stress development after the liquid nitrogen quench resulting from the temperature increase to room temperature is overlaid with the effect of the temperature increase resulting from the bottom of the oil bath (see previous section). At later desorption stages, the stress development leading to nuclei development solely derives from the temperature increase to room temperature. Therefore, the void formation in the early stages does not occur homogenously.

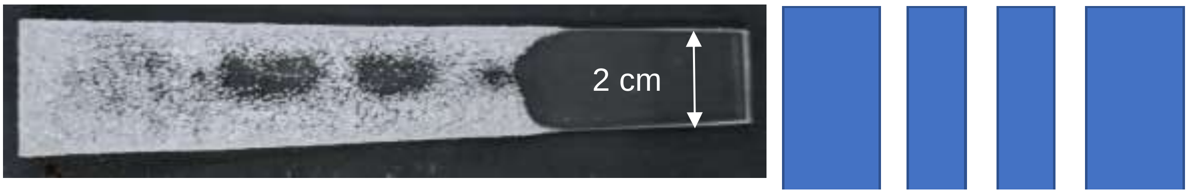

Figure 62: Void distribution in a sample that had been subject to a liquid nitrogen quench and left of a structured sample holder (structure right) for 5min before foaming.

The fact that voids develop in the quenched part upon foaming if the quench is applied before desorption is a big difference to the case of tensile stress application in which case no additional void formation could be observed in the stressed part if tensile stress was applied before desorption to lower methanol concentrations (see Figure 44). It again indicates that the hydrostatic stresses resulting from a liquid nitrogen quench are higher and therefore expand a higher number of nuclei at high methanol concentrations.

The most interesting observation is that the amount of void formation following further desorption initially increases gradually and only in the pre-quenched part. It therefore seems the nuclei in the quenched part are already in a more advanced state towards foamability and smaller desorption-induced stresses are sufficient to bring those nuclei gradually into a foamable state. It appears that the desorption-induced stresses superimpose with the stresses resulting from the previously applied quench and their combination leads to nuclei development into a foamable state. This is in accordance with the suggestion made in section 6.7 that the impact of stress on foamable nuclei development superimposes. It also contributes to the assumption (see sections 2.3.2 and 6.7) that post-critical nuclei are not necessarily foamable into foam cells upon the applicable foaming conditions, but are gradually expanded towards a foamable state by expansive stresses. Therefore, a difference between post-critical and foamable nuclei is assumed.

A nucleus state sufficient for foaming in this case seems to be reached gradually by the quench-induced (thermal) expansive stresses and the subsequent desorption-induced expansive stresses. Such applied stresses could also play a role for solid-state foaming. In solid state foaming the “thermal conditioning” (see 2.2.3.1 and (Stéphane Costeux 2014)) between the steps of the two-step process potentially also enhances the expansion of post-critical nuclei into foam cells.

Another interesting outcome of this experiment is that the difference in amount of void formation in the quenched part compared to the unquenched part decreases during desorption. And a state of homogenous foam formation is reached in the unquenched and quenched part at the same methanol concentration. This indicates that the quench does not lead to a sustained expansion of all postcritical nuclei and some might shrink back unless the quenched sample is kept at lower temperatures than 25 °C (see next section 7.3.4). Smaller nuclei have a high surface to volume ratio and are therefore more likely to shrink back on a shorter time scale.

Probably like depicted in the schematics below (Figure 64 to Figure 66), a quench expands postcritical nuclei (Figure 64). Partly they transition into a foamable state and further desorption brings more nuclei in the quenched and unquenched part towards a foamable state (Figure 65). But from the quenched ones some smaller nuclei shrink back on a shorter time scale and need to be re-expanded by desorption-induced stresses to become foamable nuclei. Therefore, at further advanced desorption stages, the amount of desorption-induced nuclei that are in a foamable state is almost equivalent with the amount of nuclei resulting from a quench followed by desorption (Figure 66).

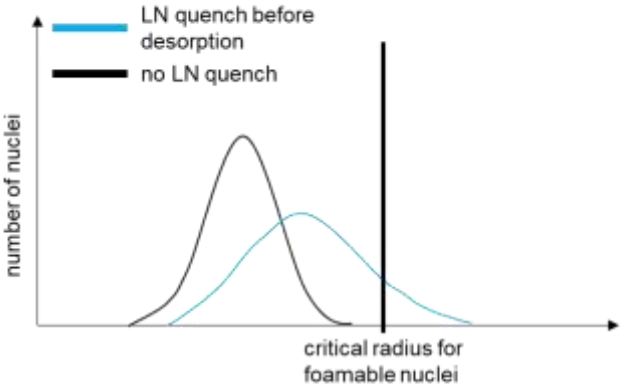

Figure 63: Schematic of potential influence of liquid nitrogen quench before methanol desorption on void development. a) the quench expands several postcritical nuclei towards a foamable state compared to the unquenched part.

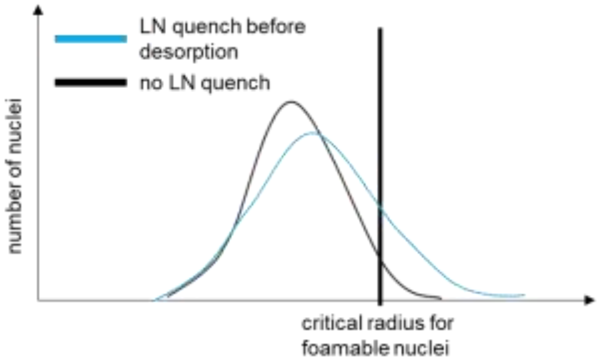

Figure 64: Upon further desorption, desorption-induced stresses bring nuclei in a foamable state in the quenched and in the unquenched part.

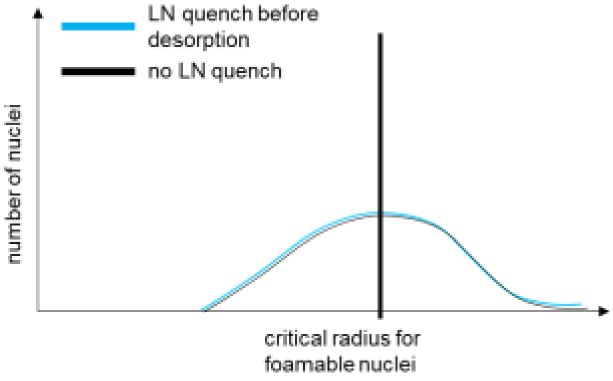

Figure 65: The expanded nuclei partly shrink back and the difference in amount of foamable nuclei between the quenched and the unquenched sample part fades.

Similar to the case of application of additional tensile stress (see chapter 6) and the quench applied after desorption, the foam properties resulting if the quench is applied before desorption are the same for quenched and unquenched part (Figure 66, see more data and discussion next section, Figure 86 and Figure 60).

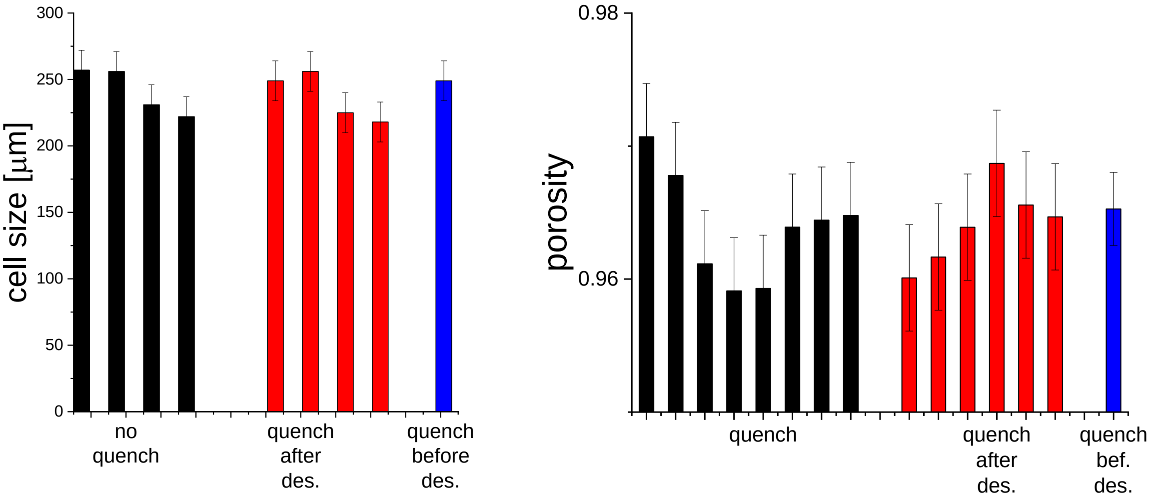

Figure 66: Cell size and porosity for foams foamed without and with a quench before or after desorption to 8 w/w% remaining methanol concentration.

This indicates that the same number of foamable nuclei is developed irrespective of when the quench is applied that has otherwise a stronger impact than the application of tensile stress. This again confirms the hypothesis that there might be a limit on the amount of post-critical nuclei. Most likely also the quench-induced stresses are not high enough to either generate more post-critical nuclei and therefore different foam properties.

The important take away is that additional stresses seem to contribute to post-critical nuclei expansion and desorption-induced stresses continue to expand these pre-expanded nuclei gradually. Therefore, nuclei development into foamable nuclei is a gradual process in which the contributing expansive stresses superimpose in their impact.

7.3.4 Void development following a liquid nitrogen quench before desorption at 5 °C

Similar to the previous section, samples were subject to a liquid nitrogen quench before desorption. In this section however, they were desorbed to lower methanol concentrations at 5 °C. They were then foamed for 60 s at 170 °C. Figure 67 shows how the foam structure develops if the liquid nitrogen quench is applied before desorption at 5 °C.

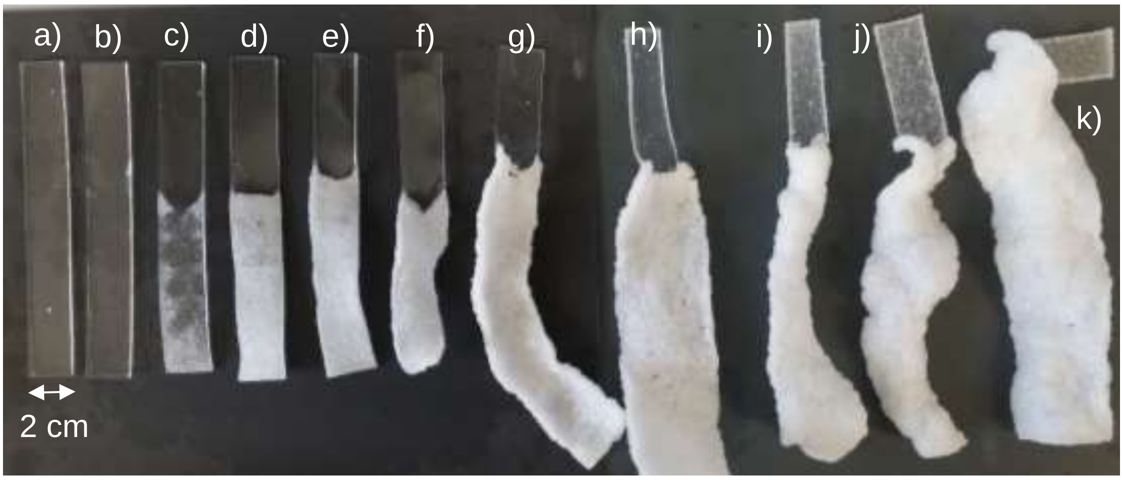

Figure 67: Samples a)-k) foamed at 170 °C for 60 s following desorption at 5 °C after a liquid nitrogen quench. From left to right: a): 18.5, b):18.2, c):17.9, d):17.4, e):16.5, f):15.9, g):14.4, h):11.8, i):10.6, j):10.1, k):9.2 w/w%.

The amount void formation at high methanol concentrations is more significant in the quenched part if the samples are desorbed at 5 °C instead of 25 °C after the liquid nitrogen quench. A porous (but not fully homogenous) structure is already achieved at around 14 w/w% (Figure 67, sample g)) remaining methanol concentration compared to 10 w/w% for desorption at 25 °C following a liquid nitrogen quench (see Figure 61, sample f)).

This is most likely a nuclei conservation effect since at 5 °C, the sample is fully under T_g and generated nuclei are less likely to collapse below T_g. Therefore, during the warming at 5 °C, more pre-expanded nuclei seem to be conserved and don’t shrink back as it was discussed in the previous section 7.3.3.

However, it has also been observed, that in the very early stages of desorption the void formation in the quenched part at 5 °C desorption temperature seems to be slower (see Figure 67 samples a) b) c) and Figure 61 samples a), b), c)). This could be resulting from the fact that the sample is fully below T_g at 5 °C and stress induced nuclei expansion is therefore initially slower. Furthermore, the lower temperature difference from – 196 °C to 5 °C compared to 25 °C results in a slower warming up process at 5 °C that could result in slower foamable nuclei formation than observed for warming up at 25 °C.

Another observation from the comparison of later stages of void development of the unquenched part between desorption at 5 and 25 °C (Figure 67 sample k) and Figure 61 sample g) and h)) was that nuclei development in the unquenched part at 5 °C is not as advanced as nuclei development at 25 °C desorption temperature at the same remaining methanol concentration at later stages of desorption. Unfortunately, the lab closure following the outbreak of SARS-CoV-2 interrupted further data collection that was supposed to obtain further evidence about the foamability after desorption at 5 °C without a quench event. However, the birefringence data presented in the next section 7.4 reveals that at 5 °C desorption temperature, almost no tensile stress state is developed in the sample core. This explains and confirms the observation that at 5 °C desorption temperature, fewer stress-induced nuclei seem to develop without a quench before desorption.

Figure 68 - Figure 70 show a comparison of foam properties resulting from either no quench and desorption at 25 °C, a quench before desorption at 5 °C and 25 °C as well as a quench after desorption at 25 °C.

The data collection for the foam characteristics had also been affected by lab closure following the outbreak of SARS-CoV-2. Therefore, data is only taken from one sample per data point and only full data sets regarding the dependence on T_1 could be collected for a quench before desorption at 5 and 25 °C.

However, the data still reveals that the liquid nitrogen quench irrespective of 5 or 25 °C desorption temperature seems not to change the foam properties in terms of cell size, porosity and nucleation density significantly as soon as full foamability is reached (see

Figure 70). Therefore, 5 °C desorption temperature after a liquid nitrogen quench seems not to be an influencing factor for the properties of the resulting homogenous foams.

Interestingly, the samples resulting from a quench followed by desorption at 25 °C seem to foam at lower foaming temperatures T_1 (145 °C instead of 155 °C) compared to samples desorbed at 5 °C following a quench. The reason could be that the sample is more rubbery at 25 °C desorption temperature which leads to nuclei shrinkage, but also facilitates nuclei expansion once desorption induced stresses emerge. Also, at 5 °C desorption temperature there seem to be almost no desorption induced stresses (see Figure 71). Therefore, the developed nuclei at 25 °C could be bigger and therefore foam at lower foaming temperatures.

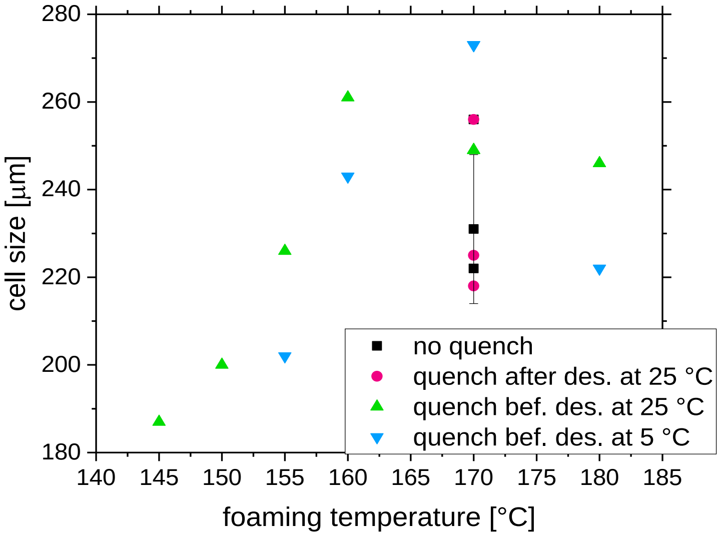

Figure 68: Comparison of cell size of foams foamed from samples that had been subject to liquid nitrogen quench before desorption at 5 and 25 °C, a liquid nitrogen quench after desorption at 25 °C and desorption at 25 °C after no quench at all.

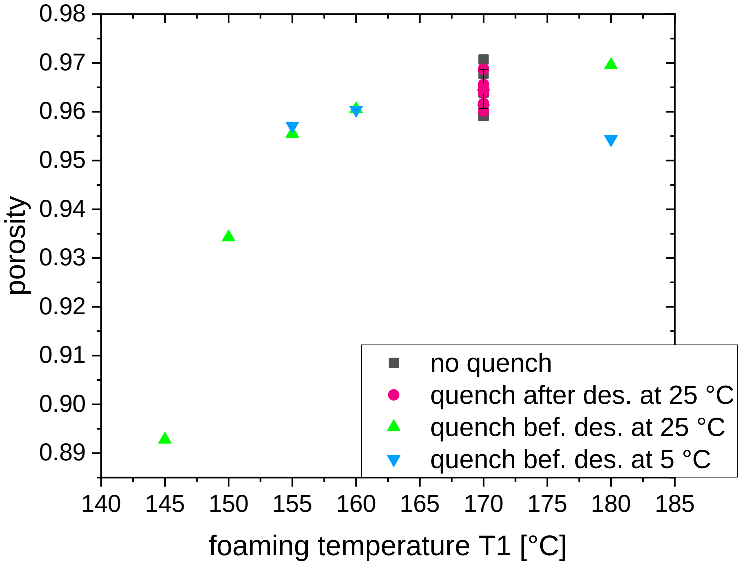

Figure 69: Comparison of porosities of foams foamed from samples that had been subject to liquid nitrogen quench before desorption at 5 and 25 °C, a liquid nitrogen quench after desorption at 25 °C and desorption at 25 °C after no quench at all.

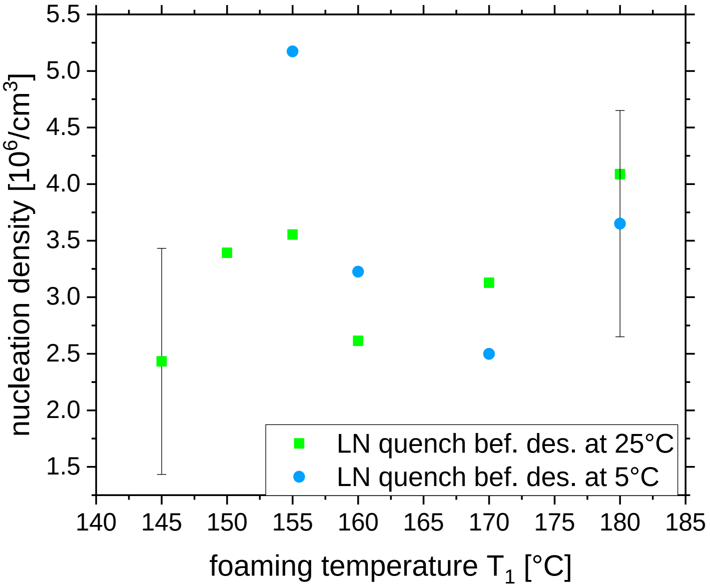

Figure 70: Comparison of nucleation densties of foams foamed from samples that had been subject to liquid nitrogen quench before desorption at 5 and 25 °C.

7.4 Stress development and geometric changes after liquid nitrogen quench

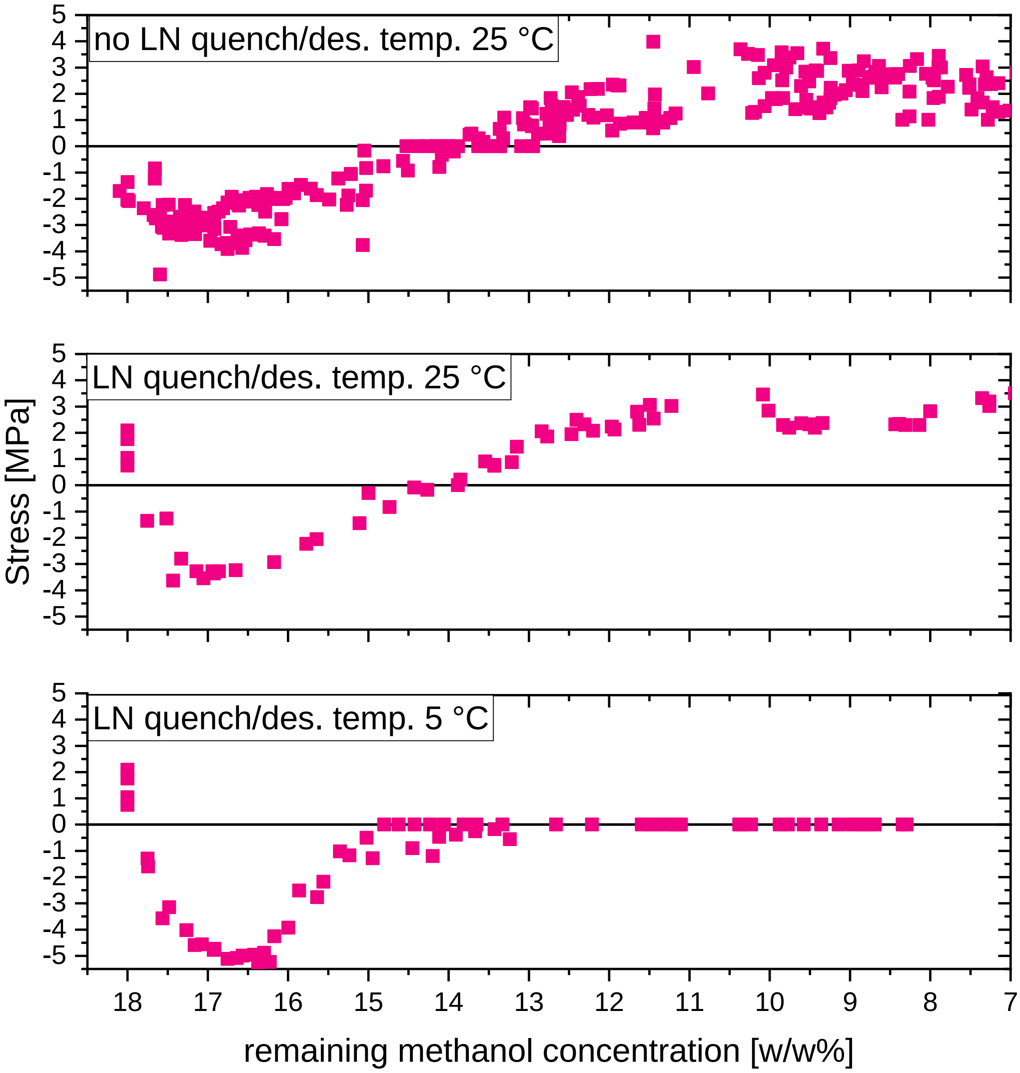

Figure 71: Stress development after a liquid nitrogen quench for desorption at 5 and 25 °C compared to no quench.

Figure 71 shows the stress development resulting from desorption at 5 °C or 25 °C following a liquid nitrogen quench at equilibrium methanol concentration. For comparison, the data for desorption at 25 °C without a quench have been plotted as well. Please note that no correction of the stress optical coefficient was applied for all data, since it is difficult to tell in how far the quench below T_g and cooling at 5 °C would have influenced the stress-optical coefficient. Potentially, it is close to $4\cdot10^{-12}$ m^2 N^{-1} following the liquid nitrogen quench and desorption at 5 °C because the lower temperature leads to a higher viscosity. Therefore, the magnitude of the stress state might be quite accurate or even underestimated for desorption at 5 °C and a little overestimated for 25 °C desorption temperature.

Therefore, it can be said that the liquid nitrogen quench followed by desorption at 5 °C leads to significantly higher compressive stresses in the sample core. The reason for this is most likely that at 5 °C, the sample is fully below its glass transition. Therefore, pressure cannot be released through geometric changes and builds up to a greater extend. This matches with the fact that there is no initial increase in sample thickness for the sample stored at 5 °C following a liquid nitrogen quench (see Figure 72). Consequently, the thickness decrease is also not different from the width decrease.

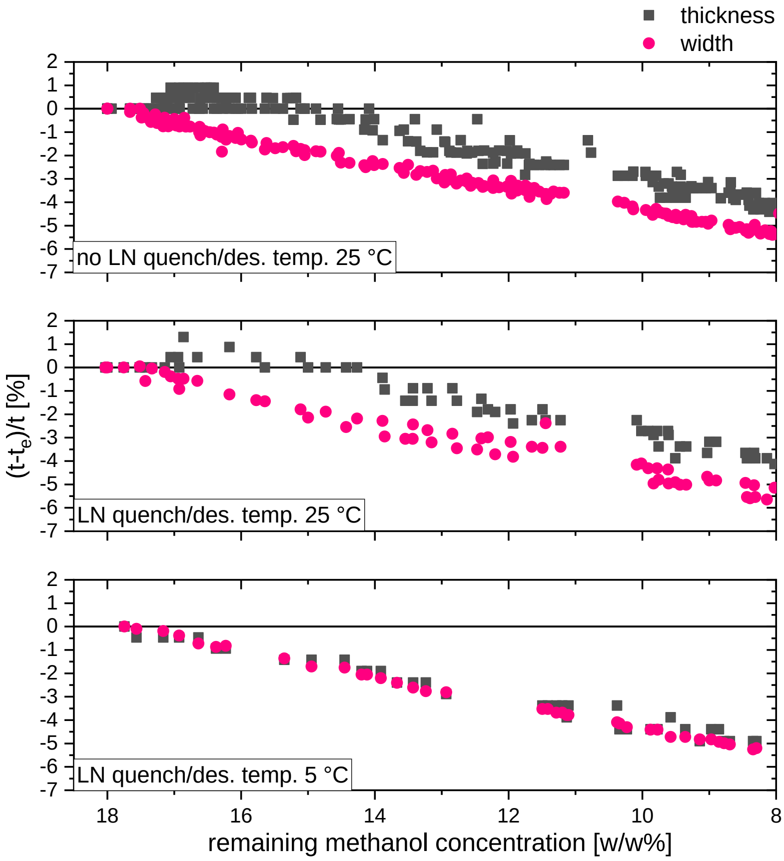

Figure 72: Geometry changes upon desorption at 5 and 25 °C following a liquid nitrogen quench in comparison to desorption at 25 °C without a quench.

Once the pressure is released, the measurable stress state at 5 °C desorption temperature following a liquid nitrogen quench is zero. This indicates that due to the glassy state of the sample, the inner layers do not contract significantly faster than the outer glassy layer. Therefore, no significant stresses build up during further desorption.

As discussed in the previous section 7.3.4, this indicates that desorption-induced stress might not play such a significant role for nuclei development in the case of desorption below T_g.

7.5 Discussion

In this chapter, it has been established that a liquid nitrogen quench leads to stress development in skin layer and sample core, most likely due to density differences resulting from the temperature increase after the quench.

If applied after methanol desorption, the quench has a higher impact on void development at high methanol concentrations compared to application of tensile stress after desorption. This indicates the quench has a higher impact on nuclei development compared to application of tensile stresses. But it also does not lead to a change in homogenous foam properties irrespective of whether it is applied before or after desorption. This confirms the hypothesis that in this case the number of foamable nuclei is limited by the number of post-critical nuclei.

If the quench is applied before desorption at 25 °C or 5 °C, it seems the impact of desorption-induced stress on nuclei development is gradually superimposing with the impact of the quench. In the beginning of desorption only the number of voids in the quenched part increases. This indicates that desorption induced stresses do not generate nuclei, because these would also develop on the unquenched part. More likely quench-induced stresses expand post-critical nuclei and desorption-induced stresses are further expanding these into foamable nuclei. This is another indication that there is a difference between post-critical and foamable nuclei.

The amount of foamed voids after a quench before desorption at 5 °C desorption temperature is higher at high methanol concentrations compared to 25 °C desorption temperature. Potentially quench-expanded nuclei are more conserved at 5 ° C. Based on these observations, it was concluded that foamable nuclei development is a gradual process and there is a difference between post-critical and foamable nuclei. This confirms the claim made in chapter 6.

Contrary to classical nucleation theory, successful foam formation is therefore not only dependent on nucleation, but also on foamable nuclei development. The fact that not every post-critical nucleus is reaching a foamable state is partly taken into account by growth theories (see section 2.3.2). However, foaming is often either described by classical nucleation theory or by growth theories in which only foam cell growth is described. This work suggests that the growth process between nucleus development and foam cell development is very important for successful foam formation and it might help to take this into account additionally to nucleation or growth theories.

Furthermore, the fact that foamable nuclei development is most likely a gradual process and temperature-induced stresses might contribute to it has the following implications for solid state foaming.

In solid state foaming the temperature increase following depressurisation is usually interpreted as a process to bring the sample above T_g in order to facilitate cell expansion.(Di Maio and Kiran 2017) It has so far not been discussed that the temperature change itself might induce stresses and stress-induced nuclei expansion. This might be a way to support the growth of foamable nuclei.

It has been described that following a two-step process in which the polymer had been cooled down to 0 °C before depressurisation in order to prevent coalescence, nucleation events could be observed during the temperature increase (dip in a warm oil bath).(Urbanczyk et al. 2010) This is a hint that also in the case of solid-state-foaming, the temperature increase leads to stress-induced nuclei expansion.

Furthermore, as described in section 2.2.3.2 the preferred continuous extrusion process for nanofoam production faces the difficulty of CO_2 mixing at the conditions necessary for achieving extrusion. One approach to improve the foaming quality is to freeze the other layer of the polymer by cooling the die in order to prevent a quick CO_2 loss.(Di Maio and Kiran 2017) In the light of the presented experiments it is plausible that the freezing not only increases the mixing quality, but potentially also induces stress development and potentially subsequent nuclei development.

7.6 Summary

It was found that a liquid nitrogen quench is leading to tensile stresses in the PMMA-methanol matrix resulting from density differences upon temperature increase after the quench.

A liquid nitrogen quench has been applied before and after desorption at 25 °C as well as before 5 °C. The resulting stress state, geometry changes and foaming properties have been characterised.

It was found that the impact of the quench on foamable nuclei development is higher compared to tensile stress development. However, the foam properties remain unchanged. Following the hypothesis made in chapter 6, it was concluded that the amount of post-critical nuclei is limited and therefore additional stresses cannot develop more foamable nuclei.

It has been observed that after a liquid nitrogen quench applied before desorption, additional void formation occurs gradually and ahead of void development in the unquenched control. It was deduced that the expansive impact of the desorption-induced stresses superimposes with the impact of the quench-induced stresses and expands post-critical nuclei gradually into a foamable state until the reservoir of post-critical nuclei is fully exploited. Furthermore, this confirms the hypothesis made in chapter 6 that there is a difference between post-critical and foamable nuclei.

The number of expanded nuclei resulting from the quench seems to be more conserved at 5 °C at which the sample is below T_g. This is also reflected in the finding that the geometry changes isotropically and no tensile stresses built up upon desorption at 5 °C. This indicates that in this case, no stress state development is necessary to reach foam formation, because quench induced nuclei are conserved below T_g.

8. Stress and foam development depending on initial methanol concentrations and desorption temperatures

As shown in chapter 5, the stress state resulting from skin development seems to have a significant effect on the nuclei development process. This raises the question of how foamability and foam structure change with a change in skin development, which should lead to a change in stress state. Since skin development is dependent on the sample T_g, the impact of different desorption temperatures on stress, geometry and foam development was investigated.

Different methanol concentrations are likely to influence phase separation (see discussion in section 2.1). Therefore, the influence of initial methanol concentrations on stress development, geometry changes and foam formation was also investigated.

Furthermore, the degree to which additional stress in the form of a liquid nitrogen quench affects void formation at different desorption conditions, as well as initial methanol concentrations, was assessed in order to gain a better understanding of the impact and limitations of stresses on foam development in dependence of desorption conditions.

The experiments for this chapter were partly affected by the lab closure during SARS-CoV-2 pandemic.

8.1 Methanol desorption at elevated temperatures

In order to study cell size development after desorption at elevated temperatures, samples fully charged with methanol (2×20×20 mm², batch 1) were desorbed down to 8 w/w% methanol content at elevated temperatures (35 °C and 40 °C). Subsequently, they were foamed by the standard procedure (see chapter 4.2).

8.1.1 Foam development

Figure 73 a) - f) shows the foam characteristics of foams resulting from foams developed after desorption at temperatures above 25 °C.

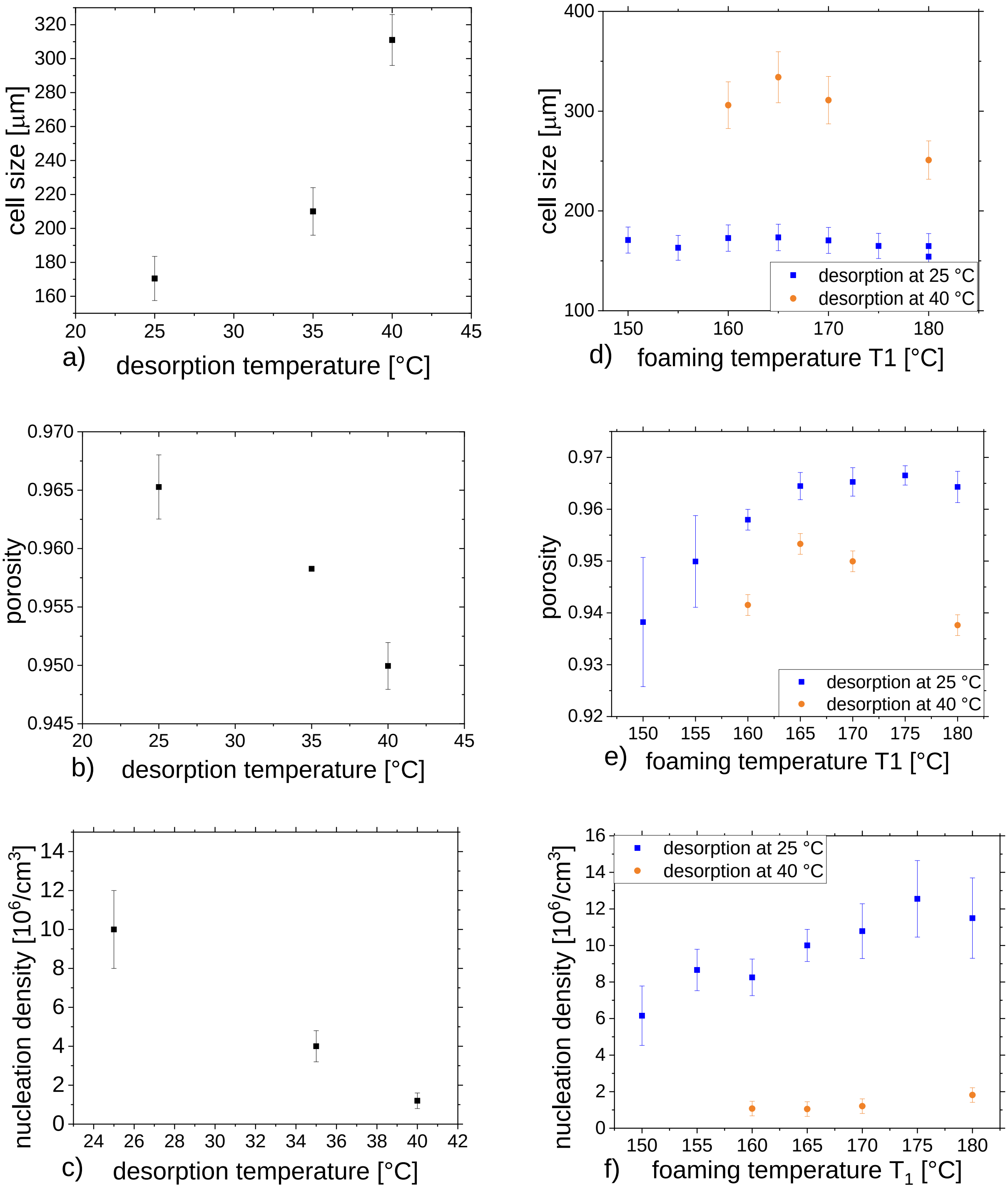

Figure 73: a), b), c): cell size, porosity and nucleation density development in dependence of desorption temperature for foams foamed at 170 °C after desorption to 8 w/w%. d), e), f): cell size, porosity and nucleation density development depending on foaming temperature for foams foamed at different T_1 after desorption to 8 w/w%.

The data points for foam properties for desorption conditions above 25 °C were taken from one sample per data point only. The error was estimated as an equivalent percentage of the standard deviation on the data of foam properties foamed with the standard process. Figure 73 a), b), c) exhibit the cell size, porosity and nucleation density for samples desorbed at 25 °C, 35 °C and 40 °C and foamed at T_1=170°C. Figure 73 d), e), f) exhibit the cell size, porosity and nucleation density for samples desorbed at 25 °C, and 40 °C foamed at different T_1 between 145 °C and 180 °C. For 35 °C no such variation in foaming temperature could be completed.

As can be seen from Figure 73, for desorption temperatures above 25 °C, the resulting cell size increases, whereas the porosity decreases. This is also reflected in Figure 74. At a desorption temperature above 40 °C, the increase in cell size and decrease in porosity is quite dramatic and not quantifiable anymore as can be seen from Figure 74(c).

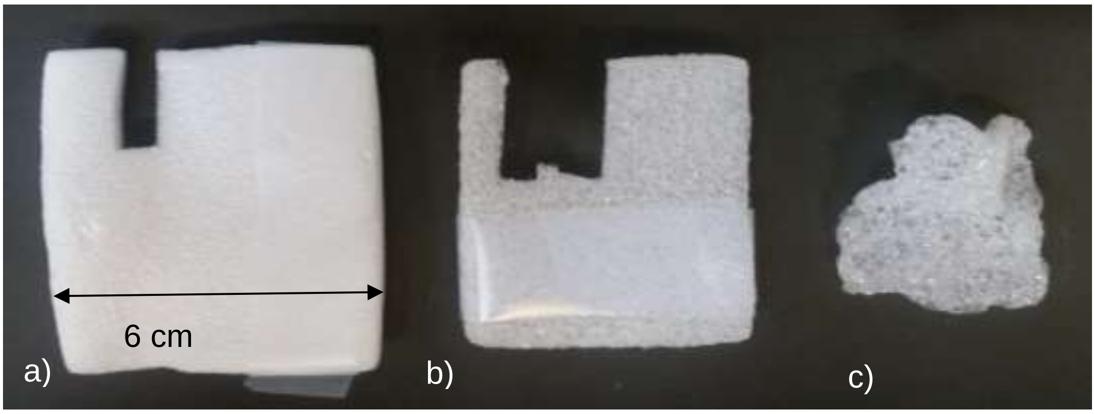

Figure 74: Foam formation after desorption to 8 w/w% methanol content at 25, 40 and 45 °C desorption temperature (left to right). Samples were foamed by the standard foaming process (T_1=170 °C, T_2=115 °C).

Furthermore, it can be seen from Figure 73 , that at 40 °C desorption temperature foams only expand from T_1=160 °C instead of 150 °C as it is the case for desorption at 25 °C. This means a higher pressure is necessary to expand the foams after desorption at higher temperatures. This is a hint that the nuclei are potentially in a less expanded state. In order to confirm this claim and explain the observed changes of cell morphology in dependence of desorption temperature, the stress state development and sample geometry are characterized in the following sections.

8.1.2 Stress development

Figure 75 shows the stress development for different desorption temperatures. The stress state was measured according to the method described in section 5.3. For desorption conducted at higher temperatures, the compressive stress that develops in the sample core in the beginning of desorption was less pronounced once a higher desorption temperature was reached. Only initial stress state measurements at which the sample hasn't reached the higher desorption temperature exhibit a higher compressive core stress.

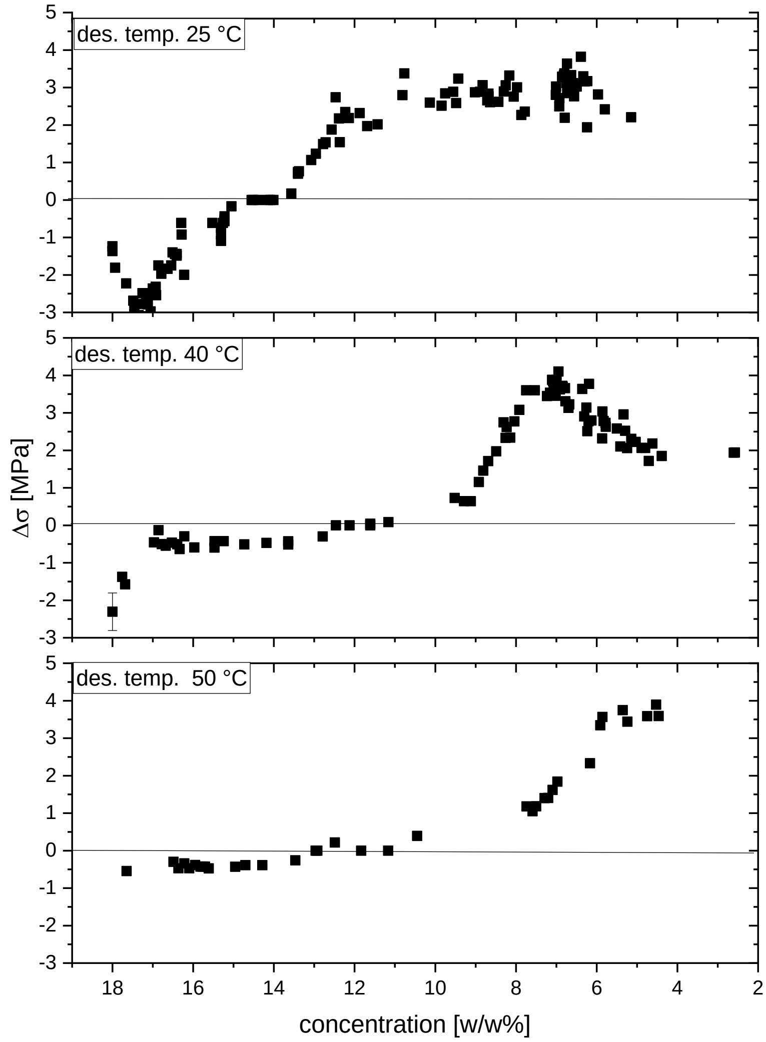

Figure 75: Stress development depending on desorption temperature. With increasing desorption temperatures, the stresses develop at lower methanol concentrations.

The reason for the lack in compressive stress development at higher desorption temperatures is most likely that at desorption temperatures above 40 °C, the methanol-desorbing sample as well as the skin are above T_g (see Figure 76) and therefore more rubbery, which resulted in lower transmitted compressive stresses.

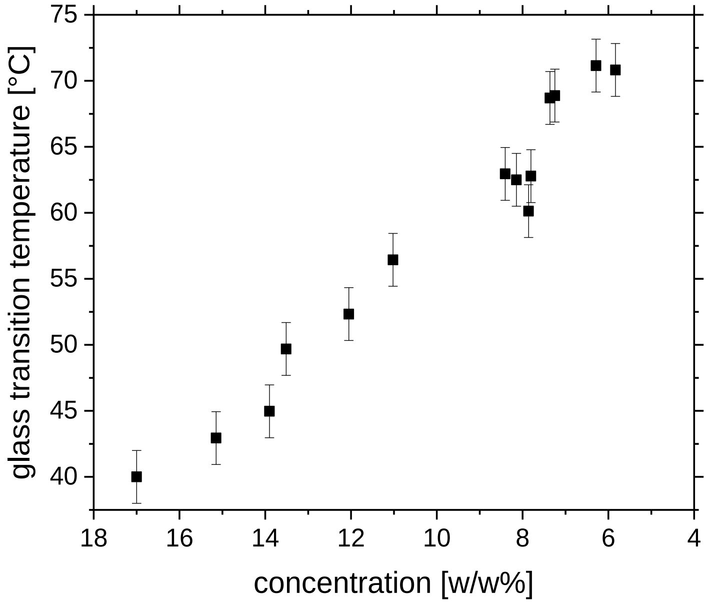

Figure 76: Dependence of glass transition temperature on methanol concentration upon desorption measured by DMA.

Furthermore, Figure 73 exhibits that the higher the desorption temperature, the lower the methanol concentration at which the compressive stress state switches to a tensile stress state. Therefore, a tensile stress (expansive) state is only developed at quite low methanol concentrations and at higher viscosities at higher desorption temperatures. Additionally, at higher temperatures, methanol is more soluble in PMMA and the drive towards phase separation and nucleation is lower. Therefore, most likely fewer nuclei develop and expand less well. And furthermore, at the same time nuclei also shrink more at higher temperatures. Therefore, desorption at higher temperatures leads most likely to fewer and smaller foamable nuclei. This most likely leads to the observed necessity for higher foaming temperatures T_1 for expansion (see Figure 73). The larger cells most likely result from the fact that there are fewer nuclei that can expand more.

At elevated desorption temperatures, the samples reach a maximum stress after which the tensile stress state decreases, while for desorption at 25 °C, the maximum stress state seems to remain almost constant once it is reached.

The decrease in maximum stress state could result from a competition between skin and core layer shrinkage at higher desorption temperatures. At elevated temperatures, the desorption rate of the core layers is higher, which potentially might lead to higher strains resulting in higher maximum stresses. But similarly, the skin is also more rubbery and potentially shrinking back faster at higher desorption temperatures. This leads to a decrease in stress in the sample core once the skin shrinkage is faster than the stress generation resulting from desorption. Whereas, at 25 °C the skin is more rigid and takes longer to shrink back and the stress state is maintained. This is also reflected in anisotropic geometry changes at 25 °C (see Figure 77), which are discussed further in the next chapter.

8.1.3 Dimensional changes upon desorption at elevated temperatures

Figure 77 shows the percentage in swelling relative to the unswollen reference state (a)) and the change in swelling relative to the equilibrium swollen state (b)) (as defined in section 3.3.8).

In the initial stages of desorption, the sample thickness increases (Figure 77 b)). The increase is higher for higher desorption temperatures. At first glance, this seems to contradict the decrease in measured compressive stress in the core. But since the sample is in a more rubbery state at elevated temperatures, the stress transferred from the higher strain is also lower. Due to sample’s rubberiness, the developing skin also has a higher impact on shape change, which leads to a more pronounced increase in thickness with desorption temperature.

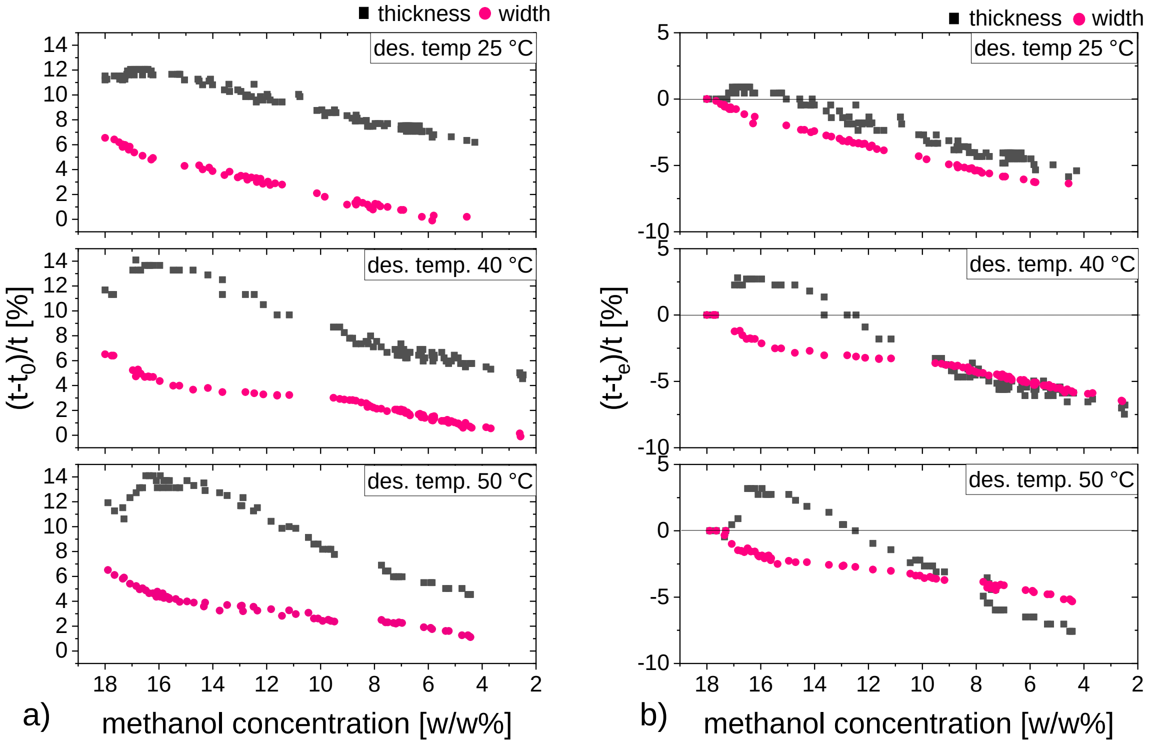

Figure 77: Changes in thickness (black marker) and width (red marker) upon methanol desorption. a): changes in dimension from zero absorption. b): Changes in dimension from equilibrium absorption.

Another reason that might result into the observed greater thickness expansion at elevated temperatures is thermal expansion, which would lead to stress-free sample expansion. The volumetric thermal expansion coefficient of methanol is around 0.001 1/K.(Dortmund Data Bank 2019) This leads to a thermal expansion of 2.5% for an increase of 25 K. This is on the scale of the observed volumetric sample expansion (1.8 %). But since the sample is only expanding in thickness and not in width, it is very likely that the major contribution to the thickness increase is imposed by the skin.

At elevated desorption temperatures swelling decreases faster in thickness compared to width at advanced desorption stages below ca. 10 w/w% methanol content. This indicates that the rate of methanol desorption is higher through the larger main faces and the thickness therefore shrinks faster than the width. The reason for this could be that the skin first builds up at the edges and the relative amount of constraining skin is therefore higher. Therefore, the width is held up by the glassy sample edges while the thickness decreases. (see discussion section 5.2).

The geometry measurements don't show a clear correlation to the stress state development (see section 8.1.2). As discussed previously this is most likely related to the fact that the stress development within the sample results from the skin and does not necessarily lead to geometric changes (see section 5.2).

8.1.4 Liquid nitrogen quench before or after desorption at elevated temperatures

In order to see in how far the stress induced by a liquid nitrogen quench can lead to foamable nuclei in cases when the desorption-induced stresses seem not to be sufficient, a fully methanol-charged sample was desorbed at 50 °C and subjected to a liquid nitrogen quench before or after desorption. For direct comparison reasons with an unquenched sample, only half of the sample strip was quenched. The quenched part will always be depicted facing towards the bottom of the presented pictures.

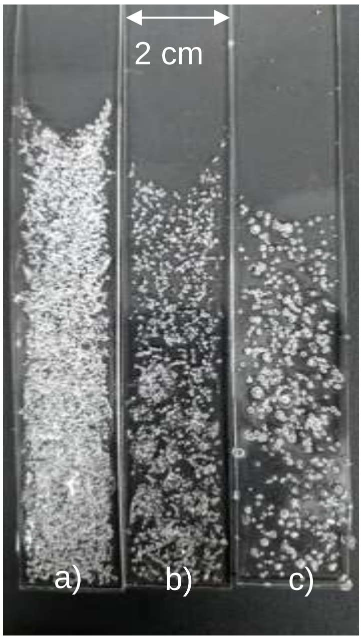

Figure 78: Samples subjected to a liquid nitrogen quench after methanol desorption to (a) 16.4, (b) 14.3 and (c) 12.1 w/w% remaining methanol concentration at 50 °C. The quenched part of the sample is on the lower part of the picture.

If the quench is applied after desorption at 50 °C (see Figure 78), its impact on cell development is decreasing with decreasing methanol concentration. This is opposite to the case of a quench after desorption at 25 °C in which case the void density after the quench increased with desorption and a much higher amount of void development was observed at comparable concentrations (see section 7.3.3).

Based on the observations made so far, the reason for this difference in void development is that at a desorption temperature of 50 °C, stresses, and therefore desorption-induced nuclei expansion, develop only below 10 w/w% remaining methanol concentration (see Figure 75) and nuclei presumably also shrink in the initial stages of desorption as at 50 °C, because the samples are above T_g above 13 w/w% remaining methanol content (see Figure 76). Therefore, the number of nuclei which the quench could further expand decreases compared to the amount available after desorption at 25 °C, where stresses developed at higher methanol concentrations (14 w/w%) provide for more further developed nuclei that would be further expanded by the quench.

This clearly shows that the quench is not introducing nucleation but expands already existing post-critical nuclei. Otherwise, a quench at similar methanol concentrations should result into a similar void structure.

This once more demonstrates that the desorption-induced stress history has a major influence on nuclei development and that desorption-induced stresses gradually develop post-critical nuclei and additional stress causes further expansion towards a foamable state.

If the samples are subject to a quench before desorption at 50 °C, the effect of an initial liquid nitrogen quench on foam cell development also seems to become less significant over the desorption period (see Figure 79). This also suggests that the nuclei are not further expanded by desorption induced stresses, because stresses only develop below 10 w/w% remaining methanol concentration at 50 °C desorption temperature and the polymer is already to rigid to allow for nuclei expansion (see Figure 75).

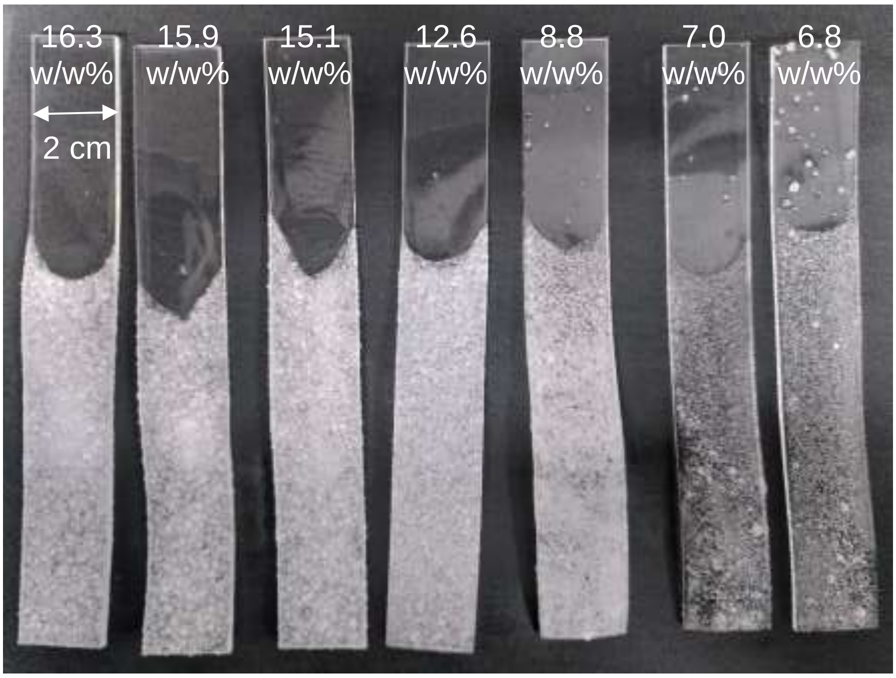

Figure 79: PMMA samples subject to a liquid nitrogen quench before desorption at 50 °C and desorbed to concentrations of 16.3, 15.9, 15.1, 12.6, 8.8, 7.0, 6.8 w/w%. The effect of the initial liquid nitrogen quench becomes less significant with decreasing methanol concentration. The quenched part of the sample is on the lower part of the picture.

It can also be seen from Figure 79 that voids in the unquenched part that only result from desorption induced stress seem to start to develop only below 10 w/w% remaining methanol concentration, which matches the onset of stress development at lower methanol concentrations (see Figure 75). Only a few voids develop in the unquenched part, which confirms that desorption induced stresses are not high enough to expand many nuclei at the lower methanol concentrations and therefore high viscosities.

8.2 Methanol desorption from higher initial methanol concentrations

In order to study the impact of initial methanol concentration on foam formation, the initial intake of methanol was increased by absorption at elevated temperatures. All samples were desorbed to 8 w/w% methanol concentration at 25 °C before foaming and foamed by the standard procedure (see 4.2). Data points on foam characteristics only result from one sample per data point.

First, it was evaluated how equilibrium methanol concentration increases with absorption temperature and what effect an increase of concentration has on T_g.

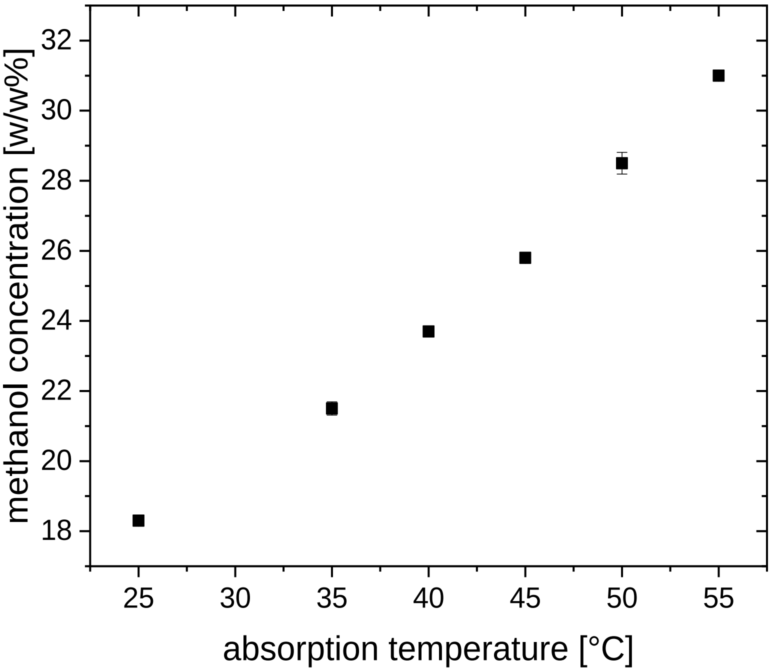

Figure 80: Methanol concentration in equilibrium depending on absorption temperature.

The methanol concentration increases with absorption temperature above 25 °C, because the glass transition temperature is decreased and the sample becomes more and more rubbery (see Figure 80). The polymer chains are therefore more flexible and can accommodate more methanol molecules. Below 25 °C absorption temperature, the equilibrium concentration does not change as has been shown by Thomas in her PhD thesis (N. Thomas 1978). The reason for this is that the PMMA-methanol system is not crossing its T_g below an absorption temperature of 25 °C (see Figure 81). Therefore, polymer chain movement does not contribute to methanol uptake and the amount of methanol reached is solely based on the Case II diffusion mechanics and therefore the total absorption is independent of absorption temperature below 25 °C. (N. Thomas 1978)

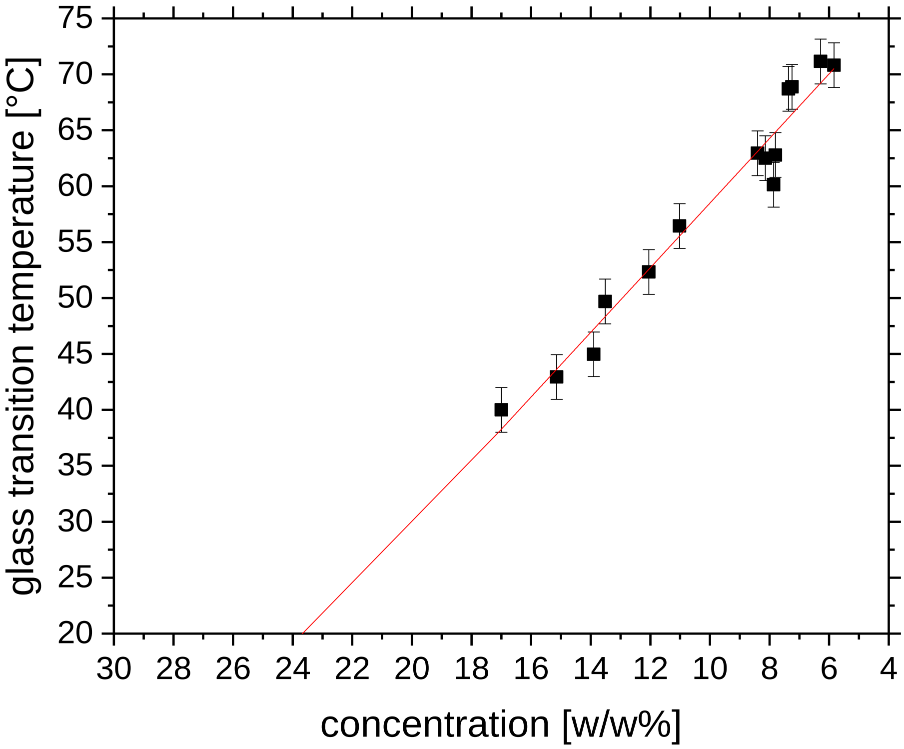

Figure 81: Linear extrapolation of glass transition temperature, measured by DMA, as a function of remaining methanol concentration

Above 23.7 w/w%, the PMMA-methanol mixture is presumed to be above its T_g at 25 °C, as can be seen from the extrapolation (red line) of data in Figure 81. The real value for glass transition temperatures at methanol concentrations might even be lower than the extrapolation, because the data below 18 °w/w% needed to be taken from desorbing samples, which would also have a skin. As described above it is not possible to achieve less than 18 w/w% methanol concentration from absorption.

For samples above 18 w/w% methanol content, it was impossible to measure the glass transition directly with dynamical mechanical without cooling the sample, because the sample is already above glass transition at room temperature at these concentrations and would need to be cooled down, to be able to cross it. Unfortunately, it was not possible to do this before the lab closure resulting from the outbreak of SARS-CoV-2.

Above initial methanol concentration of 28.5 w/w%, the samples turn opaque with a blue colour (see Figure 82), upon taking them out of methanol; below this concentration, they stay transparent. This indicates that blue light is scattered and is a hint that at higher methanol concentrations, coarser nuclei on the scale of 400 nm develop right upon phase separation. The opaqueness fades during desorption presumably because the nuclei shrink due to the low viscosity at higher methanol concentrations.

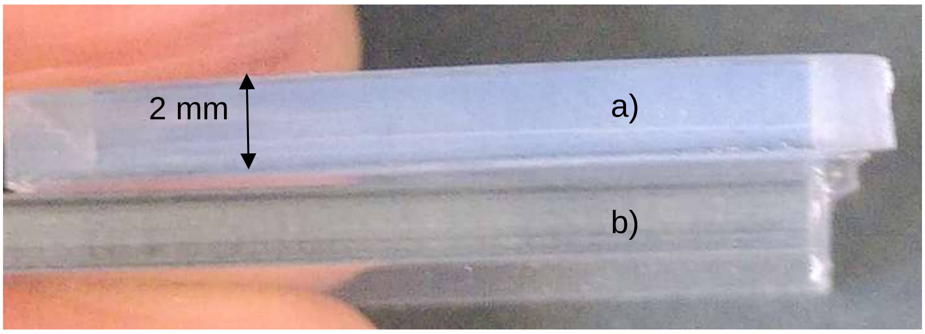

Figure 82: a) Opaque sample with methanol concentration of 28.5 w/w% right after taking out of methanol compared to b) a sample absorbed to 18 w/w% methanol content that stays transparent.

8.2.1 Foam development

Figure 84 shows cell size, porosity and nucleation density for samples foamed at T_1 = 170 °C depending on initial methanol concentration.

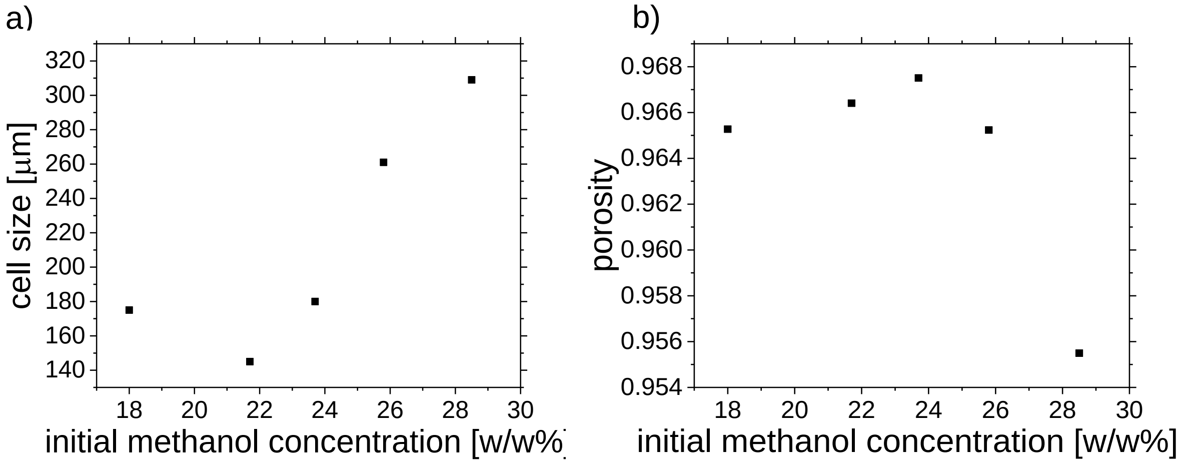

Figure 83: a) cell size and b) porosity for samples foamed at T_1 = 170 °C.

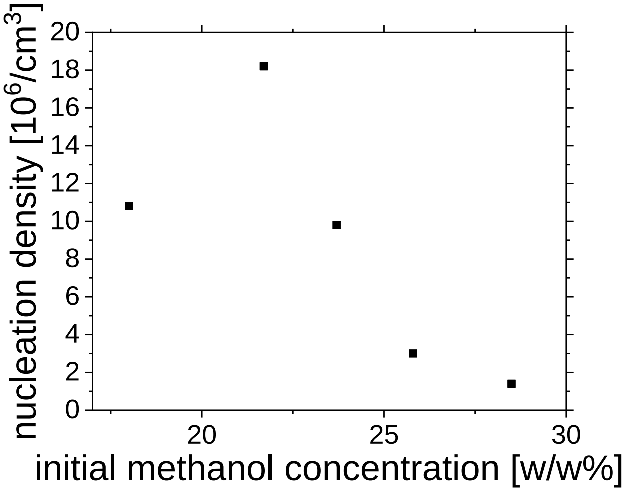

Figure 84: nucleation density for samples foamed at T_1 = 170 °C.

All samples had been desorbed to 8 w/w% remaining methanol concentration at 25 °C. The data in Figure 83 and Figure 84 show that cell size increases after desorption from initial methanol concentrations above 24 w/w%, while porosity and nucleation density severely decrease. Above this concentration, the sample is presumably above T_g (see Figure 76). This indicates that once the PMMA-methanol mixture is above its T_g, nuclei most likely coalesce leading to a lower nucleation density.

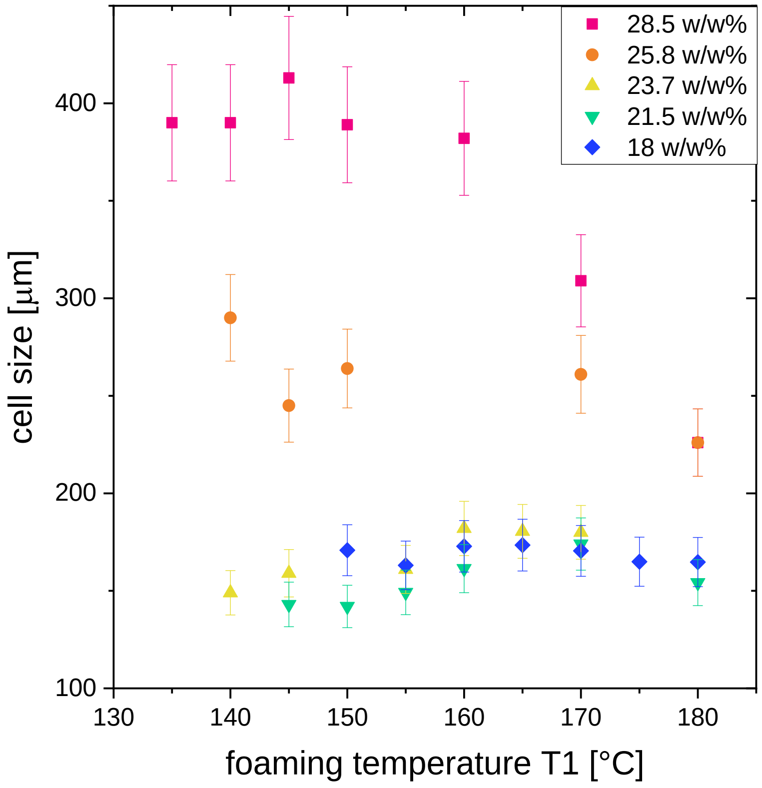

Figure 85: Foam developent depending on intial methanol concentrations after desorption to 8 w/w% and standard foaming procedure.

If one looks at cell size, porosity and nucleation density for different initial methanol concentrations for different T_1 as in Figure 85 and Figure 86, the maxima in cell size and porosity depending on T_1 shift to lower T_1 with higher initial methanol concentrations (see Figure 86). Furthermore, T_1 decreases with an increase in initial methanol concentration, making foaming possible even at 135 °C after desorption from 28.5 w/w% initial methanol concentration. This indicates that the initial sizes of the nuclei are bigger due to coalescence, and less pressure is needed to expand the nuclei. This potentially also leads to cell collapse at higher values of T_1, as indicated by the decrease in nucleation density and porosity at high T_1.

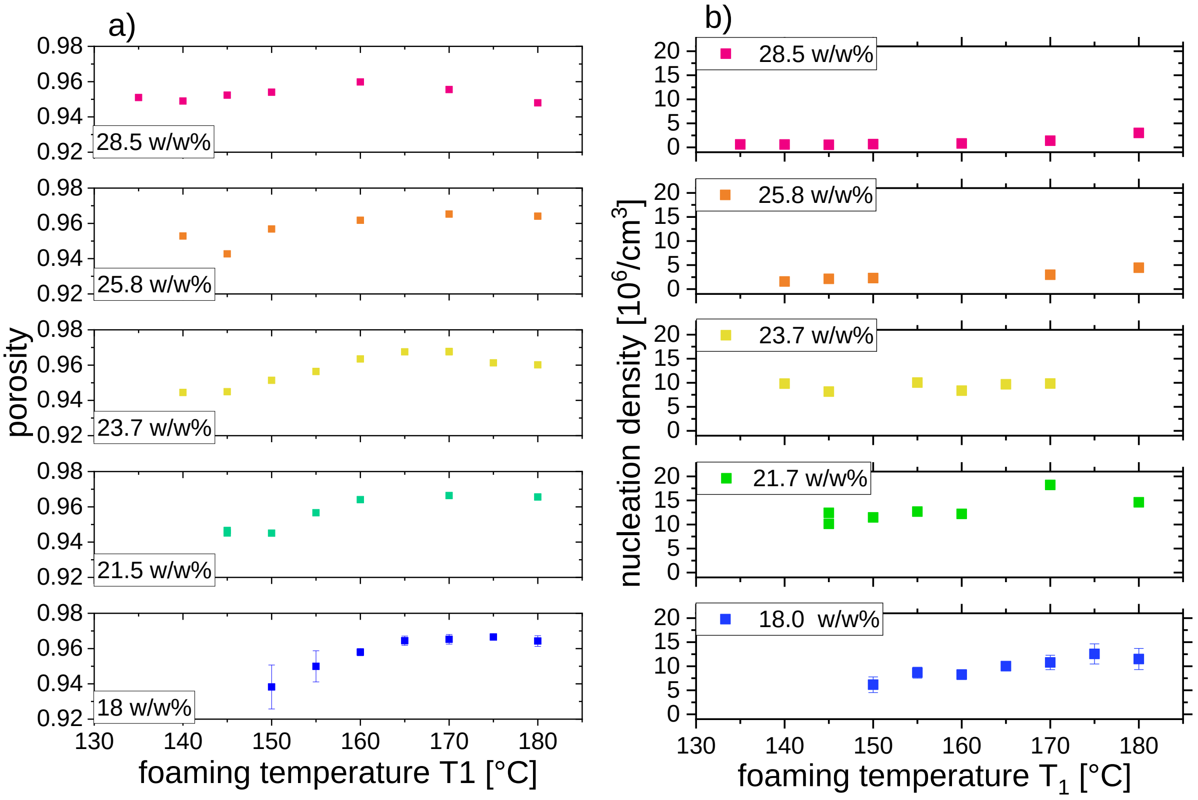

Figure 86:a): cell sizes for foaming after desorption from different methanol concentrations.b) porosity for foaming after desorption from different methanol concentrations.

Below initial methanol concentrations of 23.7 w/w%, the sizes of nuclei seem to be almost independent of foaming temperature, with a small tendency towards a decrease in cell size and increase in nucleation density. This is in accordance with the expectation that nucleation density increases with higher methanol concentrations close to, but below T_g, since the viscosity is slightly lower and more cells should be generated during phase separation and similarly more cells are expanded by desorption-induced stresses, but are still conserved below T_g.

This is similar to the observations from the solid state foaming process in which higher CO_2 concentrations would usually lead to smaller cells. (Judith Martín-de León, Bernardo, and Rodríguez-Pérez 2019)

As for the solid-state foaming process, there seems to be an ideal viscosity, close to T_g at which a maximum in nuclei develop without coalescing and are supported to grow into stable nuclei by the developing stresses. In case of phase separation above T_g however, nuclei coalesce. (Martín-de León, Bernardo, and Rodríguez-Pérez 2016)

8.2.2 Stress development

Figure 87 shows the stress development resulting from desorption from higher methanol concentrations (23.7 w/w% and 28.5 w/w%).

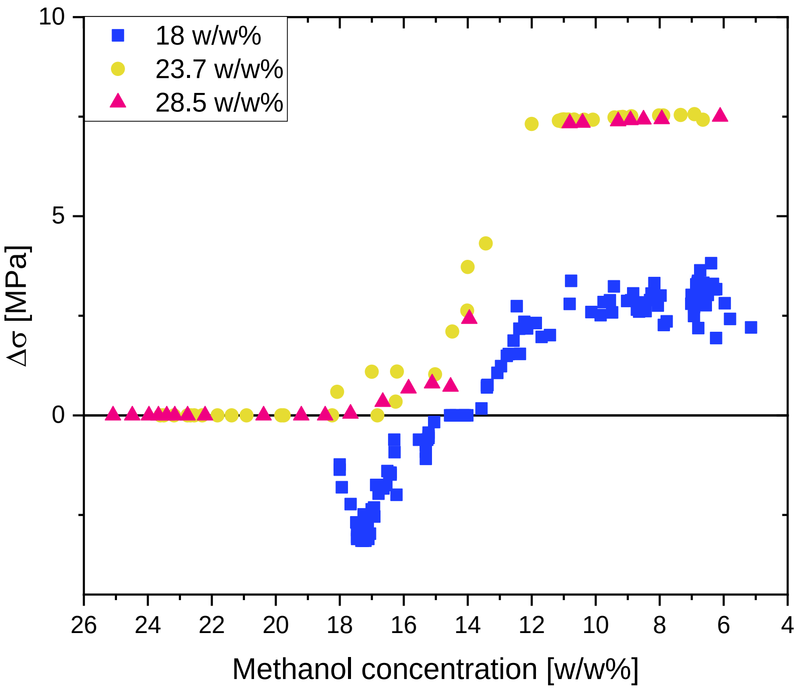

Figure 87: Stress development resulting from desorption from higher methanol concentration.

Regarding stress development during desorption from higher methanol concentrations, no compressive stress state observed in the beginning of desorption (see Figure 87). The reason for this is most likely that at higher methanol contents and therefore higher desorption rates through the skin, the skin is not developing into a contractive rigid state that would impose a measurable compressive stress state. This is in accordance with the absence of any skin-imposed thickness increase observed for the geometry measurements (see Figure 89). The stress state only starts developing below 18 w/w% methanol concentration. Presumably the viscosity is to high above 18 w/w% to allow for a stress state to develop.

The stresses developing during desorption from higher methanol concentrations are higher by a factor of two than the stresses developing from desorption from 18 w/w% methanol content. They start to develop at higher methanol concentrations and are advanced compared to stress development for desorption from 18 w/w%. The reason is likely the much higher desorption rates through the main sample phases, which explains the findings in section 8.2.3 and is described there.

The retardation for the final stage is over a retardation order (530 nm), which means that the determination of retardation via RGB fit (see section 3.3.1.2) is ambiguous (see Figure 88). Therefore, the developed RGB analysis is not possible anymore with the method developed in section 3.3.1.2. The measurement by eye is subject to an error of ca. 1 MPa resulting from ca. 100 nm of uncertainty in estimating the retardation. So, finer changes are not possible to track but the measurements still reveal a nearly two-fold increase in stress development for high initial methanol concentrations.

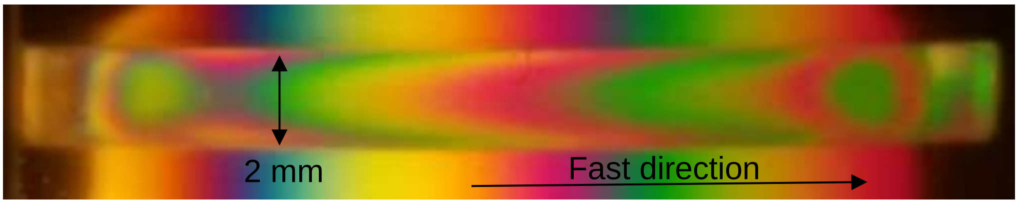

Figure 88: Stress development for sample desorbed from high intitial methanol concentration. The stresses lead to retardations above one order and therefore make an RGB fit between sample and reference ambiguous.

Within this measurement error, the stress development does not differ much for desorption from 23.7 and 28.5 w/w%. However, as discussed, the resulting cell sizes increase significantly for desorption from 28.5 w/w% compared to 23.7 w/w% when foamed after desorption to 8 w/w% methanol concentration. This is a hint that, in this case with the lower initial sample viscosities resulting from the higher methanol concentration, postcritical nuclei resulting from phase separation coalescence resulting into bigger, but fewer nuclei that develop into bigger voids. This is further discussed in the following sections 8.2.3 and 8.2.4.

8.2.3 Dimensional changes upon desorption from higher methanol concentrations

Figure 89 shows the changes in sample dimensions (calculated according to section 3.3.8) resulting from desorption from higher methanol concentrations (23.7 w/w% and 28.5 w/w%).

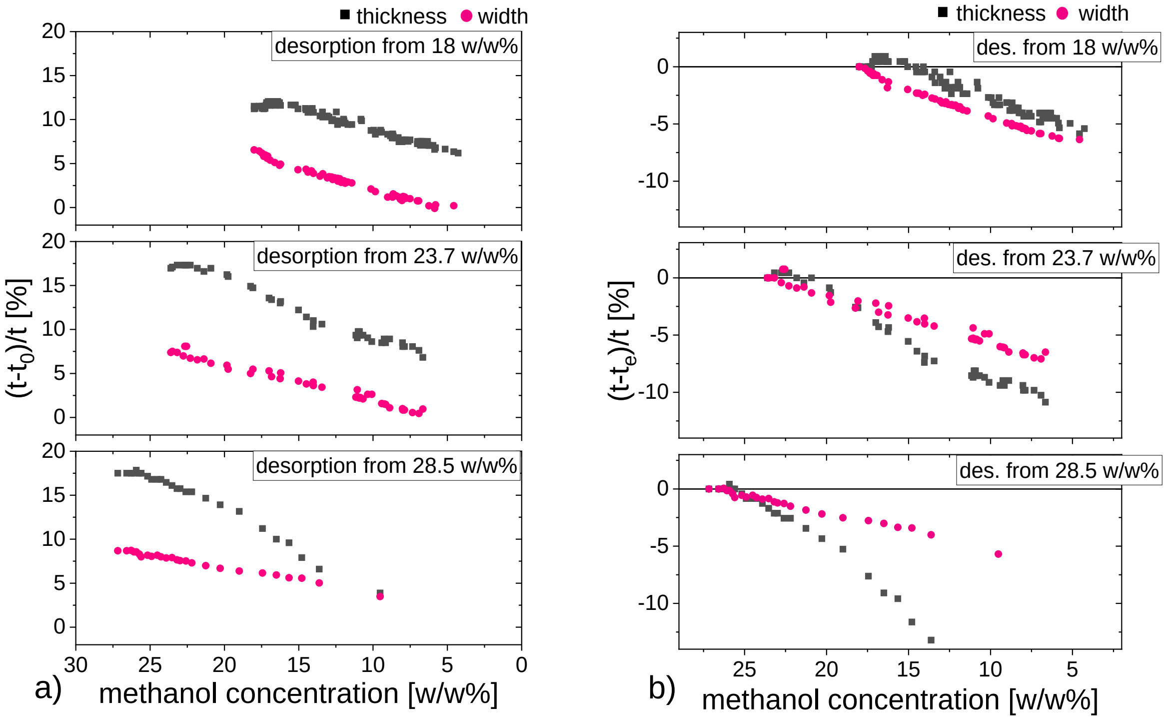

Figure 89: Change in dimensions upon methanol desorption from higher initial methanol concentrations. a) with respect to uncharged sample proportions. b) with respect to equilibrium sample proportions.

A notable difference to the geometry changes resulting from desorption at higher temperatures (see 8.1.3) is the fact that the sample thickness seems not to increase significantly in the early stages of desorption. This indicates that initially, there is no compression or shape change due to the development of skin. The reason is most likely that at higher methanol concentrations there is a higher methanol throughput through the faces keeping them rubbery.

Furthermore, the thickness decrease from equilibrium absorption is advanced compared to the width decrease above 23.7 w/w% initial methanol concentration.

Similar as for desorption at higher temperatures (see 8.2.3), this indicates that the methanol desorption is higher through the rubbery main faces compared to the smaller edges with a higher relative glassy edge content and the thickness therefore shrinks faster than the width. This should contribute to the development of tensile stresses along the width and is most likely the reason that the observed stresses (see Figure 88) are much higher than at desorption from 25 °C.

As discussed (see Figure 82), above 28.5 w/w% initial methanol content, the mixture exhibits a slight opaqueness once taken out of the methanol. The opaqueness fades over time. This indicates that initially, phase separation and coalescence is the driving force for nuclei development. These nuclei seem to decrease in size with desorption. It would therefore be plausible that such a sample could immediately be foaming since voids are already developed. But foaming is not successful in the initial stages of desorption from 28.5 w/w% initial methanol concentration. Most likely because in this case, the voids collapse before the methanol expands as described in section 4.4..

The question resulted whether nuclei shrinking could be prevented with additional stress resulting from a liquid nitrogen quench. Therefore, in the next section, it is shown how and when a sample with 28.5 w/w% initial methanol concentration is influenced by a liquid nitrogen quench.

8.2.4 Liquid nitrogen quench before and after desorption from higher methanol concentrations

A liquid nitrogen quench was applied before and after methanol desorption from 28.5 w/w% methanol concentration at 25 °C.

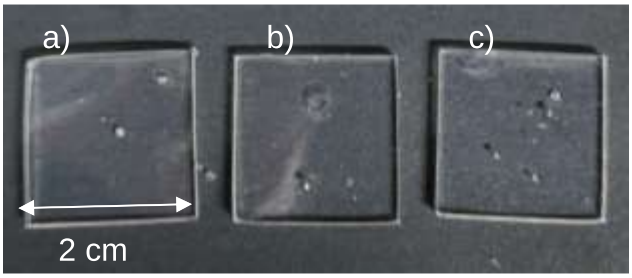

Figure 90: From left to right: a) Immediate liquid nitrogen quench and foaning after equilibrium absorption to 28.5 w/w%, b) liquid nitrogen quench before absorption to 26.9 w/w%, c) liquid nitrogen quench after desorption to 26.7 w/w% remaining methanol content.

In the early stages of desorption, a liquid nitrogen quench before or after desorption has no effect on void formation (see Figure 90).

If the quench is applied before desorption, there is also no effect on void development at more advanced stages of desorption (see Figure 91 upper row). This indicates that quench-induced nuclei expansion was not sustained due to the rubbery state at high methanol concentrations.

At later stages of desorption, a slight void development (Figure 91 (upper row)) results most likely from desorption-induced stresses.

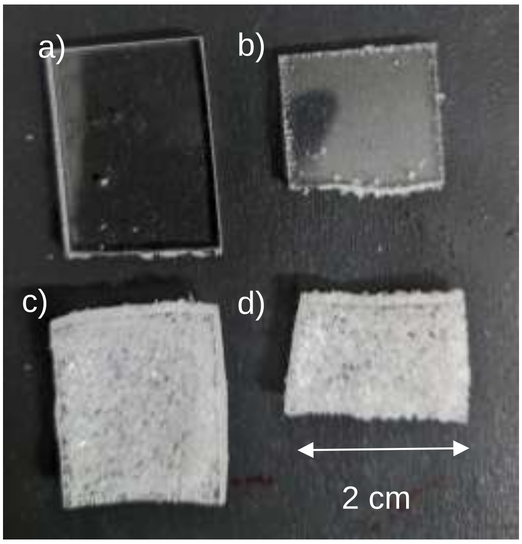

Figure 91: Top row: Sample desorbed from 28.5 w/w% after an immediate liquid nitrogen quench. Concentration at foaming: a)13.6, b) 10.3 w/w%. Bottom row: sample subject to a liquid nitrogen quench at a) 13.6, b)10.3 w/w% after desorption from 28.5 w/w%.

However, if a liquid nitrogen quench is applied after desorption from 28.5 w/w% methanol content at 25 °C to lower concentrations and therefore higher viscosities, the amount of void formation increases significantly (see Figure 91 lower row). It also enables homogenous foaming at methanol concentrations above 10 w/w% remaining methanol concentration if foaming temperature T_1 is lowered to 150 °C (see Figure 92). This indicates that the liquid nitrogen quench expands shrunken nuclei towards foamable nuclei. The resulting foamable nuclei are potentially bigger as they derive from expansion of previously coalesced nuclei. Therefore, similarly to the observations in Figure 86, the voids expand at lower foaming temperatures, but also collapse at higher foaming temperatures T_1.

Figure 92: Samples desorbed from 28.5 w/w% methanol content to 10 w/w% and quenched in liquid nitrogen after desorption. Foaming temperatures from left to right: 130, 150, 160, 170 °C.

8.3 Discussion

The question accompanying this chapter was in how far desorption conditions would influence stress-development and therefore nuclei and foam development.

With the help of birefringence measurements, it was shown that higher desorption temperatures delay stress state development towards lower methanol concentrations (around 8 w/w% compared to 14 w/w% for desorption at 25 °C). The reason is most likely that the more rubbery skin at higher temperatures accommodates the desorption-induced changes in sample shape and therefore no skin-induced stresses are developed. This is also confirmed by the initial thickness increase at higher desorption temperatures observed by the geometry measurements. The delayed start of stress state development at lower methanol concentration and therefore higher PMMA rigidity leads to less foamable nuclei that also seem to be smaller since a higher minimum foaming temperature T_1 is necessary to expand them (160 °C instead of 150°C for 25 °C desorption temperature). On the other hand, if the initial methanol concentration is high enough for the polymer to be above T_g, nuclei coalesce and foam already at lower minimum foaming temperatures T_1 (135 °C instead of 150 °C). This indicates that the nuclei are bigger. Therefore, desorption conditions seem to influence nuclei size as well and foam cell size.

That nuclei grow to different sizes is also plausible in the light that it was confirmed that nuclei development is a gradual process in which desorption-induced stress and additional stress superimpose. This was shown by the fact that the impact of a liquid nitrogen quench on void development at the same desorption achieved methanol concentration is different depending on desorption temperature (see section 8.1.4). Therefore, the impact of the quench depends on the desorption temperature and the accompanied stress development. Therefore, the quench has fewer nuclei available to bring into a foamable state after desorption above 25 °C, when the stress state development is delayed. The impact of the quench is therefore dependent on the desorption history and on the amount of pre-expanded nuclei, which it can further expand. This confirms the findings of the previous chapter that post-critical nuclei are most likely gradually expanded by desorption-induced stress and therefore nuclei development is limited if desorption-induced stress development is limited. As the quench at similar remaining methanol concentrations, but with different desorption histories leads to different amounts of void formation, it is clearly indicated that the quench does not trigger nucleation, which at the same concentration should lead to the same amount of nuclei and foam voids. It is more likely it contributes to nuclei expansion of pre-existing nuclei that are in different states depending on desorption conditions and therefore the quench results into different amounts of foamable nuclei after different desorption conditions. Therefore, nucleation and nuclei development into foamable nuclei are not identical, but most likely different processes subject to different influencing conditions.

Post-critical nuclei most likely develop upon taking the sample out of methanol as shown by the development of opacity upon taking the sample out of methanol at higher methanol concentrations. These initial post-critical nuclei develop further into foamable nuclei depending on desorption conditions, which determine expansional stress development and viscosity.

Therefore, it can be clearly stated that desorption conditions are determining foam properties due to their influence on stress state development and viscosity that determine the growth of post-critical into foamable nuclei.

8.4 Summary

Methanol desorption was conducted at higher desorption temperatures up to 50 °C and the resulting stress state, geometry changes and foam properties characterized. It was found that methanol desorption at elevated temperatures delays stress state development, which delays nuclei expansion to higher viscosities and reduces the amount of foamable nuclei. Therefore, fewer nuclei have space to grow into bigger cells. Furthermore, the nuclei seem to be smaller as they need higher minimum foaming temperatures (160 °C instead of 150 °C) to expand.

It was also found that a liquid nitrogen quench leads to less void development if applied after desorption at higher desorption temperature. This connected to the delay in stress-state development at 50 °C, since there are fewer pre-expanded voids resulting from desorption-induced stress which the liquid nitrogen-induced stress could expand into a foamable state. This is in accordance with the hypothesis that foamable nuclei develop gradually as a result of stress development and that the impact of stresses superimposes.

Furthermore, desorption from higher methanol concentrations was conducted and stress state, geometry development and resulting foams were characterised. At high methanol concentrations, the samples become opaque upon being taken out of methanol. This indicates that they are phase separating and nucleating at this step, but also coalescing.

In accordance with this it was found that higher initial methanol concentrations lead to fewer but potentially bigger nuclei that expand at lower minimum foaming temperatures (135 °C instead of 150 °C) with increase in initial methanol concentration. It was found that stress development occurs at higher concentrations compared to desorption from 18 w/w% and is much higher presumably due to an anisotropic shrinkage of sample thickness compared to width.

Regarding an effect of liquid nitrogen before or after desorption from 28.5 w/w% initial methanol content, it was found that opposite to the case of initial methanol concentration of 18 w/w%, no impact is sustained if the quench is applied before desorption. Most likely because the lower PMMA viscosity at higher methanol concentrations leads to nuclei shrinkage. But the quench increases foamability at higher remaining methanol concentrations if applied after desorption from high methanol concentrations above 18 w/w/% methanol concentrations.

Therefore, desorption conditions in terms of temperature and initial concentration have a great influence on foam property development. They mostly seem to influence nuclei expansion which seems not to be identical with nucleation.

9. FE model of the hydrostatic component of desorption-induced stress

Birefringence measurements give information about the stress state in terms of difference in the principal stresses. In order to obtain the hydrostatic component of the desorption-induced stress, the stress state imposed by the skin on a methanol desorbing slab of PMMA was modelled by finite element (FE) simulations using the software package COMSOL 5.3a employing Structural Mechanics and Heat Transfer modules. The deviatoric stress state, as assessed by the retardation obtained from the birefringence measurements and measured Young's modulus, was used as to validate the FE simulations.

Initially, the general model setup will be described followed by a detailed description of parameter estimation and assignment.

9.1 Model considerations

In order to set up a realistic FE model (FEM) of the real stress state, a sample geometry must be assigned with the material parameters and constraints that reflect the real stress state.

From earlier experimental work (see section 5.1), it is known that the local stress state results from the glassy skin layer that froze in an expanded state. The dependence of the Young's modulus on local methanol concentration leads to a local Young's modulus in each layer, which generates a local strain in each material layer. These two parameters (local strain and modulus) generate the stress state. Both are unknown at the state of desorption and need to be estimated as described in the following sections. However, the total Young's modulus and the retardation can be measured (see chapter 5) and they are therefore employed as validation.

The skin can be assumed to consist of a single thin layer of PMMA as it is not identifiable as a thicker layer in the birefringence measurements (Figure 93). Therefore, it should be below the resolution of the birefringence images, which is 5 µm.

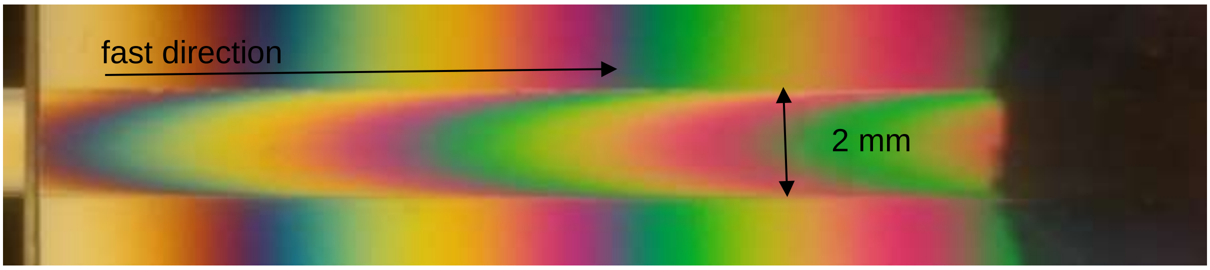

Figure 93: A sample during desorption.The skin is not identifiable.

9.1.1 Estimation of local strain values

The strain is likely to be below 1% as stress optical effects result from strains of the magnitude up to 1%.(Shafiee, Tagaya, and Koike 2010) Furthermore, the sample itself is only swollen up to 5% at lower remaining methanol concentrations at which the strain should be highest. So, an upper boundary limit of 1% for the strain seems plausible.

It is assumed that the change in length Δl (see Figure 94) resulting from the skin is the same in every layer. The layer lengths decrease towards the core. The layers meet at the stress-free axes as depicted in Figure 94. Therefore, the strain increases linearly towards the sample core. These considerations also confirm that the stress σ_3 across the sample thickness that results from the constraints of the small faces is negligible as it does not contribute to the stress state in the sample core. The stress state is therefore resulting mostly from the stress development caused by the skin on the main faces σ_1 and σ_2

The strain at the skin was set to 0% and linearly increased towards the centre. The value in the centre was varied between 0 and 0.35% as this leads to the most accurate results as described below. This was done by assigning a coefficient of thermal expansion and a temperature as described in section 9.2.

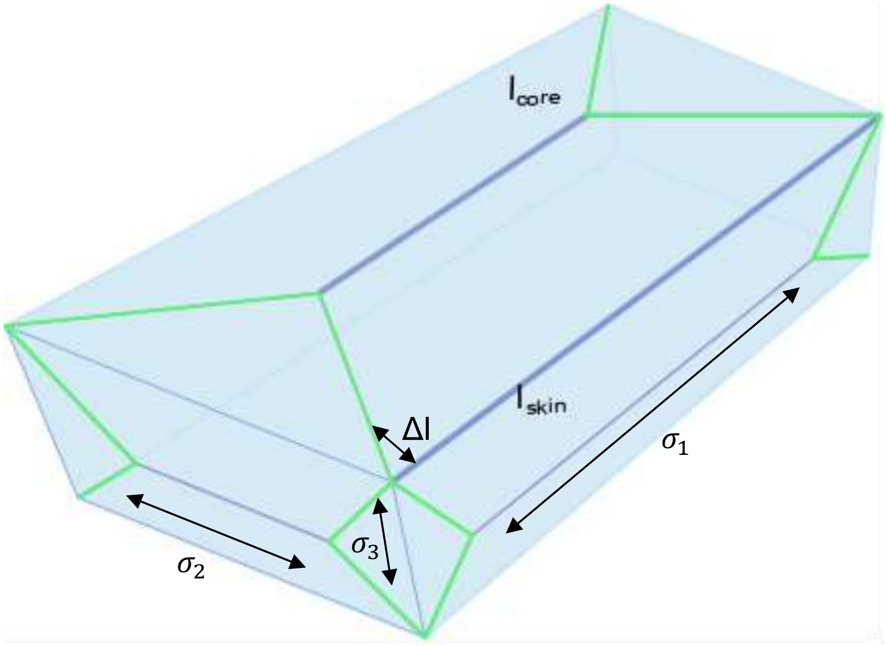

Figure 94: Sample with neural axes in green. The Δl caused by the skin has a higher relative impact on the core layer.

9.1.2 Estimation of local Young's modulus

For the Young's modulus assignment, it is expected that only the skin layers are methanol free, whereas the inner layers are still with a higher methanol content that is not distributed linearly. It is assumed that the inner Young's modulus is largely lower in the center and only close to the glassy value at the skin. Therefore, the local Young's modulus profile was assigned to be parabolic across the sample thickness. The parabola was approximated by the following piece-wise linear functions, given in table in Figure 85.

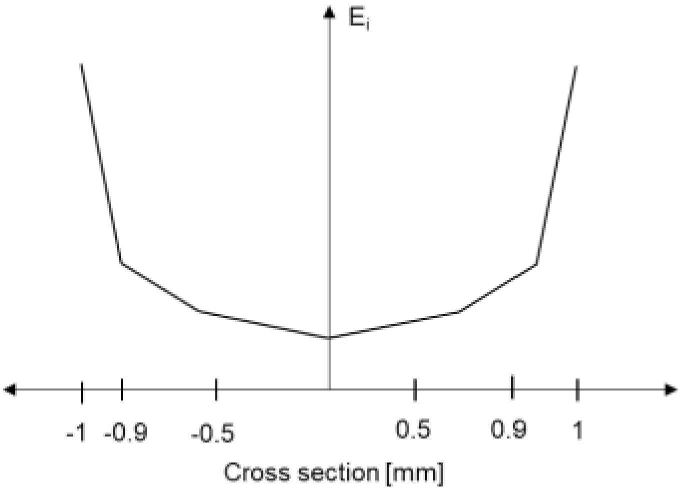

thickness [mm]	linear approximation [GPa]
- 1	1.33
- 0.9	$(1.33-E_i)/2+E_i$
- 0.5	$(1.33-E_i)\cdot 0.1+E_i$
0	E_i
0.5	$(1.33-E_i)\cdot 0.1+E_i$
0.9	$(1.33-E_i)/2+E_i$
1	1.33

Figure 95: Approximated Young's modulus across sample cross section imposed on the FE geometry.

The local Young’s modulus E_i is estimated to be between that of pure PMMA (1.33±0.05 GPa) at the skin and the measured total modulus close to full equilibrium concentration of 18 w/w% methanol content, which is 0.15±0.05 GPa (see Figure 39).

The Young’s modulus change across the length of the sample is neglected since it is insignificant compared to the distribution across the thickness.

9.2 Details of model setup and parameter assignment

To set up the FE model in COMSOL, a geometry with the experimental dimensions of 2x20x100 mm^3 was created in the software. The mesh was set as a Physics-controlled mesh with the finest possible element size (element size between 0.025 and 2.5 mm).

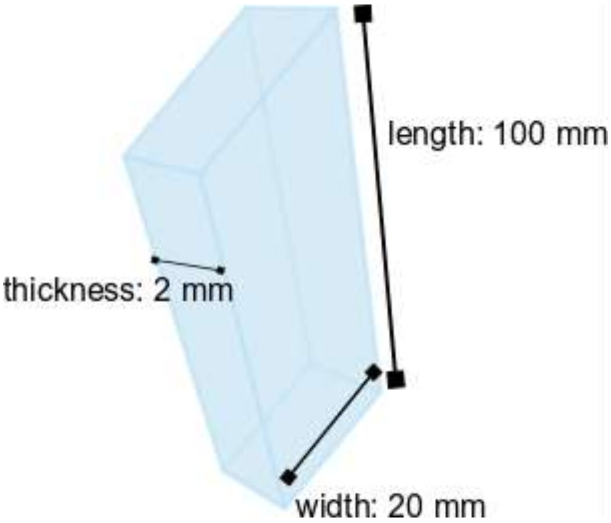

Figure 96: sample dimensions in simulation

The strain ε within the FE geometry was imposed via the thermal expansion coefficient α. ΔT was chosen to be 70 K.[4] and α was set depending on the chosen strain.

The choice of ΔT has no influence on the material properties in the FE setup other than on the coefficient of thermal expansion. It was initially chosen for convenience reasons to have a convenient number for α (0.0001) at 0.7% strain, which was used for the model setup initially.

The boundary conditions for the FE model in Comsol would require one of the material's faces to be constrained. This would put a strain on the geometry. Therefore, the geometry was put in a box of material (air) with a nominal Young's modulus of 1 Pa. The constrain was assigned to the box faces and because of its low Young's modulus, it transmits a negligible stress to the sample. So, the sample can be regarded as free standing.

---

[4] The suggestion to impose the strain via the thermal expansion coefficient was made by Dr James Dean

9.3 Parameter variation and model validation

FE simulations were conducted for all possible parameter combinations of inner Young's modulus E_i and inner strain assignment for E_i between 0.2 and 1 GPa (step size 0.0125 GPa) and core strain between 0 and 0.35% with step size of 0.025 and some additional steps with step size of 0.0125 between 0.25 and 0.3 % strain since more data was needed in this area to derive retardation and hydrostatic tension from a sample with around 8 w/w% remaining methanol content in the FE setup.

The total FEM Young's modulus, the FEM retardation and hydrostatic tension were determined for each of the potential variations of E_i and pre-strain. The total Young's modulus in the FE model is derived from FE modelling of the strain response to an applied tensile stress. Retardation and hydrostatic tension can be returned for each point in the FEM geometry.

In order to obtain the correct developed hydrostatic tension for a certain methanol concentration, the FEM retardation depending on pre-strain and E_i (defining total Young's modulus) was matched with the real retardation depending on the total Young's modulus (Figure 97). As shown before, the total Young's modulus is linearly dependent on methanol concentration (see Figure 39). This way a value for hydrostatic tension depending on remaining methanol concentration can be deduced from the FEM simulation (Figure 98 a) and b)). The hydrostatic tension for a sample desorbed to 8 w/w% remaining methanol concentration is therefore around 1MPa derived from the model.

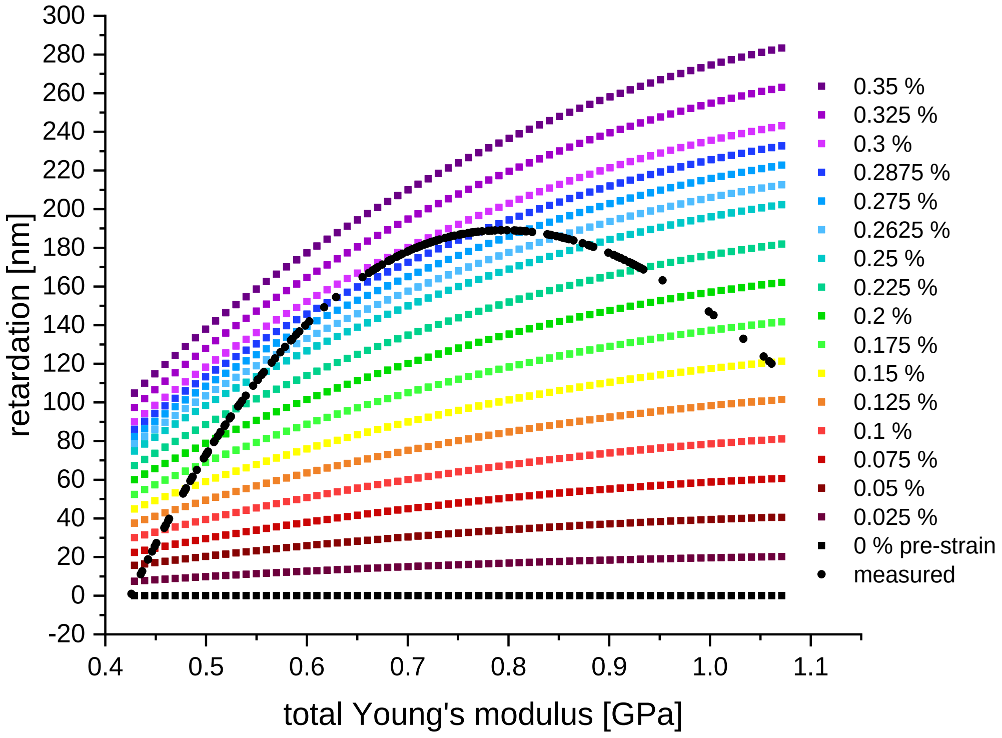

Figure 97: Match of experimentally and FEM determined retardation in order to deduce hydrostatic tension from the setup that leads to the match.

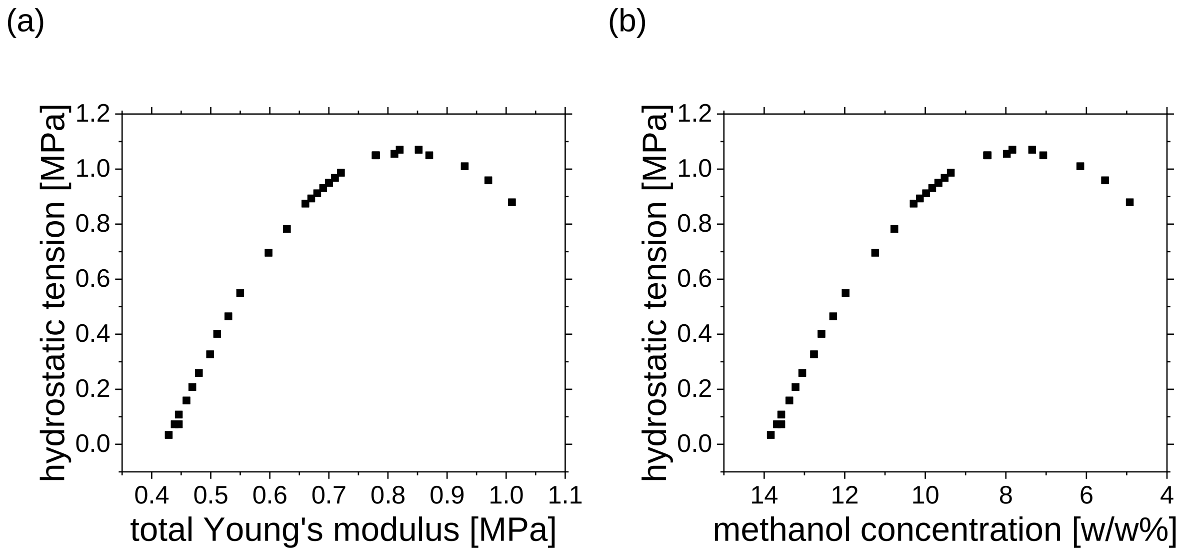

Figure 98: (a) Hydrostatic tension depending on total Young's modulus, (b) Hydrostatic tension depending on methanol concentration.) shows the original measured retardation of a sample desorbed to 8 w/w% measured with a full λ waveplate as well as a quartz wedge.

Figure 99 b) shows the retardation resulting from the FE model corresponding to a stress state at 8 w/w% remaining methanol concentration (Figure 99 a)) and Figure 99 c) the resulting hydrostatic stress.

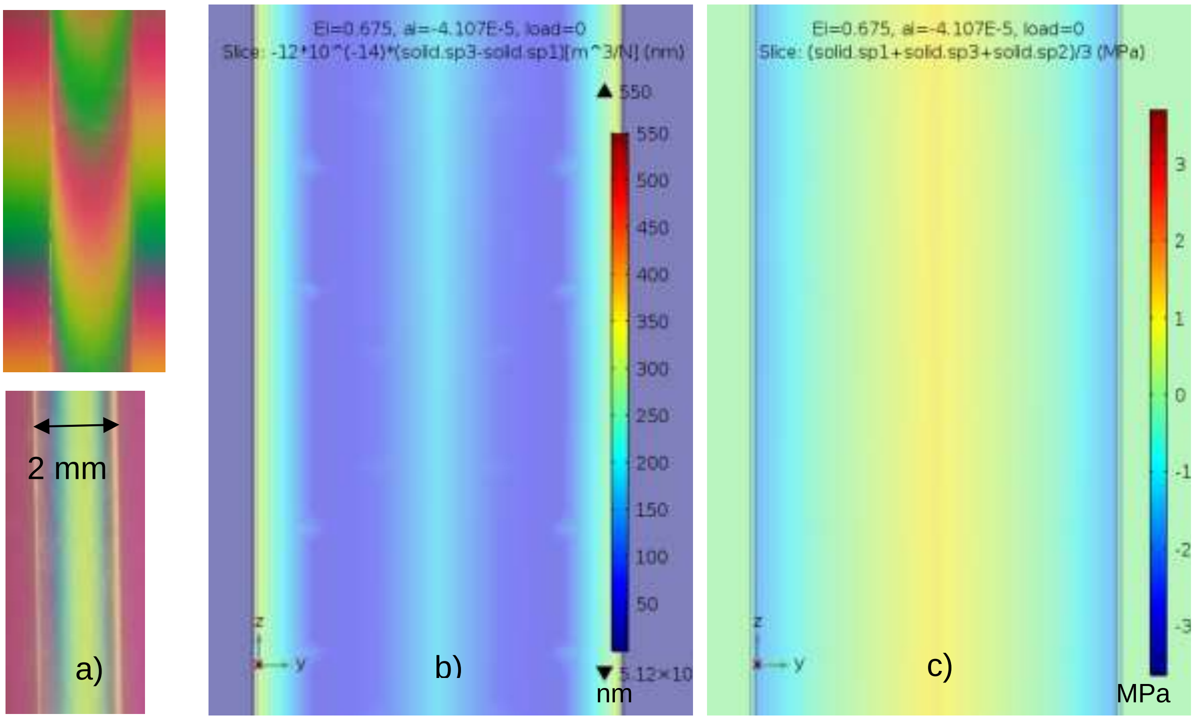

Figure 99: a) measured retardation of 200 nm in the core of a sample desorbed to 8 w/w% methanol content. b) modelled retardation of 200 nm in the sample core of a sample desorbed to 8 w/w%. c) FE analysis of hydrostatic tension in sample core of a sample desorbed to 8 w/w%.

Note that the principal stresses change sign in the compressed skin (σ_1 becoming negative, σ_3 becoming positive). The sign of retardation therefore changes for a measurement with a retardation plate. In the FE plot, the principal stresses are automatically ordered by magnitude respecting signs $\sigma_1 > \sigma_2 > \sigma_3$. This means a sign change from positive to negative changes assignment and eliminates the sign change for retardation between σ_1 and σ_3 since they were swapped. Therefore, the FE model does not show a sign change. For the determination of hydrostatic tension, all stresses are employed and therefore the sign change from tensile core stress to compression in the skin is visible (

c)).

The FE model corresponding to a stress state at 8 w/w% remaining methanol concentration approximates the measured stress distribution across the sample width approximately (see Figure 100). The match is less well across the whole sample width, which potentially relates to the fact that the linearly approached desorption induced stress state is not fully linear. However, parabolical approximations led to a dip for retardation in the sample centre. This is most likely related to the interaction of the sample layers that impose less tensile stress state on each other if there is less difference in tensile stress state between them. Which means that if the difference in tensile stress between layers decreases like around the centre of a parabola, the tensile stress in the layers decreases.

However, the modelled stress state still approaches the observed birefringence distribution and it is reasonable to assume that the modeled hydrostatic stress in the sample centre should not differ by more than a magnitude. This is supported by the fact that as will be shown in the next section, an additional tensile stress on the order of MPa, does not change the hydrostatic tension by more than a magnitude either.

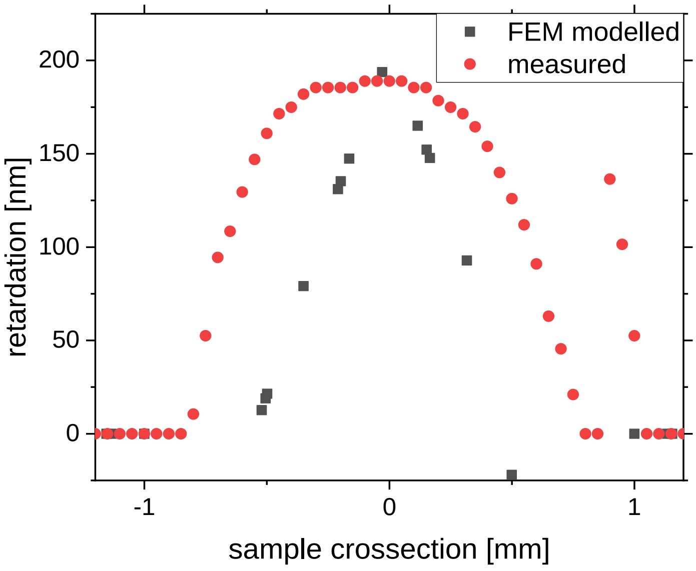

Figure 100: Distribution of retardation across the sample thickness. Measured from birefringence with a quartz wedge (red) and resulting from the FE model at 8 w/w% remaining methanol content (black).

9.4 Influence of tensile stress on hydrostatic tension

Figure 101 shows the hydrostatic tension depending on relevant pre-strains (see Figure 97) and methanol concentration. The hydrostatic tension resulting from the pre-strain is on the same magnitude as the hydrostatic tension resulting from the added tensile stress. Furthermore, its magnitude levels off with lower methanol concentrations. On the one hand this indicates that tensile stress generates a magnitude of hydrostatic tension that makes it plausible that tensile stress contributes to nuclei expansion. On the other hand, it also shows that its magnitude is leveling off and it might not be high enough at lower methanol concentrations to expand nuclei sufficiently.

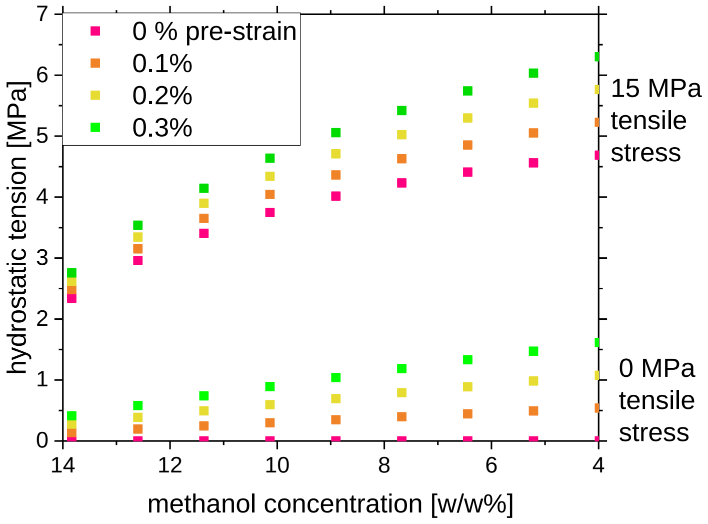

Figure 101: Hydrostatic tension in dependece of additional stress of 15 MPa fror different pre-strains

The model does not fully explain, why additional tensile stress cannot generate enough nuclei below 9.43 w/w% remaining methanol content even though it is above the value of 1 MPa. The reason could be that in this case not all nuclei are sustained at higher methanol concentrations and lower viscosities, because even if they are expanded, they shrink back quicker.

9.5 Discussion and summary

The magnitude of hydrostatic tension resulting from desorption-induced stress development is deduced with the help of a FE model. It estimates the magnitude around 8 w/w% remaining methanol concentration to be at 1 MPa. Additional tensile stress leads to 4 MPa hydrostatic tension around 8 w/w% remaining methanol content. Therefore, desorption-induced and tensile stress generated hydrostatic tension are on the same magnitude and it seems plausible that both lead to the same effect, namely the increase of nuclei towards foamable nuclei.

The hydrostatic tension is a magnitude lower than the hydrostatic stresses involved in sold state foaming (depressurisation rate around 100 MPa/s (section 2.2.3)). Given that the nucleation density achieved with solid state foaming differs by a factor of 10^9, 1 MPa desorption induced hydrostatic tension is within the expectation that desorption-induced hydrostatic tension is most likely lower than the hydrostatic tension involved in sold state foaming, but not in a completely different range.

10. Conclusions and prospects

The question accompanying this work was how to increase the nucleation density in polymer foams and in particular in nanofoams. The standard process for nanofoam generation employs CO_2 as a foaming agent and therefore also comprises a depressurisation step, which is not well observable in detail or experimentally accessible.

The guiding idea for this thesis was to develop an analogous, but more observable process that gives an insight into the solid-state foaming process that helps to understand and improve it towards the generation of foams with lower cell sizes and densities. Therefore, a novel foaming process was developed utilizing PMMA and methanol.

In **chapter 4**, the novel foaming process was developed based on PMMA and methanol and characterized. It essentially comprises methanol absorption up to equilibrium followed by methanol desorption at 25 °C below 8.5 w/w% remaining methanol content. The desorption step was found to be crucial for homogenous foam formation. The optimum in cell size and porosity of the resulting foam was found for a foaming procedure of 1 min at $T_1 = 170$ °C in a silicone oil bath and a stabilization step of 8 min in another silicone oil bath at 115 °C.

It was found that cell size is different for the two employed manufacturing batches of PMMA, that are theoretically the same product, but differ in dispersity. The batch 1 PMMA with the higher weight average molecular weight ($M_w = 1{,}968{,}000$ g mol^{-1} compared to 1,911,500 g mol^{-1}) leads to smaller cell sizes, but similar porosity (175 µm compared to 250 µm, both with 0.965 porosity). This tendency is also observed for nanofoams.(Van Loock et al. 2019)

After desorption at 25 °C, the cell size was found to be almost independent of foaming temperature T_1. However, changing T_1 significantly influences the nucleation density and porosity. Therefore, it was concluded that foaming conditions after desorption at 25 °C don't change the number of expanded nuclei sufficiently enough that they have an impact on cell size, but only on porosity and nucleation density.

In **chapter 5**, it was qualitatively and quantitatively established that the underlying reason for the necessity of desorption is stress development. Qualitatively the stress development results from a methanol-desorbed skin-layer that becomes glassy in an extended state when the sample is still almost fully swollen and therefore sets subsequently methanol desorbing core layers into tension. This theory was backed up by geometry measurements that revealed the shape changing impact of the skin layer. Quantitatively, birefringence measurements revealed that a tensile stress state develops in the sample core upon desorption. The maximum extent of tensile stress state development occurs at 8 w/w% remaining methanol concentration, which is the concentration below which homogenous foam formation is possible. Therefore, it was concluded that tensile stress development is an important condition for foam development in this process. The stress development was also found to be of elastic nature (i.e. recoverable). Since samples with released stress also foam, it was concluded that it is the stress history which contributes to nuclei development rather than the present stress state.

In **chapter 6**, it was established that application of additional tensile stress after desorption to lower methanol concentrations increases the number of foamable nuclei relative to the unstressed control and leads to homogenous foam formation in samples with up to 9.4 w/w% remaining methanol concentration, compared to 8.5 w/w% otherwise. The number of voids compared to the unstressed control increases with the magnitude of tensile stress at higher methanol concentrations above 8.5 w/w%. However, no significant change in foam properties was observed for methanol concentrations at which also the unstressed control foamed homogenously. This indicates that the magnitude of tensile stresses was not high enough to expand significantly more nuclei than those that are expanded during desorption for the employed PMMA brand. It was therefore hypothesized that foamable nuclei develop from a reservoir of post-critical nuclei that are developed upon phase separation. And once the reservoir is exhausted no more nuclei can expand unless significantly higher stresses are applied that would generate additional post-critical nuclei. However, a change in cell size resulting from additional stress application before foaming has been observed for another PMMA brand, which indicates that in principal additional stresses can lead to a change in foam properties in cases when the reservoir is probably not fully exhausted by desorption induced stress or the additional stress is high enough to generate additional post-critical nuclei. This also indicates that the PMMA properties play a major role for the properties of the here developed foam.

It was found that the applied tensile stress has an influence on foam formation within the elastic regime. It can therefore be concluded that the main impact of additional stresses does not result from void formation in the sense of crazing.

The application of additional compressive pressure erases nucleation if applied above 64 MPa before foaming, which indicates that nuclei are formed and can also be destroyed before foaming.

In **chapter 7**, a liquid nitrogen quench was established as a possibility to introduce a higher stress state compared to application of tensile stress. It leads to more void formation at higher methanol concentrations. The underlying mechanism of stress development accompanying a liquid nitrogen quench was identified to be the generation of density differences between the sample layers resulting from the temperature increase after the quench.

It was found that if the quench was applied before desorption, gradually a larger number of voids were developed in the quenched part upon desorption while no voids developed in the unquenched part upon initial desorption. Therefore, it was concluded that desorption-induced stresses do not generate nuclei, because they would also lead to voids in the unquenched part. Instead the quench seems to further expand nuclei that are already closer to being foamable nuclei as a result of the quench. Therefore, less desorption induced stresses are needed to reach foamable nuclei states in the quenched part of the sample.

It was also concluded from this that post-critical nuclei expansion towards foamable nuclei is a gradual process in which the nuclei are expanded step by step and the contributing expansion mechanisms can superimpose. Furthermore, this confirms the hypothesis made in chapter 6 that there is a difference between post-critical and foamable nuclei and the desorption-induced stresses superimpose with the impact of the quench on nuclei expansion towards foamable nuclei. Therefore, foaming seems not only dependent on the generation of post-critical nuclei, but also on post-critical nuclei expansion towards foamable nuclei.

Furthermore, it was found that foamable nuclei resulting from a liquid nitrogen quench at equilibrium concentration are more conserved at low desorption temperatures (5 °C instead of 25 °C).

The impact of a liquid nitrogen quench on nuclei development seems to be higher than that of tensile stress. However, neither method leads to a change in foam properties compared to an unstressed sample. This confirms the hypothesis of chapter 6 that there is a limited reservoir of post-critical nuclei. This reservoir is already exhausted by desorption-induced stresses that bring all post-critical nuclei into a foamable state and hence additional stress application has no impact once the reservoir is exhausted.

In **chapter 8**, the influence of methanol concentration and desorption temperature on foam properties was studied. It was found that an increase in desorption temperature delays the stress state development towards lower methanol concentrations at which nuclei expansion is prevented by the PMMA's lower ductility. The reason for the delay in stress development is most likely the delayed development of the skin layer at higher desorption temperatures that keep the whole sample above T_g. This results in fewer foamable nuclei that are smaller since they are foaming at higher minimum foaming temperatures T_1 compared to desorption at 25 °C. They grow into bigger cells. This demonstrates the importance of desorption history for the resulting foam structure within this foaming process.

It was found that a liquid nitrogen quench after desorption at higher temperatures does have a lower impact on void development than a liquid nitrogen quench after desorption at 25 °C to the same methanol concentration. This indicates that a liquid nitrogen quench expands pre-existing and also pre-expanded nuclei, which derive from desorption-induced stresses and are therefore fewer in number in the case of desorption at higher temperatures at which stress development is delayed. This strongly supports the finding that foamable nuclei develop gradually and desorption-induced stresses and additional stresses superimpose.

It was also found that the initial methanol concentration has a major impact on nuclei coalescence if phase separation occurs above T_g. This is particularly indicated by the fact that samples with high initial methanol concentrations turn opaque upon taking them out of methanol. The nuclei also foam at a lower minimum foaming temperature T_1, which is assumed to result from the larger foamable nuclei deriving from coalescence. Since they are therefore fewer foamable nuclei they were found to grow into bigger voids. Therefore, initial methanol concentration has an impact on foam properties. Furthermore, this supports the hypothesis that nuclei develop upon phase separation and expand, coalesce or collapse depending on desorption conditions. Therefore, as also shown in chapter 6 and 7 nucleation resulting from phase separation is not identical with the development into foamable nuclei and in order to decrease cell size both processes have to be optimized.

In summary, there seem to be three ways of influencing foam structure:

1. Change in phase separation conditions by change in material properties, material concentration and thermal conditions to change the number of postcritical nuclei
2. Change in desorption conditions by change in temperature or applied stress state to change the number of foamable nuclei
3. Change in foaming conditions (in this case oil bath temperature and duration) to change the number of foamed nuclei

In **chapter 9**, the magnitude of hydrostatic stress development was studied with the aid of FE modelling. It was found that the hydrostatic stress development upon desorption is of the order of 1 MPa. Although this is one order of magnitude lower than the hydrostatic tensions resulting from depressurisation, it is still of a size which can potentially be expected to have an impact on nucleation density in the case of solid-state foaming.

***In short summary** in order to learn about void development mechanisms in solid state foaming, which could contribute to the generation of nanofoams with lower cell size and densities, an analogous novel foaming process was developed utilizing PMMA* *and methanol. For the here developed foaming process it was found that desorption-induced hydrostatic stress development was a necessary condition for achieving a foam. It was shown that this stress development provides for gradual post-critical nuclei expansion into foamable nuclei. It was shown that additional sources of hydrostatic tension can superimpose with desorption induced hydrostatic tension and accelerate the nuclei expansion towards a foamable state. It was concluded that post-critical nuclei need to be brought into a foamable state and that there is a difference between post-critical and foamable nuclei (definition see section 3.3.4).*

It was observed that post-critical nuclei are developed upon phase separation depending on polymer properties, methanol concentration and temperature. The development into foamable nuclei was shown to be highly dependent on methanol concentration and desorption temperature that influence the stress state development in the polymer.

Altogether, three mechanisms and their accompanying conditions could be identified as being influential on foam properties: phase separation and consequent post-critical nuclei development, desorption-induced or other forms (e.g. triggered by temperature differences or externally applied) of hydrostatic stress development that lead to foamable nuclei, and the foaming process.

In particular, desorption and thermally induced hydrostatic stresses are likely to occur in the CO_2 *employing solid state foaming process as well and therefore a potentially cell size influencing factor for the* CO_2 *employing nanofoam formation process has been identified.*

The influence of process accompanying hydrostatic stresses other than the CO_2 *depressurisation that support the development from post-critical towards foamable nuclei, which can also be accelerated by external stress application seems not to have been identified by other research as a significant contribution towards foam formation before.*

The implications and prospects for solid state foaming are the following:

In general, the fact that nuclei growth into foamable nuclei is not necessarily identical with the nucleation event and is a gradual process is a view on the foaming process that might also be helpful for solid state foaming in order to improve process conditions towards more successful expansion rather than only nucleation. It might be helpful to theoretically describe the growth of a post-critical nucleus to a foamable nucleus theoretically or consider and implement it into existing theoretical descriptions.

In more detail, the CO_2 depressurisation leads to desorption as well as to adiabatic cooling and a consequent temperature increase. Qualitatively, both of these should have a stress-inducing impact like methanol desorption and a liquid nitrogen quench, which might also contribute to nuclei development. This is therefore a new aspect in the description of the solid-state foaming process.

The question for the solid-state foaming process is in how far the stress development resulting from desorption and temperature increase following adiabatic cooling influences foam properties quantitatively.

Reports about solid state foaming describe that in solid state foaming the samples are “often transparent” after the depressurisation step and “not much expanded” and that “a thermal conditioning step” is necessary to achieve nuclei expansion. This is interpreted as a necessity to bring the sample in a rubbery regime to allow for nuclei expansion by the gas. (Stéphane Costeux 2014) However, it could be as well that the necessity of a temperature increase results from an accompanied stress development that has a significant impact on nuclei development. In this case an important part of nuclei development would take place between the depressurisation and expansion step, which is essentially an extended desorption step after depressurisation. As has been shown, nuclei development during desorption is severely influenced by desorption conditions such as temperature and solvent concentration.

In solid state foaming the impact on foam formation of the conditions such as e.g. temperature and duration between depressurisation and foaming have not been subject to systematic research. If desorption-induced stress development is a contributing factor in the solid-state foaming process, the conditions between the steps would be an important tool to potentially influence foam properties. It would be therefore interesting to research the impact of changing desorption conditions between the steps in solid state foaming more systematically.

Furthermore, it would be interesting to find out whether additional stress application in between the steps would contribute towards a change in foam properties. Therefore, it would be interesting to apply in practice additional stresses after depressurisation and look into their impact on nuclei development.

Since it was found that application of stress and desorption-induced stress superimpose, it would also be interesting to see whether multiple repeats of additional stress would superimpose and be beneficial for nuclei development.

It has also been shown additional stresses don’t have an impact at too high or low viscosities. If additional stress application was applied in solid state foaming it would therefore be important to find the right viscosity at which stress-induced nuclei development occurs.

Furthermore, it has been shown that the PMMA molecular weight seems to have a major influence on foam properties. It would therefore be interesting to systematically vary this and investigate its impact on foam property development.

Appendix

A.1 Fick's law

Fick's first law states that the flux of particles is proportional to the gradient of concentration:

$$J = -D\frac{\partial C}{\partial x}$$

This only applies if the concentration C does not vary with time. The non-steady state is described by Fick's second law:(Comyn 1985)

$$\frac{\partial C}{\partial t} = \frac{\partial}{\partial x}D(\frac{\partial C}{\partial x})$$

A.2 Solubility parameters

Solubility parameters take the strength of the attraction between the molecules of a substance into account. For a liquid they can be calculated based on the energy of vaporization per unit volume V.(Dack 1975) The product equals the cohesive energy density c.e.d. C.e.d. is defined as the energy that is required to separate all molecules in a material from each other.(Treloar 2005, p.147).

$$\delta^2 = c.e.d. = \frac{\Delta U_{Vap}}{V} \qquad (1)$$

For polymers it is necessary to sum up the individual contributions of the chemical structure that contribute to the strength of attraction between its molecules. Usually it is referred to the Hildebrand solubility parameter δ, which does not take into account polar contributions. (Young and Lovell 2011) Hansen solubility parameters differentiate between dispersion forces δ_d, hydrogen bonding δ_H and dipole forces δ_p.(Koenhen and Smolders 1975) χ is then given by:(Arnold 2010)

$$\chi = \frac{V_S[(\delta_{S,d} - \delta_{P,d})^2 + (\delta_{S,p} - \delta_{P,p})^2 + (\delta_{S,H} - \delta_{P,H})^2]}{RT} \qquad (2)$$

Furthermore, the χ parameter is dependent on the temperature. This plays a role for the phase separation behavior in case of temperature induced phase separation. Experimentally, it has been proven that χ is also dependent on concentration itself, which is theoretically neglected. (Qian, Mumby, and Eichinger 1991)

A.3 Osmotic pressure

Osmotic pressure $\boldsymbol{\pi}$ is defined by the difference in chemical potential of the solvent μ_1 in the mixture and in its pure state μ_0.

$$\mu_1 - \mu_0 = -\boldsymbol{\pi} V_1 \qquad (28)$$

For a non-dilute system $\boldsymbol{\pi}$ can be expressed as:

$$\boldsymbol{\pi} = \frac{\mathrm{RT}}{V_1}(\ln\phi_1 + \left(1 - \frac{1}{x}\right)\phi_2 + \chi\phi_2 \qquad (29)$$

ϕ_1, ϕ_2 are the volume fractions of the solvent and polymer respectively. R is the universal gas constant. x is the number of polymer segments with the molar volume of the solvent. And χ represents the χ-parameter.

It can also be described as the pressure that must be applied to a solution to stop the inflow of a solvent, which is caused by the differences in chemical potential of a polymer solution and the pure solvent.(Atkins and Paula 2010)

For the nucleation of a solvent from a polymer the difference in chemical potentials is the difference between the chemical potential of the solvent μ_0 and the chemical potential of the solvent mixed in the polymer μ_1.(Han and Dae Han 1990) It can be expressed by Flory-Huggins theory.(Han and Dae Han 1990), (Young and Lovell 2011)

$$\mu_1 - \mu_0 = RT(\ln\phi_1 + \left(1 - \frac{1}{x}\right)\phi_2 + \chi{\phi_2}^2) \qquad (30)$$

A.4 Explanation colour change and birefringence

If the retardation is an even multiple of half a wavelength, the phase shift $\boldsymbol{\varphi}$ is a multiple of 2π and the recombined light is again parallel to the polariser and perpendicular to the analyser. As a consequence the analyser blocks this wavelength and the light transmitted by the analyser is missing this colour.

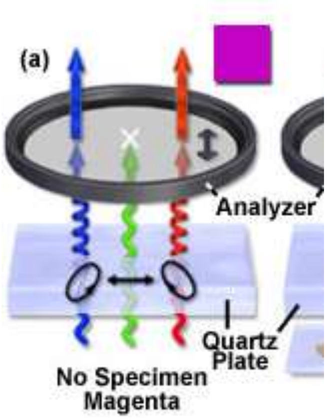

Figure 102: Depending on the change in polarization a wavelength is filtered out by the polarizer leading to a change in colour. (“Light and Color - Optical Birefringence | Olympus Life Science” n.d.)

For a retardation of e.g. one wavelength of green light, the transmitted light is magenta. For retardations on the order of one wavelength a retardation of one wavelength is unambiguous. Higher orders of retardation can result when the path difference is a larger multiple of different wavelengths, which gives rise to multiple extinction conditions. Therefore, for higher orders of retardation, the colours resulting from birefringence are a combination of serveral colours missing from the spectrum.

A.5 Python Code for shift map

The code was mostly written by Dr Jerónimo Terrones and slightly modified by Andrew Fowler and Angelika Beinert

```
import sys
import numpy as np
from PIL import Image, ImageFilter

for i in range(1,2):

    class toy_class():
        def __init__(self,args):
            for _key in args.keys():
                setattr(self,_key,args[_key])

    d={"direc":"25_40_1", "file":"test", \
      'scale_factor': '10', 'scale_method':'LANCZOS', 'normalize':'True', \
      'lines2avg':'10', 'individualized':'False', 'tolerance':'50'}

    args = toy_class(d)

    #print(args)

    #Opening and resizing Input Image:
    input_image = Image.open("D:\\PhD\\Bilder\\"+args.direc+"\\"+args.file+str(i)+"\\in.png")

    if args.scale_factor == 1:
        resized_image = input_image
    else:
        resized_image = input_image.resize([input_image.size[0]//int(args.scale_factor),
            input_image.size[1]//int(args.scale_factor)],eval('Image.' + args.scale_method))

    #resized_image.show()

    #Extracting pixel RGB data:
    image_pixels = np.array(resized_image)

    #'Normalizing' image (if requested):
    processed_pixels = image_pixels
    rows = image_pixels[:,0,0].size
    cols = image_pixels[0,:,0].size
    if args.normalize:
        for row in range(rows):
            for col in range(cols):
                processed_pixels[row,col,:]                                                      =
np.round((image_pixels[row,col,:]/np.linalg.norm(image_pixels[row,col,:]))*255)

    #Forming and saving the processed image
    processed_image = Image.fromarray(processed_pixels)
    processed_image.save("D:\\PhD\\Bilder\\"+args.direc+"\\"+args.file+str(i)+"\\out.bmp")

    ################################
    # Calculation of the shift map #
    ################################

    #Creating the avgd reference:
    reference = np.mean(processed_pixels[0:int(args.lines2avg),:,:],0)

    #Initialising the shift profile matrix:
    shift_profile = np.empty((rows,cols))
```

```
for row in range(rows):
    #Creating the flag vector:
    flag_used = np.zeros((cols,1), dtype=bool)
    for colref in range(cols):
        for colIMG in range(cols):
            j = colIMG;
            #Performing comparison btw current reference and image pixel
            if ((abs(processed_pixels[row,colIMG,0]-reference[colref,0]) <= int(args.tolerance))
                and (abs(processed_pixels[row,colIMG,1]-reference[colref,1]) <= int(args.tolerance))
                and (abs(processed_pixels[row,colIMG,2]-reference[colref,2]) <= int(args.tolerance))
                and not flag_used[colIMG]):
                flag_used[colIMG] = True
                break
        shift_profile[row,colref] = int(j-colref)

#Saving shift profile:
np.savetxt("D:\\PhD\\Bilder\\"+args.direc+"\\"+args.file+str(i)+"\\out.csv",shift_profile, fmt='%i', delimiter=',')
```

A.6 Derivation integral term

R refers to radius

$$\Delta \mathrm{G}(R) = -n(R) * (\mu_{old} - \mu_{new}) - \frac{4\pi}{3}R^3\Delta P + \int_{p_0}^{p} V(p)dp + 4\pi R^2\gamma \tag{31}$$

$$\frac{dV}{V} = -\frac{dp}{k} \Leftrightarrow \int_{V}^{V}\frac{dV}{V} = -\int_{p_0}^{p}\frac{dp}{k} \Leftrightarrow \ln V - \ln V_0 = -\frac{p-p_0}{k} \Leftrightarrow$$

$$V(p) = V_0 \exp\left(-\frac{p-p_0}{k}\right)$$

$$\Rightarrow \int_{p_0}^{p} V(p)dp = V_0 \int_{p_0}^{p} \exp\left(-\frac{p-p_0}{k}\right)dp = k\,V_0\left(-\exp\left(\frac{p-p_0}{k}\right)+1\right)$$

$$\text{since: } p - p_0 \ll k \Rightarrow \text{-exp}\left(\frac{p-p_0}{k}\right) = -1$$

$$\Rightarrow \int_{p_0}^{p} V(p)dp \approx 0$$

A.7 DSC traces

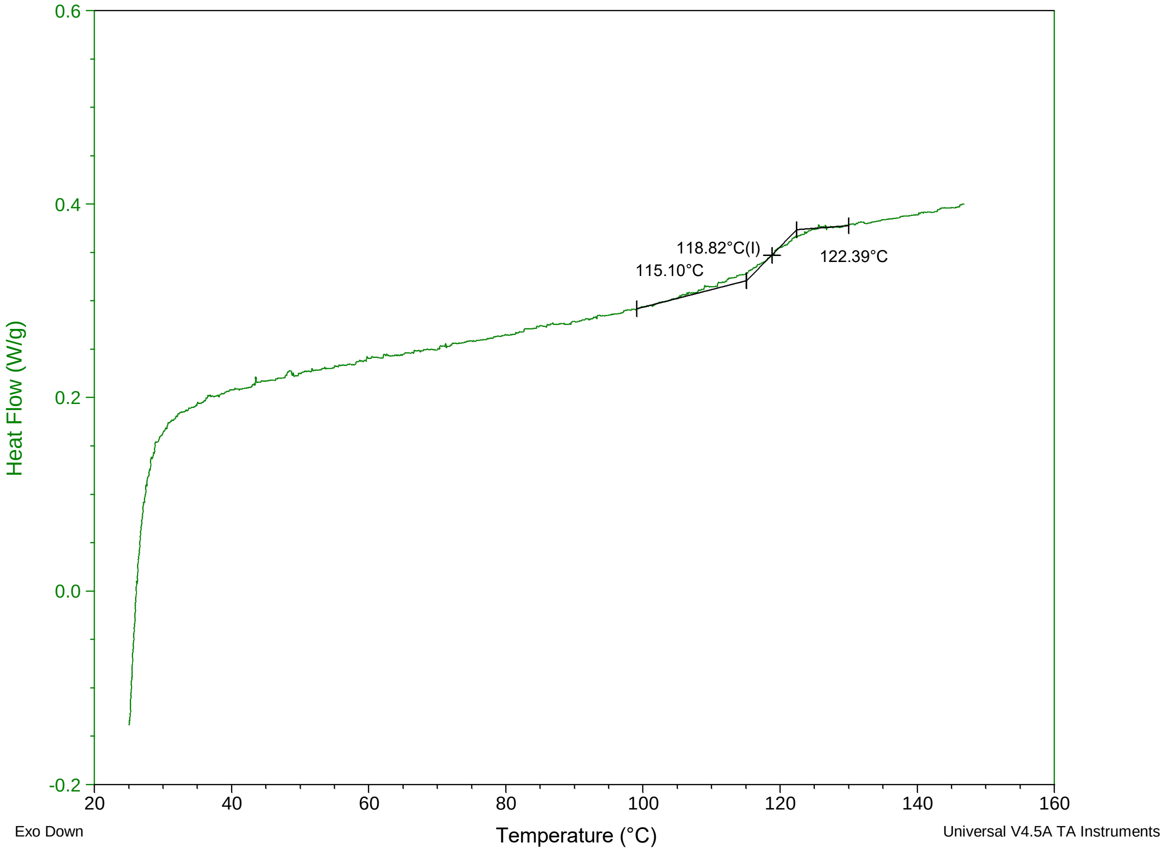

Figure 103: DSC trace from 2nd cycle of batch 1 PMMA

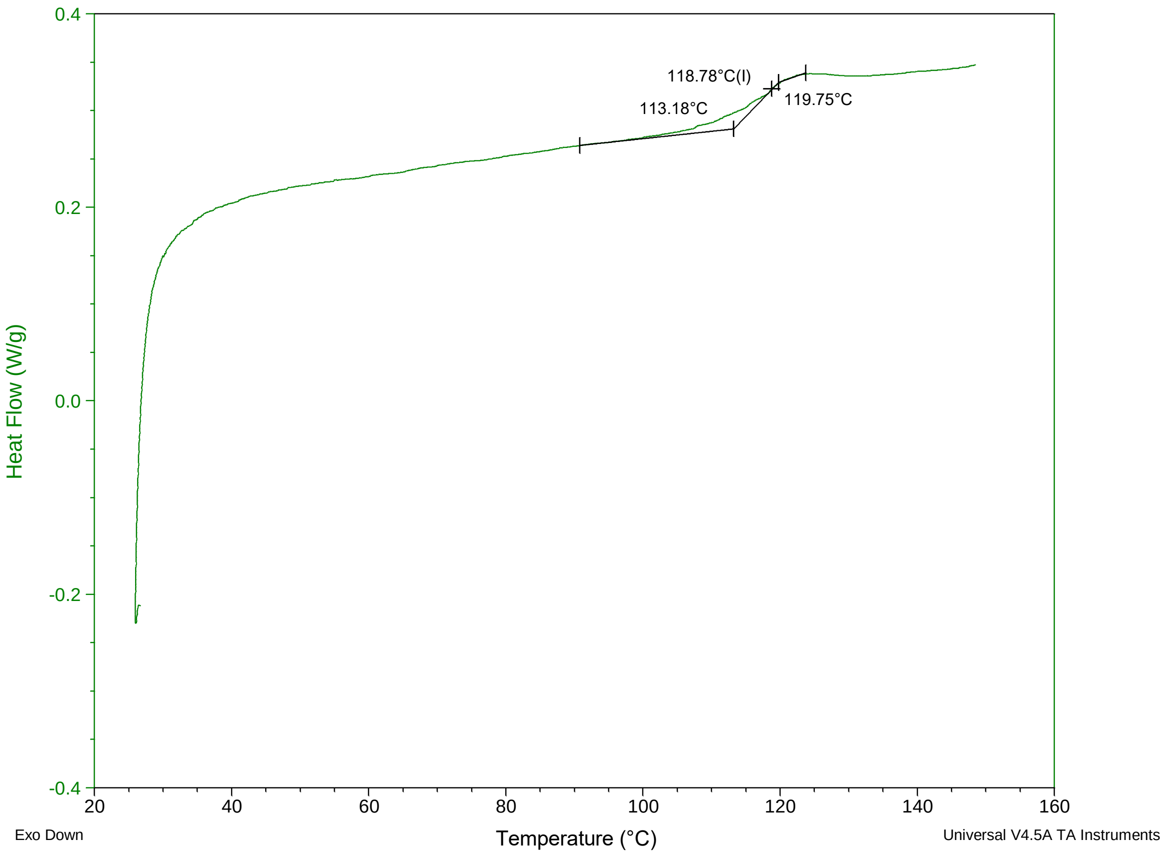

Figure 104: DSC trace from 2nd cycle of batch 2 PMMA

Abbreviations

Most abbreviations are defined upon use. However, some are used repeatedly and therefore defined here:

PMMA	Polymethylmethacrylate
PC	Polycarbonat
CO_2	carbon dioxide
DMA	Dynamic Mechanical Analysis
DSC	Dynamic Scanning Calorimetry
TGA	Thermo Gravimetric Analysis
SEM	scanning electronic microscopy
p	pressure
V	volume
T	temperature
t	time
R	radius or universal gas constant
k	Bolzmann constant
T_g	glass transition temperature
G_{mix}	Gibb’s free energy of the mixed state
χ	Flory-Huggins polymer-solvent interaction parameter
α	thernal expansion coefficient
$\sigma_1 > \sigma_2 > \sigma_3$	principal stresses
ε	strain
ΔΓ	retardation
ς	stress optical coefficient
E_i	Youngs’ modulus
µ	chemical potential or micron

T_1	temperature of silicone oil bath employed for foaming
t_1	foaming time
T_2	temperature of stabilizing silicone oil bath
t_2	stabilisation duration
n	refractive index

List of Figures

List of Tables

Bibliography

Adams, R, H H M Balyuzi, and R E Burge. 1978. “The Structure of Amorphous Polystyrene by X-Ray Scattering and Simple Conformational Analysis.” *JOURNAL OF MATERIALS SCIENCE* 13: 391–401. http://download.springer.com/static/pdf/212/art%253A10.1007%252FBF00647784.pdf?originUrl=http%3A%2F%2Flink.springer.com%2Farticle%2F10.1007%2FBF00647784&token2=exp=1490016348~acl=%2Fstatic%2Fpdf%2F212%2Fart%25253A10.1007%25252FBF00647784.pdf%3ForiginUrl%3Dhttp%253A%252F%252Flink.springer.com%252Farticle%252F10.1007%252FBF00647784*~hmac=edb9b794b6d66cce6a4faf8789c7025931da632a6deb31d17f7eaf30280bb7bc.

Albalak, Ramon J., Zehev Tadmor, and Yeshayahu Talmon. 1990. “Polymer Melt Devolatilization Mechanisms.” *AIChE Journal* 36 (9): 1313–20. https://doi.org/10.1002/aic.690360904.

Alfrey, Turner. 1947. “The Influence of Solvent Composition on the Specific Viscosities of Polymer Solutions.” *Journal of Colloid Science* 2 (1): 99–114. https://doi.org/10.1016/0095-8522(47)90013-5.

Arnold, J.C. 2010. “A Free-Volume Hole-Filling Model for the Solubility of Liquid Molecules in Glassy Polymers 1: Model Derivation.” *European Polymer Journal* 46 (5): 1131–40. https://doi.org/10.1016/j.eurpolymj.2010.01.016.

Atkins, Peter, and Julio de Paula. 2010. *Atkins’ Physical Chemistry*. OUP Oxford. https://books.google.co.uk/books/about/Atkins_Physical_Chemistry.html?id=BV6cAQAAQBAJ&pgis=1.

Aubert, J.H., and R.L. Clough. 1985. “Low-Density, Microcellular Polystyrene Foams.” *Polymer* 26 (13): 2047–54. https://doi.org/10.1016/0032-3861(85)90186-7.

Bernardo, Victoria, Judith Martín-de León, Ester Laguna-Gutiérrez, and Miguel Ángel Rodríguez-Pérez. 2017. “PMMA-Sepiolite Nanocomposites as New Promising Materials for the Production of Nanocellular Polymers.” *European Polymer Journal* 96 (November): 10–26. https://doi.org/10.1016/j.eurpolymj.2017.09.002.

Cahn, John W. 1965. “Phase Separation by Spinodal Decomposition in Isotropic Systems.” *The Journal of Chemical Physics* 42 (1): 93. https://doi.org/10.1063/1.1695731.

Caneba, Gerard T., and David S. Soong. 1985. “Polymer Membrane Formation through the Thermal-Inversion Process. 1. Experimental Study of Membrane Structure Formation.” *Macromolecules* 18 (12): 2538–45. https://doi.org/10.1021/ma00154a031.

Carter, Walter C., Robert L. Scott, and Michael Magat. 1946. “The Viscosity-Molecular Weight Relation for Natural Rubber1.” *Journal of the American Chemical Society*, no. 68,8: 1480–83.

Castro, AJ. 1981. Methods for making microporous products. *US Patent 4,247,498*, issued 1981. http://www.google.com/patents?hl=en&lr=&vid=USPAT4247498&id=Q_Y0AAAAEBAJ&oi=fnd&dq=Methods+for+making+microporous+products&printsec=abstract.

Chen, Lee, Xiang Wang, Rich Straff, and Kent Blizard. 2002. “Shear Stress Nucleation in Microcellular Foaming Process.” *Polymer Engineering & Science* 42 (6): 1151–58. https://doi.org/10.1002/pen.11019.

Comyn, J., ed. 1985. *Polymer Permeability*. Dordrecht: Springer Netherlands. https://doi.org/10.1007/978-94-009-4858-7.

Costeux, Stéphane. 2014. “CO 2 -Blown Nanocellular Foams.” *Journal of Applied Polymer Science* 131 (23): n/a-n/a. https://doi.org/10.1002/app.41293.

Costeux, Stéphane, and Devin Foether. 2015. *Continuous Extrusion of Nanocellular Foam*.

Costeux, Stephane, Hyun Jeon, Shana Bunker, and Irfan Khan. 2012. “Nanocellular Foams from Acrylic Polymers: Experiments and Modeling.” In *SPE FOAMS 2012 Conference*. https://www.researchgate.net/publication/260985490_Nanocellular_foams_from_acrylic_polymers_Experiments_and_modeling.

Crank, John. 1975. *The Mathematics of Diffusion*. Clarendon Press.

Dack, M. R. J. 1975. “The Importance of Solvent Internal Pressure and Cohesion to Solution Phenomena.” *Chemical Society Reviews* 4 (2): 211. https://doi.org/10.1039/cs9750400211.

David L. Tomasko, *, Hongbo Li, Dehua Liu, Xiangmin Han, Maxwell J. Wingert, and L. James Lee, and Kurt W. Koelling. 2003. “A Review of CO2 Applications in the Processing of Polymers.”

“DoITPoMS - TLP Library Stress Analysis and Mohr’s Circle - Representing Stress as a Tensor.” n.d. Accessed January 27, 2020. https://www.doitpoms.ac.uk/tlplib/metal-forming-1/stress_tensor.php.

Dortmund Data Bank. 2019. “Thermal Expansion Coefficient of Methanol from Dortmund Data Bank.” 2019. http://www.ddbst.com/en/EED/PCP/CEC_C110.php.

Ehrenstein, Gottfried W, Gabriela. Riedel, and Pia. Trawiel. 2004. *Thermal Analysis of Plastics : Theory and Practice*. Munich; Cincinnati: Hanser ; Hanser Gardner Publications [distributor].

Einstein, A. 1905. “Über Die von Der Molekularkinetischen Theorie Der Wärme Geforderte Bewegung von in Ruhenden Flüssigkeiten Suspendierten Teilchen.” *Annalen Der Physik* 322 (8): 549–60. https://doi.org/10.1002/andp.19053220806.

Elder, Robert M., Tyler R. Long, Erich D. Bain, Joseph L. Lenhart, and Timothy W. Sirk. 2018. “Mechanics and Nanovoid Nucleation Dynamics: Effects of Polar Functionality in Glassy Polymer Networks.” *Soft Matter* 14 (44): 8895–8911. https://doi.org/10.1039/C8SM01483C.

Estravis, Sergio, Alan H. Windle, Martin van Es, and James A. Elliott. 2020. “Thermodynamic Limits on Cell Size in the Production of Stable Polymeric Nanocellular Materials.” *Polymer* 186 (January): 122036. https://doi.org/10.1016/J.POLYMER.2019.122036.

Favelukis, Moshe, Zehev Tadmor, and Raphael Semiat. 1999. “Bubble Growth in a Viscous Liquid in a Simple Shear Flow.” *AIChE Journal* 45 (4): 691–95. https://doi.org/10.1002/aic.690450404.

Ferriol, M., A. Gentilhomme, M. Cochez, N. Oget, and J.L. Mieloszynski. 2003. “Thermal Degradation of Poly(Methyl Methacrylate) (PMMA): Modelling of DTG and TG Curves.” *Polymer Degradation and Stability* 79 (2): 271–81. https://doi.org/10.1016/S0141-3910(02)00291-4.

Flory, Paul J. 1942. “Thermodynamics of High Polymer Solutions.” *The Journal of Chemical Physics* 10 (1): 51. https://doi.org/10.1063/1.1723621.

Forest, C., P. Chaumont, P. Cassagnau, B. Swoboda, and P. Sonntag. 2015. “CO2 Nano-Foaming of Nanostructured PMMA.” *Polymer* 58 (February): 76–87. https://doi.org/10.1016/j.polymer.2014.12.048.

Freyman, T.M., I.V. Yannas, and L.J. Gibson. 2001. “Cellular Materials as Porous Scaffolds for Tissue Engineering.” *Progress in Materials Science* 46 (3–4): 273–82. https://doi.org/10.1016/S0079-6425(00)00018-9.

Gałka, Piotr, Jolanta Kowalonek, and Halina Kaczmarek. 2014. “Thermogravimetric Analysis of Thermal Stability of Poly(Methyl Methacrylate) Films Modified with Photoinitiators.” *Journal of Thermal Analysis and Calorimetry* 115 (2): 1387–94. https://doi.org/10.1007/s10973-013-3446-z.

Gennes, Pierre-Gilles de. 1979. *Scaling Concepts in Polymer Physics*. Cornell University Press. https://books.google.com/books?hl=en&lr=&id=ApzfJ2LYwGUC&pgis=1.

Guo, Huimin. 2015. “Solid-State Polymer Nanofoams.” https://digital.lib.washington.edu:443/researchworks/handle/1773/35253.

Guo, Huimin, Andrei Nicolae, and Vipin Kumar. 2015. “Solid-State Poly(Methyl Methacrylate) (PMMA) Nanofoams. Part II: Low-Temperature Solid-State Process Space Using CO2 and the Resulting

Morphologies.” *Polymer* 70: 231–41. https://doi.org/10.1016/j.polymer.2015.06.031.

Guo, M.C, and Y.C Peng. 2003. “Study of Shear Nucleation Theory in Continuous Microcellular Foam Extrusion.” *Polymer Testing* 22 (6): 705–9. https://doi.org/10.1016/S0142-9418(03)00004-7.

Han, James H., and Chang Dae Han. 1990. “Bubble Nucleation in Polymeric Liquids. II. Theoretical Considerations.” *Journal of Polymer Science Part B: Polymer Physics* 28 (5): 743–61. https://doi.org/10.1002/polb.1990.090280510.

Handa, Y. Paul, and Zhiyi Zhang. 2000. “A New Technique for Measuring Retrograde Vitrification in Polymer-Gas Systems and for Making Ultramicrocellular Foams from the Retrograde Phase.” *Journal of Polymer Science Part B: Polymer Physics* 38 (5): 716–25. https://doi.org/10.1002/(SICI)1099-0488(20000301)38:5<716::AID-POLB9>3.0.CO;2-N.

Harvey, E. Newton, D. K. Barnes, W. D. McElroy, A. H. Whiteley, D. C. Pease, and K. W. Cooper. 1944. “Bubble Formation in Animals. I. Physical Factors.” *Journal of Cellular and Comparative Physiology* 24 (1): 1–22. https://doi.org/10.1002/jcp.1030240102.

Holl, M. R., V. Kumar, J. L. Garbini, and W. R. Murray. 1999a. “Cell Nucleation in Solid-State Polymeric Foams: Evidence of a Triaxial Tensile Failure Mechanism.” *Journal of Materials Science* 34 (3): 637–44. https://doi.org/10.1023/A:1004527603363.

Holl, M R, V Kumar, J L Garbini, and W R Murray. 1999b. “Cell Nucleation in Solid-State Polymeric Foams: Evidence of a Triaxial Tensile Failure Mechanism” 3 (9): 637–44. https://pdfs.semanticscholar.org/fd1c/9e398614cf386af98726cd8a6c58a7216690.pdf.

Huggins, Maurice L. 1941. “Solutions of Long Chain Compounds.” *The Journal of Chemical Physics* 9 (5): 440. https://doi.org/10.1063/1.1750930.

Hung, Wei-Lun, Da-Ming Wang, Juin-Yih Lai, and Shang-Chih Chou. 2016. “On the Initiation of Macrovoids in Polymeric Membranes – Effect of Polymer Chain Entanglement.” *Journal of Membrane Science* 505 (May): 70–81. https://doi.org/10.1016/j.memsci.2016.01.021.

Kashchiev, Dimo. 2000. *Nucleation : Basic Theory with Applications*. Butterworth Heinemann. https://books.google.co.uk/books/about/Nucleation.html?id=beLcgIp-p6EC&redir_esc=y.

Koenhen, D. M., and C. A. Smolders. 1975. “The Determination of Solubility Parameters of Solvents and Polymers by Means of Correlations with Other Physical Quantities.” *Journal of Applied Polymer Science* 19 (4): 1163–79. https://doi.org/10.1002/app.1975.070190423.

Koros, W.J., and G.K. Fleming. 1993. “Membrane-Based Gas Separation.” *Journal of Membrane Science* 83 (1): 1–80. https://doi.org/10.1016/0376-7388(93)80013-N.

Kuhn, Werner, and F. Grün. 1942. “Beziehungen Zwischen Elastischen Konstanten Und Dehnungsdoppelbrechung Hochelastischer Stoffe.” *Kolloid-Zeitschrift* 101 (3): 248–71. https://doi.org/10.1007/BF01793684.

Lee, S. T., and J. A. Biesenberger. 1989. “A Fundamental Study of Polymer Melt Devolatilization. IV: Some Theories and Models for Foam-Enhanced Devolatilization.” *Polymer Engineering and Science* 29 (12): 782–90. https://doi.org/10.1002/pen.760291206.

Lee, Shau-Tarng. 1994. “More Experiments on Thermoplastic Foam Nucleation.” *Journal of Cellular Plastics* 30 (5): 444–53. https://doi.org/10.1177/0021955X9403000502.

León, Judith Martín-de, Victoria Bernardo, and Miguel Ángel Rodríguez-Pérez. 2019. “Nanocellular Polymers: The Challenge of Creating Cells in the Nanoscale.” *Materials* 12 (5). https://doi.org/10.3390/MA12050797.

León, Judith Martín-de, Victoria Bernardo, Ester Laguna-Gutiérrez, and Miguel Ángel Rodríguez-Pérez. 2020. “Influence of the Viscosity of Poly(Methyl Methacrylate) on the Cellular Structure of Nanocellular Materials.” *Polymer International* 69 (1): 72–83. https://doi.org/10.1002/pi.5920.

Leung, Siu N., Anson Wong, Lilac Cuiling Wang, and Chul B. Park. 2012. “Mechanism of Extensional Stress-Induced Cell Formation in Polymeric Foaming Processes with the Presence of Nucleating Agents.” *The Journal of Supercritical Fluids* 63 (March): 187–98.

https://doi.org/10.1016/J.SUPFLU.2011.12.018.

"Light and Color - Optical Birefringence | Olympus Life Science." n.d. Accessed May 15, 2020. https://www.olympus-lifescience.com/en/microscope-resource/primer/lightandcolor/birefringence/.

Lloyd, Douglas R., Kevin E. Kinzer, and H.S. Tseng. 1990. "Microporous Membrane Formation via Thermally Induced Phase Separation. I. Solid-Liquid Phase Separation." *Journal of Membrane Science* 52 (3): 239–61. https://doi.org/10.1016/S0376-7388(00)85130-3.

Loock, Frederik Van, Victoria Bernardo, Miguel Angel Rodríguez Pérez, and Norman A. Fleck. 2019. "The Mechanics of Solid-State Nanofoaming." *Proceedings of the Royal Society A: Mathematical, Physical and Engineering Sciences* 475 (2230): 20190339. https://doi.org/10.1098/rspa.2019.0339.

Loock, Frederik Van, and Norman A. Fleck. 2018. "Deformation and Failure Maps for PMMA in Uniaxial Tension." *Polymer* 148 (July): 259–68. https://doi.org/10.1016/j.polymer.2018.06.027.

Maio, Ernesto Di, and Erdogan Kiran. 2017. "Foaming of Polymers with Supercritical Fluids and Perspectives on the Current Knowledge Gaps and Challenges." *The Journal of Supercritical Fluids*, November. https://doi.org/10.1016/J.SUPFLU.2017.11.013.

Martín-de León, Judith, Victoria Bernardo, and Miguel Rodríguez-Pérez. 2016. "Low Density Nanocellular Polymers Based on PMMA Produced by Gas Dissolution Foaming: Fabrication and Cellular Structure Characterization." *Polymers* 8 (7): 265. https://doi.org/10.3390/polym8070265.

Martín-de León, Judith, Victoria Bernardo, and Miguel Ángel Rodríguez-Pérez. 2017. "Key Production Parameters to Obtain Transparent Nanocellular PMMA." *Macromolecular Materials and Engineering* 302 (12): 1700343. https://doi.org/10.1002/mame.201700343.

Martini, Jane Ellen. 1981. "The Production and Analysis of Microcellular Foam." https://dspace.mit.edu/handle/1721.1/15748.

Matsuyama, Hideto, Stephane Berghmans, and Douglas R Lloyd. 1998. "Formation of Hydrophilic Microporous Membranes via Thermally Induced Phase Separation." *Journal of Membrane Science* 142 (2): 213–24. https://doi.org/10.1016/S0376-7388(97)00330-X.

Merritt, D. R., and F. Weinhaus. 1978. "The Pressure Curve for a Rubber Balloon." *American Journal of Physics* 46 (10): 976–77. https://doi.org/10.1119/1.11486.

Miller, Dustin, Pavee Chatchaisucha, and Vipin Kumar. 2009. "Microcellular and Nanocellular Solid-State Polyetherimide (PEI) Foams Using Sub-Critical Carbon Dioxide I. Processing and Structure." *Polymer* 50 (23): 5576–84. https://doi.org/10.1016/j.polymer.2009.09.020.

Nam, Yoon Sung, and Tae Gwan Park. 1999. "Biodegradable Polymeric Microcellular Foams by Modified Thermally Induced Phase Separation Method." *Biomaterials* 20 (19): 1783–90. https://doi.org/10.1016/S0142-9612(99)00073-3.

Notario, B., J. Pinto, and M.A. Rodriguez-Perez. 2016a. "Nanoporous Polymeric Materials: A New Class of Materials with Enhanced Properties." *Progress in Materials Science* 78 (February): 93–139. https://doi.org/10.1016/j.pmatsci.2016.02.002.

———. 2016b. "Nanoporous Polymeric Materials: A New Class of Materials with Enhanced Properties." *Progress in Materials Science* 78–79 (June): 93–139. https://doi.org/10.1016/J.PMATSCI.2016.02.002.

Notario, B., J. Pinto, E. Solorzano, J.A. de Saja, M. Dumon, and M.A. Rodríguez-Pérez. 2015. "Experimental Validation of the Knudsen Effect in Nanocellular Polymeric Foams." *Polymer* 56 (January): 57–67. https://doi.org/10.1016/j.polymer.2014.10.006.

Okolieocha, Chimezie, Daniel Raps, Kalaivani Subramaniam, and Volker Altstädt. 2015. "Microcellular to Nanocellular Polymer Foams: Progress (2004–2015) and Future Directions – A Review." *European Polymer Journal* 73 (December): 500–519. https://doi.org/10.1016/j.eurpolymj.2015.11.001.

Parthasarathy, Raghuveer. 2008. “Http://Physics-Server.Uoregon.Edu/~raghu/TeachingFiles/Winter08Phys352/Notes_Diffusion.Pdf.” 2008. http://physics-server.uoregon.edu/~raghu/TeachingFiles/Winter08Phys352/Notes_Diffusion.pdf.

Pick, M., R. Lovell, and A. H. Windle. 1979. “Detection of Elastic Strain in an Amorphous Polymer by X-Ray Scattering.” *Nature* 281 (5733): 658–59. https://doi.org/10.1038/281658a0.

Pinto, Javier, Belen Notario, Raquel Verdejo, Michel Dumon, Stephane Costeux, and Miguel Angel Rodriguez-Perez. 2017. “Molecular Confinement of Solid and Gaseous Phases of Self-Standing Bulk Nanoporous Polymers Inducing Enhanced and Unexpected Physical Properties.” *Polymer* 113 (March): 27–33. https://doi.org/10.1016/J.POLYMER.2017.02.046.

“Polymer Foam Market Size | Global Industry Forecast Report, 2027.” n.d. Accessed August 29, 2020. https://www.grandviewresearch.com/industry-analysis/polymer-foam-market.

Qian, Caibao, Stephen J. Mumby, and B. E. Eichinger. 1991. “Phase Diagrams of Binary Polymer Solutions and Blends.” *Macromolecules* 24 (7): 1655–61. https://doi.org/10.1021/ma00007a031.

Qingping Guo, and Jin Wang, Chul B. Park*, and Masahiro Ohshima. 2006. “A Microcellular Foaming Simulation System with a High Pressure-Drop Rate.” https://doi.org/10.1021/IE060105W.

Ramesh, N. S., Don H. Rasmussen, and Gregory A. Campbell. 1994. “The Heterogeneous Nucleation of Microcellular Foams Assisted by the Survival of Microvoids in Polymers Containing Low Glass Transition Particles. Part I: Mathematical Modeling and Numerical Simulation.” *Polymer Engineering and Science* 34 (22): 1685–97. https://doi.org/10.1002/pen.760342206.

Reverchon, E., E. Schiavo Rappo, and S. Cardea. 2006. “Flexible Supercritical CO2-Assisted Process for Poly(Methyl Methacrylate) Structure Formation.” *Polymer Engineering & Science* 46 (2): 188–97. https://doi.org/10.1002/pen.20438.

Salvatore Iannace, Chul B. Park. 2015. *Biofoams: Science and Applications of Bio-Based Cellular and Porous Materials*. CRC Press. https://books.google.com/books?hl=en&lr=&id=AHe9CgAAQBAJ&pgis=1.

Samitsu, Sadaki, Rui Zhang, Xinsheng Peng, Mohan Raj Krishnan, Yoshihisa Fujii, and Izumi Ichinose. 2013. “Flash Freezing Route to Mesoporous Polymer Nanofibre Networks.” *Nature Communications* 4 (January): 2653. https://doi.org/10.1038/ncomms3653.

Shafiee, Houran, Shotaro Beppu, Shuhei Iwasaki, Akihiro Tagaya, and Yasuhiro Koike. 2015. “Mechanisms of Orientational and Photoelastic Birefringence Generation of Methacrylates for the Design of Zero-Zero-Birefringence Polymers.” *Polymer Engineering & Science* 55 (6): 1330–38. https://doi.org/10.1002/pen.24072.

Shafiee, Houran, Akihiro Tagaya, and Yasuhiro Koike. 2010. “Mechanism of Generation of Photoelastic Birefringence in Methacrylate Polymers for Optical Devices.” *Journal of Polymer Science Part B: Polymer Physics* 48 (19): 2029–37. https://doi.org/10.1002/polb.22082.

Smolders, C. A., J. J. Aartsen, and A. Steenbergen. 1971. “Liquid-Liquid Phase Separation in Concentrated Solutions of Non-Crystallizable Polymers by Spinodal Decomposition.” *Kolloid-Zeitschrift & Zeitschrift Für Polymere* 243 (1): 14–20. https://doi.org/10.1007/BF01500609.

Smoluchowski, M. von. 1906. “Zur Kinetischen Theorie Der Brownschen Molekularbewegung Und Der Suspensionen.” *Annalen Der Physik* 326 (14): 756–80. https://doi.org/10.1002/andp.19063261405.

Song, Seung-Won, and John M. Torkelson. 1994. “Coarsening Effects on Microstructure Formation in Isopycnic Polymer Solutions and Membranes Produced via Thermally Induced Phase Separation.” *Macromolecules* 27 (22): 6389–97. https://doi.org/10.1021/ma00100a024.

———. 1995. “Coarsening Effects on the Formation of Microporous Membranes Produced via Thermally Induced Phase Separation of Polystyrene-Cyclohexanol Solutions.” *Journal of Membrane Science* 98 (3): 209–22. https://doi.org/10.1016/0376-7388(94)00189-6.

Strobl, Gert R. 1997. *The Physics of Polymers: Concepts for Understanding Their Structures and*

Behaviour. Springer Science & Business Media. https://books.google.co.uk/books/about/The_Physics_of_Polymers.html?id=ENi4O_5QRWEC&pgis=1.

Student, Ralf. 2007. “No Title.” *PhD Thesis*, no. https://core.ac.uk/download/pdf/45268798.pdf.

Thomas, N.L., and A.H. Windle. 1980. “A Deformation Model for Case II Diffusion.” *Polymer* 21 (6): 613–19. https://doi.org/10.1016/0032-3861(80)90316-X.

Thomas, N.L, and A.H Windle. 1981. “Diffusion Mechanics of the System PMMA-Methanol.” *Polymer* 22 (5): 627–39. https://doi.org/10.1016/0032-3861(81)90352-9.

Thomas, Noreen. 1978. “Transport Mechanisms Associated with Swelling of PMMA by Methanol.” *PhD Dissertation*.

Tomasko, David L., Adam Burley, Lu Feng, Shu-Kai Yeh, Koki Miyazono, Sharath Nirmal-Kumar, Isamu Kusaka, and Kurt Koelling. 2009. “Development of CO2 for Polymer Foam Applications.” *The Journal of Supercritical Fluids* 47 (3): 493–99. https://doi.org/10.1016/J.SUPFLU.2008.10.018.

Treloar, L.R.G. 1958. *The Physics of Rubber Elasticity*. OUP Oxford. https://books.google.co.uk/books/about/The_Physics_of_Rubber_Elasticity.html?id=-iyDehYpoAQC&pgis=1.

Tsai, Fu Jya, and John M. Torkelson. 1990a. “The Roles of Phase Separation Mechanism and Coarsening in the Formation of Poly(Methyl Methacrylate) Asymmetric Membranes.” *Macromolecules* 23 (3): 775–84. https://doi.org/10.1021/ma00205a014.

———. 1990b. “Microporous Poly(Methyl Methacrylate) Membranes: Effect of a Low-Viscosity Solvent on the Formation Mechanism.” *Macromolecules* 23 (23): 4983–89. https://doi.org/10.1021/ma00225a018.

Urbanczyk, Laetitia, Cédric Calberg, Christophe Detrembleur, Christine Jérôme, and Michaël Alexandre. 2010. “Batch Foaming of SAN/Clay Nanocomposites with ScCO2: A Very Tunable Way of Controlling the Cellular Morphology.” *Polymer* 51 (15): 3520–31. https://doi.org/10.1016/J.POLYMER.2010.05.037.

Volmer, M., and A. Weber. 1926. “Keimbildung in Übersättigten Gebilden.” *Zeitschrift Für Physikalische Chemie* 119U: 277. https://doi.org/10.1515/zpch-1926-11927.

Vonka, Michal, Andra Nistor, Adam Rygl, Miloš Toulec, and Juraj Kosek. 2016. “Morphology Model for Polymer Foams Formed by Thermally Induced Phase Separation.” *Chemical Engineering Journal* 284 (January): 357–71. https://doi.org/10.1016/j.cej.2015.08.105.

Wang, Guilong, Jinchuan Zhao, Lun Howe Mark, Guizhen Wang, Kejing Yu, Chongda Wang, Chul B. Park, and Guoqun Zhao. 2017. “Ultra-Tough and Super Thermal-Insulation Nanocellular PMMA/TPU.” *Chemical Engineering Journal* 325 (October): 632–46. https://doi.org/10.1016/j.cej.2017.05.116.

Wang, Guilong, Jinchuan Zhao, Kejing Yu, Lun Howe Mark, Guizhen Wang, Pengjian Gong, Chul B. Park, and Guoqun Zhao. 2017. “Role of Elastic Strain Energy in Cell Nucleation of Polymer Foaming and Its Application for Fabricating Sub-Microcellular TPU Microfilms.” *Polymer* 119 (June): 28–39. https://doi.org/10.1016/J.POLYMER.2017.05.016.

Whang, K., C.H. Thomas, K.E. Healy, and G. Nuber. 1995. “A Novel Method to Fabricate Bioabsorbable Scaffolds.” *Polymer* 36 (4): 837–42. https://doi.org/10.1016/0032-3861(95)93115-3.

Witte, P. van de, P.J. Dijkstra, J.W.A. van den Berg, and J. Feijen. 1996. “Phase Separation Processes in Polymer Solutions in Relation to Membrane Formation.” *Journal of Membrane Science* 117 (1–2): 1–31. https://doi.org/10.1016/0376-7388(96)00088-9.

YH, Xu, and Pitot HC. 2003. “An Improved Stereologic Method for Three-Dimensional Estimation of Particle Size Distribution From Observations in Two Dimensions and Its Application.” *Computer Methods and Programs in Biomedicine* 72 (1). https://doi.org/10.1016/S0169-2607(02)00115-3.

Young, Robert J., and Peter A. Lovell. 2011. *Introduction to Polymers, Third Edition*. CRC Press. https://books.google.co.uk/books/about/Introduction_to_Polymers_Third_Edition.html?id=ImQg2MK8NtkC&pgis=1.

Zhuang, Wenhao, and Erdogan Kiran. 1998. “Kinetics of Pressure-Induced Phase Separation (PIPS) from Polymer Solutions by Time-Resolved Light Scattering. Polyethylene + n-Pentane.” *Polymer* 39 (13): 2903–15. https://doi.org/10.1016/S0032-3861(97)00593-4.

List of publications and awards

PUBLICATION:

Stress as a necessary condition for foam formation in PMMA/methanol foams
16th International Conference on Advances in Foam Materials & Technology
Montreal, Canada, 2018
Angelika M. Beinert, Martin van Es, Alan H. Windle, James A. Elliott

CONFERENCE PRESENTATIONS:

FOAMS 2018, Montreal, Canada
Nucleation – just a lot of stress? (talk)
Angelika M. Beinert, Martin van Es, Alan H. Windle, James A. Elliott

FOAMS 2018, Montreal, Canada
Characterisation of skin-induced hydrostatic stress and its influence on nucleation (poster)
Angelika M. Beinert, Martin van Es, Alan H. Windle, James A. Elliott

FOAMS 2017 Bayreuth, Germany
Polymer foam creation in PMMA and methanol – a way towards understanding cell size control (poster)
Angelika M. Beinert, Martin van Es, Alan H. Windle, James A. Elliott

AWARD:

Reedy Scholarship award at FOAMS 2018 conference
Award for best student contribution